REPORT DOCUMENTATION PAGE

Form Approved
OMB No. 0704-0188

1. AGENCY USE ONLY (Leave Blank)	2. REPORT DATE	3. REPORT TYPE AND DATES COVERED
	1997	Final

4. TITLE AND SUBTITLE
Ultrafast Spatiotemporal Coupling in Nonlinear Dispersive Media

5. FUNDING NUMBERS

6. AUTHORS
Andrew T. Ryan

AFRL-SR-BL-TR-98

0034

7. PERFORMING ORGANIZATION NAME(S) AND ADDRESS(ES)
The Institute of Optics
University of Rochester

9. SPONSORING/MONITORING AGENCY NAME(S) AND ADDRESS(ES)
AFOSR/NI
110 Duncan Avenue, Room B-115
Bolling Air Force Base, DC 20332-8080

AGENCY REPORT NUMBER

11. SUPPLEMENTARY NOTES

12a. DISTRIBUTION AVAILABILITY STATEMENT
Approved for Public Release

12b. DISTRIBUTION CODE

13. ABSTRACT *(Maximum 200 words)*
See attached.

19980115 193

14. SUBJECT TERMS			15. NUMBER OF PAGES
			16. PRICE CODE
17. SECURITY CLASSIFICATION OF REPORT	18. SECURITY CLASSIFICATION OF THIS PAGE	19. SECURITY CLASSIFICATION OF ABSTRACT	20. LIMITATION OF ABSTRACT
Unclassified	Unclassified	Unclassified	UL

Ultrafast Spatiotemporal Coupling in Nonlinear Dispersive Media

by

Andrew T. Ryan

Submitted in Partial Fulfillment

of the

Requirements for the Degree

Doctor of Philosophy

Supervised by

Professor Govind P. Agrawal

The Institute of Optics

The College

School of Engineering and Applied Sciences

University of Rochester

Rochester, New York

1997

For my friend Mike Flora,

who reminded me why

when I had forgotten how.

Curriculum Vitae

The author was born in Plattsburgh, New York on 13 October 1966. He attended the State University of New York College at Oswego from 1986 to 1990. He graduated Magna Cum Laude with a Bachelor of Science degree in Physics. He came to the University of Rochester in the fall of 1990 and began graduate studies in Optics. He received an Air Force Office of Scientific Research Laboratory Graduate Fellowship in 1992. He collaborated with Dr. John J. Kester at the Frank J. Seiler Research Laboratory in Colorado Springs, Colorado in 1993. In 1991 he began his thesis research under the supervision of Professor Govind P. Agrawal. His research interests were in the area of nonlinear optics and ultrashort pulse propagation.

Publications

A. T. Ryan, V. C. Wong and M. C. Gupta, "Photorefractive Instability Compensation in Quasi-Phasematched Second-Harmonic Generation in Li:TaO_3 Waveguides," submitted to J. Appl. Phys. (1997)

A. T. Ryan, "Spatiotemporal-Coupling-Induced Pulse Shaping via Spatial Soliton Beam Steering," to be submitted to J. Opt. Soc. Am. B (1997)

A. T. Ryan and G. P. Agrawal, "Spatiotemporal Coupling in Dispersive Nonlinear Planar Waveguides," J. of Opt. Soc. Am. B **12**, 2382 (1995)

A. T. Ryan and G. P. Agrawal, "Pulse Compression and Spatial Phase Modulation in Normally Dispersive Nonlinear Kerr Media," Optics Letters **20**,306-309 (1995)

A. T. Ryan and G. P. Agrawal, "Steering of Optical Beams in Nonlinear Kerr Media by Spatial Phase Modulation," Optics Letters **18**, 1795-1797 (1993)

A. T. Ryan, G. P. Agrawal, G. R. Gray and E. C. Gage, "Optical-Feedback-Induced-Chaos and its Control in Multimode Semiconductor Lasers," IEEE J. Quantum Electron., **QE-30**, 668-679 (1994)

G. R. Gray, A. T. Ryan, G. P. Agrawal and E. C. Gage, "Control of Optical-Feedback-Induced Laser Intensity Noise in Optical Data Recording," Optical Engineering **32**, 739-745 (1993)

Acknowledgments

Part of the process of going through graduate school is that you learn that there really is no such thing as purely independent research. The work presented in the thesis would not have been possible without the technical assistance of many colleagues and the unwavering support of many friends and my family.

I would like to acknowledge the support of the Cornell National Supercomputing Facility. Were it not for their grant of supercomputing time, the simulations would still be running. The Z-scan experiments were greatly aided by contributions from several people. Dr. George Fischer provided many useful discussions. Dr. Bob Bridges did most of the design work on the Ti:Sapphire laser system. Dr. Robert W. Boyd provided me with a back-up argon pump laser when our tube failed. Dr. Samson Janekhe provided conjugated polymer solutions for the Z-scan experiments. Samples of high-index glass were also provided by Dr. Nicholas Borrelli and Dr. Bruce Aitken at Corning Inc. I would also like to thank the Air Force Office of Scientific Research Laboratory Graduate Fellowship Program for both funding three years of my stay here in Rochester and providing me with a perfectly good reason to spend a summer in Colorado Springs. While in Colorado, Dr. John Kester taught me a great deal about what it means to be an experimentalist for which I will be forever grateful. I have learned a bit more about experimental work from Dr. Mool C. Gupta at Kodak with whom I have been working for the past eight months as a 'pre'-doc. I would also like to thank Dr. Gupta for tolerating my infrequent absences to finish writing this thesis. It took longer than both of us ever suspected it would.

Many of my friends have also pointed out that this took longer than they thought it would too. But their good-humored chiding did not detract from the benefit of their support and camaraderie over the years. When they taught me how to play golf, Dave Fischer and John LaFleche may not have done much to reduce the fraction of my life spent in graduate school, but they certainly made the experience more enjoyable. Dave, Mike Van Leeuwen and Craig Olson were also great about making themselves available to play basketball or watch just about any sport you could put a beer in front of (which is, I guess, all of them). I have a feeling that in the years to come watching the Super Bowl or the NCAA Tournament is just not going to be the same without their insightful, occasionally cynical but usually humorous commentary. My friends from home, Jeff Dumas and Mike Flora, were also great for entertaining me when I managed on occasion to escape Rochester. Even when I couldn't make it home, Mike and Jeff provided many an entertaining and enlightening hour on the telephone.

And then there's volleyball. I will always consider the night my volleyball team, Mom Plays Hockey, won the league championship as one of the highlights of my time in Rochester. And I will always regret that my other commitments prevented me from providing my teammates, Duncan Crawford, Dan Harrington, Bridget Petraitis, Warren and Melissa Grice, with the level of play with which they had become accustomed in the seasons that followed and coincided with the beginning of the writing of this thesis. I will also always regret that another volleyball friend, Debbie Wilson, has become a less-significant part of my life because of the strain put on our relationship by writing a thesis while working as a post-doc. Debbie was a wonderful source of support for as long as she could be.

I have also received a great deal of support and laughs from friends with whom I do not play any sports. The (nearly) always friendly countenance of my former officemate and now Dr. Lisa Liou was usually enough to make me believe that coming in to school that day wasn't a mistake. Lisa still has the most rewarding laugh of anyone I know. In the past year, the almost never cheerful greeting of Dr. Stojan Radic has always made me feel that my life wasn't so bad in comparison. But in reality, Stojan's constant enthusiasm for coffee, tasteless humor and scientific discussions has done much to help me keep my sanity over the past few months. Perhaps more importantly, Stojan's disciplined, determined work ethic has also provided me with a standard I am still striving to meet but which has been invaluable in preventing this writing process to drag on any further.

My thesis advisor Dr. Govind Agrawal really belongs in several of these groups. Although I have yet to play volleyball, basketball or golf with him, Dr. Agrawal has always been readily available as a source of technical information, encouragement and good humor. I think I learned more sitting in the chair opposite his desk than any other place I have ever been. I will always be grateful for all of his cheerful assistance and insightful comments over the years.

Finally I would like to thank my family. Mike, Greg, Pat (yes, even Pat), Frances, Mary and Matt have been wonderful providers of support, inspiration and motivation for all of my life. It has not always been easy keeping in touch over the distance and the years but when we do find the time it is always nice to feel their love and concern for me and my life. I would also like to thank my parents for providing me with such a great group of siblings. My mother and father will probably never know how

much those Sunday morning phone calls have meant to me over the years. I could not have done it without them.

Abstract

In this thesis the results of a systematic investigation into the behavior of ultrashort optical pulses propagating in dispersive media with a Kerr nonlinearity (and intensity-dependent refractive index) are presented. The effect of the nonlinear index is to couple the spatial and temporal behaviors of the optical field together in a process known as spatiotemporal coupling. In the first chapter, a review of the previous work done in describing spatiotemporal coupling is presented as well as a discussion of its relevance to the remaining chapters.

Optical wave propagation in general is described by Maxwell's equations. In the second chapter Maxwell's equations are used to derive the various forms of the nonlinear Schrödinger equation (NSE) which describe optical wave propagation in the presence of a Kerr nonlinearity. The different forms of the NSE account for different propagation geometries and conditions. The numerical model based on the NSE which is used to derive many of the results in the remainder of the thesis is also described. In chapter three, the numerical model is employed to give a thorough description of the dynamics of the pulse behavior in the presence of spatiotemporal coupling. An explanation of enhanced beam-broadening in self-defocusing media and localized pulse compression in normally dispersive self-focusing media are presented.

The remaining two chapters describe experimental conditions under which spatiotemporal coupling may become important. In chapter four, the model is used to describe a means to exploit the ultrafast Kerr nonlinearity to achieve pulse compression with spatial phase modulation. The process relies on the nonlinear coupling among the overlapping

subbeams produced by the modulation resulting in an intensity-dependence of the steering angles of the several peaks of the modulated pulse. In the fifth and final chapter, the influence of spatiotemporal coupling on Z-scan measurements of the nonlinear refractive index is discussed. A numerical investigation followed by an attempt at experimental verification shows that spatiotemporal pulse reshaping may lead to errors in measurements of the nonlinear index and nonlinear absorption performed via the Z-scan technique.

Table of Contents

List of Figures

Chapter 1

Introduction

1.1 Background

The beginning of the study of nonlinear optics was virtually concurrent with the invention of the laser[1,2] in 1960. The strength of the optical fields produced by lasers gave rise to such novel phenomena as self-focusing and self-trapping which warranted a more thorough understanding of the influence of an intense optical field on the medium in which it propagates. Self-focusing and self-trapping arise from an intensity-dependent refractive index (also known as a Kerr-type nonlinearity). The index of refraction of a Kerr material is given by $n = n_0 + n_2 I$ where I is the intensity of the optical field and the parameter n_2 is known as the nonlinear refractive index. However, the intensity-dependent refractive index is by no means the only phenomenon which the field of nonlinear optics seeks to describe. It is merely the one on which this thesis will concentrate. More complete descriptions of these and other effects have been compiled in the texts by Shen,[3] Boyd,[4] and Agrawal.[5]

The field of ultrafast optics also came to the fore with the invention of the laser.[1,2] The first optical laser was a flash-pumped ruby laser which produced "ultrafast" nanosecond (10^{-9} s) pulses.[2] As new tools were developed which produced shorter pulses, the term "ultrafast" took on new meaning. It is now generally accepted[6] that an ultrafast optical pulse is one with a duration or width $T_0 \leq 10$ ps, although the results contained

in this work generally refer to pulses of 100 fs (10^{-13} s) or shorter. Through the 1980s colliding-pulse modelocked (CPM) lasers lead the way into the femtosecond domain[7,8] with the first sub-100 fs pulses being generated in 1981 using a CPM laser.[7] A CPM laser was also in 1987 used to produce the shortest pulses ever recorded,[8] only 6 fs wide. In that experiment pulses from the CPM laser were first amplified and then passed through a fiber-grating-prism compressor[3] to achieve the result. Since that time, efforts in ultrafast pulse generation have been directed at creating less-complicated devices with a broader range of wavelengths from which to choose. The most significant development in these areas has been the Ti:Al_2O_3 laser.[9] In 1990, Spence et al.[9] were able to achieve self-modelocking by slightly realigning a modified Ti:Sapphire laser (Spectra-Physics Model 3900 CW). They coined the term "self-modelocking" because this laser had no elements designed specifically to produce modelocking (e.g. modulators or saturable absorbers). With intracavity dispersion compensation, they were able to achieve pulse widths less than 100 fs. Since that time, progress with Ti:Al_2O_3 lasers and the new class of related solid state lasers (Nd:YLF, Cr:LiSAF, etc.) has been rapid and widespread.[10-13] Recently the emphasis in research has switched to amplification of these pulses to millijoule levels[14-17] and to broadening the wavelength range still further through the use of optical parametric oscillators (OPO's).[18-20] The result of these efforts is that access to high-power femtosecond light sources is now almost commonplace.

Ultrafast optics and nonlinear optics are connected in that ultrafast pulses, because of their high peak powers, are frequently used to investigate nonlinear phenomena. In particular there have been a variety of techniques developed in recent years for measuring the nonlinear

refractive index of materials.[21-28] Early n_2 measurements exploited three-wave[21] and four-wave[22,23] mixing geometries. Interferometric techniques[24,25] have also been proposed which are quite sensitive, yet frequently quite complicated. More recently Sheik-Bahae[26,27] and co-workers introduced the Z-scan technique. The basic idea behind this technique is to measure the spatial distortions in the far-field resulting from the phase accumulated by a focused beam passing through a nonlinear material. Since its introduction, several innovations[28-34] have increased the accuracy and applicability of the Z-scan technique. Results have been presented for Z-scans performed using top-hat beams,[28] an eclipsed far-field,[29] arbitrarily shaped beams[30] and thick media,[31] as well as two-color arrangements[32,33] and a method for measuring the polarization dependence of the nonlinear response of crystals.[34] Further, pump-probe arrangements[35,36] have been employed to determine the response time of the material being investigated.

In all of the measurements discussed above an unchanging pulse shape has been assumed. This assumption is perfectly valid for a broad range of experimental parameters that include picosecond pulses or samples much thinner than the Rayleigh range of the beam. However, for the ubiquitous Ti:Al_2O_3 laser and other sub-picosecond sources there are conditions under which the pulse may be reshaped upon propagation through materials that are thinner than the Rayleigh range of the beam.[37] The result is that the reshaping in time changes the spatial distribution of the accumulated phase which in turn alters the far-field. This process is known as spatiotemporal coupling. The significance of spatiotemporal coupling is demonstrated in Fig. (1.1), where we plot the results of the

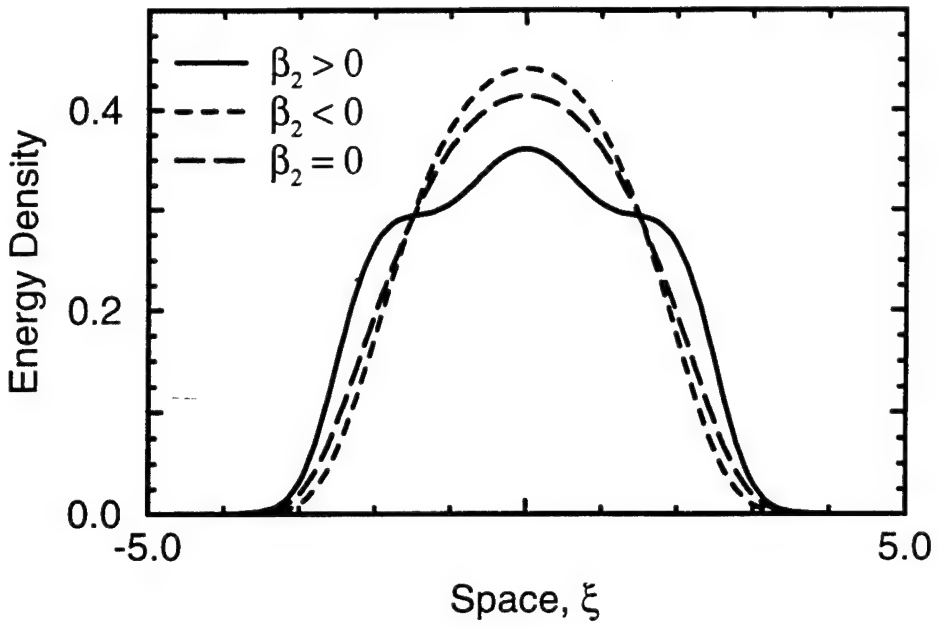

Figure (1.1) Time-integrated spatial energy distribution of an ultrashort pulse after propagating one diffraction length through a nonlinear dispersive medium for the cases of normal dispersion, anomalous dispersion and no dispersion. The dispersion produces changes in the beam shape via ultrafast nonlinear spatiotemporal coupling .

numerical simulation of the propagation of a spatially one-dimensional pulse through a nonlinear dispersive medium under three different assumptions: normal dispersion ($\beta_2 > 0$), anomalous dispersion ($\beta_2 < 0$) and no-dispersion ($\beta_2 = 0$). Clearly, the spatial far-field intensity distributions will be different for the three different dispersion cases. This difference is due to nonlinear ultrafast spatiotemporal coupling.

1.2 Overview

What we suggest in Fig. (1.1) is what we intend to demonstrate in this document: in order to use ultrashort pulses in nonlinear optics

experiments a clearer understanding of the evolution of the pulse shape (than that provided by the dispersionless approximation) as it propagates under the influence of diffraction, dispersion and the nonlinearity is needed. Fortunately, work in this area has been proceeding for over three decades.

Initially the research, directed at understanding the self-trapping of light predicted by Askar'yan[38] in 1962, was motivated by the discovery of damage tracks in laser crystals. The first papers[39,40] on the topic used a continuous-wave (cw) approximation with the nonlinear Schrödinger equation (NSE) to estimate self-trapping[39] conditions and self-focusing[40] thresholds for intense beams in nonlinear media. Later, Zakharov and Shabat[41] used the inverse scattering method to obtain soliton solutions of the one-dimensional NSE as well as a more complete description of two-dimensional self-focusing. Hasegawa and Tappert[42] followed with numerical simulations demonstrating the stability of the soliton solutions with respect to noise, perturbations and absorption. These one-dimensional results were significant in that they applied to the interaction of dispersive effects in the time-domain with the self-focusing nonlinearity. Since that time the study of one-dimensional fields, corresponding to pulses propagating in optical fibers, has been extensive and pulse behavior in fibers is now well understood.[3] The first discussion of the effect of spatial self-focusing on the shape of the pulse was presented by Marburger[43] in 1967, although his work was done in the dispersionless limit.

Throughout the 1970's much work was done both theoretically and experimentally investigating self-focusing phenomena. Bjorkholm and Ashkin[44] presented the results of the first quantitative experimental

investigation of self-focusing and self-defocusing. They tuned a dye laser through the sodium resonance to exploit the changing sign of the nonlinear index, and so investigate both phenomena. Later, Askar'yan and Mukhamadzhanov[45] investigated wave collapse using 10 ns pulses from a ruby laser focused into a nitrobenzene cell. An important innovation in the theoretical investigation of self-focusing was made by Anderson[46,47] who employed a variational approach to the problem which helped determine the dynamics of the beam width as a function of propagation distance.

The experimental demonstration of fiber solitons lead to an increased interest in three-dimensional solitons, or "light bullets." Marburger[43] had demonstrated that self-focusing could change the pulse shape but little was known about the effect of self-focusing on the pulse shape when dispersion was included in the model. Zharova et al.[48] presented the first results discussing the self-focusing of short pulses in the presence of dispersion. They found that normal dispersion can work as a mechanism to create temporal structures in the collapsing wave. Shortly thereafter Silberberg[49] demonstrated that in the anomalous dispersion regime three dimensional soliton solutions to the three-dimensional NSE exist but are unstable. This result was followed by the work of Desaix, Anderson and Lisak[50] who employed a variational approach to describe the dynamics of a collapsing wave obtained for different assumptions about the input field. They described the different behavior of Gaussian, hyperbolic secant and paraxial waves in one, two and three dimensions and compared them to the results of numerical simulations for the same assumptions. Chernev and Petrov[51,52] performed a more thorough numerical investigation of self-focusing pulses in normally dispersive

media and described both the pulse-splitting phenomenon discussed by Zharova et al.[48] as well as the phase characteristics of the collapsing wave. Rothenberg[53] presented similar results almost simultaneously. Recently, many of these results were verified experimentally by workers at Cornell[54] who demonstrated pulse splitting with sub-100-fs pulses self-focusing in BK7 glass in the normal dispersion regime.

Much of the multidimensional work in the past five years has been concerned with the behavior of optical pulses propagating in the anomalous-dispersion regime. The effects of the paraxiality of the NSE,[55-57] full-wave models based directly on Maxwell's equations,[58,59] saturable nonlinearities,[59,60] higher-order nonlinearities,[61] temporal phase modulation[62] and higher-order dispersion[63] have all been discussed in the context of wave collapse or light bullets. However, Luther and co-workers[64] have presented extensive numerical and analytical results describing the effect of normal dispersion on wave collapse. Some progress[65-67] has even been made describing multidimensional focusing occurring in a Ti:Al_2O_3 laser, a normally dispersive medium. We have investigated the dynamics of pulse behavior[35,68] in both the normal- and anomalous-dispersion regimes of self-defocusing and self-focusing media. Our work, as will be seen in the remainder of this thesis, has focused on the dynamics of beam and pulse shape due to the nonlinear spatiotemporal coupling implied by the NSE.

In chapter 2 we derive the multidimensional NSE and discuss the conditions under which the dimensionality can be reduced. We show how the NSE implies a spatiotemporal coupling and give a more thorough description of what precisely is meant by that expression. We

also describe the numerical model, based on the NSE, (and its limitations) used to simulate optical field propagation.

In chapter 3 we thoroughly describe optical pulse propagation in nonlinear dispersive media. We numerically investigate the interplay of diffraction, dispersion and the nonlinearity for spatially one and two-dimensional pulses for both self-focusing and self-defocusing nonlinearities in both normally and anomalously dispersive media.

In chapter 4 we will discuss beam steering via spatial phase modulation in nonlinear dispersive media. We numerically demonstrate how spatial solitons can influence the efficiency of the beam steering process. We then show how nonlinear spatiotemporal coupling can be exploited to shape as well as steer ultrashort pulses.

In chapter 5 we discuss the implications of spatiotemporal coupling for Z-scan experiments. We look at the results of simulations of spatially one-dimensional Z-scans using ultrashort pulses. These results show qualitatively how spatiotemporal coupling affects the measurements when an actual three-dimensional Z-scan is performed. We then discuss the results of Z-scan experiments performed with a Ti:Al_2O_3 laser and look for qualitative confirmation of the conclusions derived from our simulations.

1.3 References

1. A. L. Schawlow and C. H. Townes, "Infrared and opticcal masers", Phys. Rev. **112**, 1940 (1958)

2. T. H. Maiman, "Stimulated optical radiation in ruby masers," Nature **187**, 493 (1960)

3. Y. R. Shen, *The Principles of Nonlinear Optics*, (Wiley, New York, 1984)

4. R. W. Boyd, *Nonlinear Optics*, (Academic Press, San Diego, 1992)

5. G. P. Agrawal, *Nonlinear Fiber Optics*, 2nd ed. (Academic Press, San Diego, 1995)

6. I. A. Wamsley and J. D. Kafka, "Ultrafast nonlinear optics," in *Contemporary Nonlinear Optics*, G. P. Agrawal and R. W. Boyd, Eds., (Academic Press, San Diego, 1992)

7. C. V. Shank, R. L. Fork. R. Yen. R. H. Stolen, and W. J. Tomlinson, "Compression of femtosecond optical pulses," Appl. Phys. Lett. **40**, 761 (1982)

8. R. L. Fork, C. H. Brito Cruz, P. C. Becker, C. V. Shank, "Compression of optical pulses to six femtoseconds by using cubic phase compensation," Opt. Lett. **12**, 483 (1987)

9. D. E. Spence, P. N. Kean, and W. Sibbett, "60-fsec pulse generation from a self-mode-locked Ti:sapphire laser," Opt. Lett. **16**, 42 (1991)

10. J. P. Likfroman, G. Grillon, M. Joffre, C. LeBlanc, A. Mignus, and A. Antonetti, "Generation of 27 fs pulses of 70 kW peak power at 80 MHz repetition rate using a cw self-pulsing Ti:Sapphire laser," Appl. Phys. Lett. **58**, 2061 (1991)

11. U. Keller, G. W. 'tHooft, W. H. Know, and J. E. Cunningham, "Femtosecond pulses from a continuously self-starting passively mode-locked Ti:sapphire laser," Opt. Lett. **16**, 1022 (1991)

12. J. Zhou, G. Taft, C.-P. Huang, M. M. Murnane, H. C. Kapteyn, I. P. Christov, "Pulse evolution in a broad-bandwidth Ti:sapphire laser," Opt. Lett. **19**, 1149 (1994)

13. I. P. Christov, M. M. Murnane, H. C. Kapteyn, J. Zhou, C. Huang, "Fourth-order dispersion limited solitary pulses," Opt. Lett. **19**, 1465 (1995)

14. M. Lenzner, C. Spielmann, E. Wintner, F. Krausz, A. J. Schmidt, "Sub-20-fs, kilohertz-repetition-rate Ti:sapphire amplifier," Opt. Lett. **20**, 1397 (1995)

15. G. J. Crofts, X. Banti, M. J. Damzen, "Tunable Phase conjugation in a Ti:sapphire amplifier," Opt. Lett. **20**, 1634 (1995)

16. S. Backus, J. Peatross, C. P. Huang, M. M. Murnane, H. C. Kapteyn, "Ti:sapphire amplifier producing millijoule-level, 21 fs pulses at 1 kHz," Opt. Lett. **20**, 2000 (1995)

17. A. Dienes, J. P. Heritage, C. Jasti, and M. Y. Hong, "Femtosecond optical pulse amplification in saturated media," J. Opt. Soc. Am. B **13**, 725 (1996)

18. J. Ringling, O. Kittelmann, F. Noack, G. Korn, J. Squier, "Tunable femtosecond pulses in the near vaccuum ultraviolet generated by frequency conversion of amplified Ti:sapphire laser pulses," Opt. Lett. **18**, 2035 (1993)

19. G. M. Gale, M. Cavallari, T. J. Driscoll, F. Hache, "Sub-20-fs tunable pulses in the visible from an 82 MHz optical parametric oscillator," Opt. Lett. **20**, 1562 (1995)

20. J. M. Dudley, D. T. Reid, E. Ebrahimzadeh, W. Sibbet, "Characteristics of a non critically phase matched Ti:sapphire pumped femtosecond optical parametric oscillator," Opt. Comm. **104**, 419 (1994)

21. R. Adair, L. L. chase, and S. A. Payne, "Nonlinear refractive index measurement of glasses using three-wave mixing, " J. Opt. Soc. Am. B **4**, 875 (1987)

22. S. R. Friberg and P. W. smith, "Nonlinear optical glasses for ultrafast optical switches," IEEE J. Quantum Electron. **QE-23**, 2089 (1987)

23. C. Malouin, A. Villeneuve, G. Vitrant, R. A. Lessard, "Degenerate four-wave mixing geometry in thin-film waveguides for nonlinear materials characterization," Opt. Lett. **21**, 21 (1996)

24. M. J. Moran, C. Y. she, and R. L. Carman, "Interferometric measurements of nonlinear refractive-index coefficient relative to CS_2 in laser-system-related materials," IEEE J. Quantum Electron. **QE-11**, 259 (1975)

25. R. Trebino, C. C. Hayden, "Antiresonant-ring transient spectroscopy," Opt. Lett. **16**, 493 (1991)

26. M. Sheik-Bahae, A. A. Said, and E. W. Van Stryland, "High sensitivity single beam n_2 measurement," Opt. Lett. **14**, 955 (1989)

27. M. Sheik-Bahae, A. A. Said, T.-H. Wei, D. J. Hagan, E. W. Van Stryland, "Sensitive measurements of optical nonlinearities using a single beam," IEEE J. Quant. Electron. **26**, 760 (1990)

28. W. Zhao, P. Palffy-Muhoray, "Z-scan technique using top-hat beams," Appl. Phys. Lett. **63**, 1613 (1993)

29. T. Xia, D. J. Hagan, M. Sheik-Bahae, and E. W. Van Stryland, "Eclipsing Z-scan measurement of $\lambda/10^4$ wave-front distortion," Opt. Lett. **19**, 317 (1994)

30. R. E. Bridges, G. L. Fischer, R. W. Boyd, "Z-scan measurement technique for non-Gaussian beams and arbitrary sample thicknesses," Opt. Lett. **20**, 1821 (1995)

31. J. A. Herrmann, R. G. McDuff, "Analysis of spatial scanning with thick optically nonlinear media," J. Opt. Soc. Am. B **10**, 2056 (1993)

32. H. Ma, A. S. L. Gomes, and C. B. de Araujo, "Measurements of nondegenerate optical nonlinearity using a two-color single beam method," Appl. Phys. Lett. **59**, 2666 (1991)

33. M. Sheik-Bahae, J. Wang, R. DeSalvo, D. J. Hagan, and E. W. Van Stryland, "Measurement of nondegenerate nonlinearities using a two-color Z-scan," Opt. Lett. **17**, 260 (1992)

34. R. DeSalvo, M. Sheik-Bahae, A. A. Said, D. J. Hagan, and E. W. Van Stryland, "Z-scan measurements of the anisotropy of nonlinear refraction and absorption in crystals," Opt. Lett. **18**, 194 (1993)

35. K. Y. Tseng, K. S. Wong, and G. K. L. Wong "Femtosecond time-resolved Z-scan investigations of optical nonlinearities in ZnSe," Opt. Lett. **21**, 180 (1996)

36. J. Wang, M. Sheik-Bahae, A. A. Said, D. J. Hagan, E. W. Van Stryland, "Time-resolved Z-scan measurements of optical nonlinearities," J. Opt. Soc. Am. B **11**, 1009 (1994)

37. A. T. Ryan, G. P. Agrawal, "Spatiotemporal coupling in dispersive nonlinear planar waveguides," J. Opt. Soc. Am. B **12**, 2382 (1995)

38. G. A. Askar'yan, "Effects of the gradient of a strong electromagnetic beam on electrons and atoms," Sov. Phys. JETP **15**, 1088 (1962)

39. R. Y. Chiao, E. Garmire, C. H. Townes, "Self-trapping of optical beams," Phys. Rev. Lett. **13**, 479 (1964)

40. P. L. Kelly, "Self-focusing of optical beams," Phys. Rev. Lett. **15**, 1005 (1965)

41. V. E. Zakharov, A. B. Shabat, "Exact theory of two-dimensional self-focusing and one-dimensional self-modulation of waves in nonlinear media," Sov. Phys. JETP **34**, 62 (1972)

42. A. Hasegawa, F. Tappert, "Transmission of stationary nonlinear optical pulses in dispersive dielectric fibers. I Anomalous dispersion," Appl. Phys. Lett. **23**, 142 (1973)

43. J. H. Marburger, "Self-focusing as a pulse sharpening mechanism," IEEE J. Quant. Electron. **QE-3**, 415 (1967)

44. J. E. Bjorkholm, A. Ashkin, "cw self-focusing and self-trapping of light in sodium vapor," Phys. Rev. Lett. **32**, 129 (1974)

45. G. A. Askar'yan and M. A. Mukhamadzhanov, "Experimental investigation of beam collapse during the self-focusing in a nonlinear medium," JETP Lett. **229**, 247 (1979)

46. D. Anderson,"Stationary self-trapped laser beams in plasma," Physica Scripta **18**, 35 (1978)

47. D. Anderson, A. Bondeson, and M. Lisak, "A variational approach to perturbed soliton equations," Phys. Lett. A **67A**, 331 (1978)

48. N. A. Zharova, A. G. Litvak, T. A. Petrova, A. M. Sergeev, A. D. Yunakovskii, "Multiple fractionation of wave structures in a nonlinear medium," JETP Lett. **44**, 13 (1986)

49. Y. Silberberg, "Collapse of optical pulses," Opt. Lett. **15**, 1282 (1990)

50. M. Desaix, D. Anderson, M. Lisak, "Variational approach to collapse of optical pulses," J. Opt. Soc. Am. B **8**, 2082 (1991)

51. P. Chernev and V. Petrov, "Self-focusing of light pulses in the presence of normal group-velocity dispersion," Opt. Lett. **17**, 172 (1992)

52. P. Chernev and V. Petrov, "Self-focusing of short light pulses in dispersive media," Opt. Comm. **87**, 28 (1992)

53. J. E. Rothenberg, "Pulse splitting during self-focusing in normally dispersive media," Opt. Lett. **17**, 583 (1992)

54. J. K. Ranks, R. W. Schirmer and A. L. Gaeta, "Observation of Pulse Splitting in Nonlinear Dispersive Media," Phys. Rev. Lett. **77**, 3783 (1996)

55. M. D. Feit, J. A. Fleck, Jr., "Beam nonparaxiality, filament formation, and beam breakup in the self-focusing of optical beams," J. Opt. Soc. Am. B **5**, 633 (1988)

56. G. R. Hadley, "Multistep method for wide-angle beam propagation," Opt. Lett. **17**, 1743 (1992)

57. H. E. Hernandez-Figueroa, "Nonlinear nonparaxial beam-propagation method," Electron. Lett. **30**, 352 (1994)

58. R. W. Ziolkowski, J. B. Judkins, "Full-wave vector Maxwell equation modeling of the self-focusing of ultrashort optical pulses in a nonlinear Kerr medium exhibiting finite response time," J. Opt. Soc. Am. B **10**, 186 (1993)

59. S. Chi, Q Guo, "Vector theory of self-focusing of an optical beam in Kerr media," Opt. Lett. **20**, 1598 (1995)

60. J. M. Soto-Crespo, D. R. Heatley, E. M. Wright, N. N. Akhmediev, "Stability of the higher-bound states in a saturable self-focusing medium," Phys. Rev. A **44**, 636 (1991)

61. V. M. Malkin, "On the analytic theory for stationary self-focusing of radiation," Physica D **64**,251 (1993)

62. X. D. Cao, G. P. Agrawal, C. J. McKinstrie, "Self-focusing of chirped optical pulses in nonlinear dispersive media," Phys. Rev. A **49**, 4085 (1994)

63. V. I. Karpman, "Influence of high-order dispersion on self-focusing. I. Qualitative investigation," Phys. Lett. A **160**, 531 (1991); V. I. Karpman and A. G. Shagalov, "Influence of high-order dispersion on self-focusing. II. Numerical investigation," Phys. Lett. A **160**, 538 (1991)

64. G. G. Luther, A. C. Newell, J. V. Moloney, "The effects of normal dispersion on collapse events," Physica D **74**, 59 (1994)

65. I. P. Christov, H. C. Kapteyn, M. Murnane, C-P. Huang, J. Zhou, "Space-time focusing of femtosecond pulses in a Ti:sapphire laser," Opt. Lett. **20**, 309 (1995)

66. R. E. Bridges, R. W. Boyd, and G. P. Agrawal, "Multidimensional coupling owing to optical nonlinearities. I. General formulation," J. Opt. Soc. Am. B **13**, 553 (1996);

67. R. E. Bridges, R. W. Boyd, and G. P. Agrawal, "Multidimensional coupling owing to optical nonlinearities. II. Results," J. Opt. Soc. Am. B **13**, 560 (1996)

68. A. T. Ryan and G. P. Agrawal, "Pulse compression and spatial phase modulation in normally dispersive nonlinear Kerr media," Opt. Lett. **20**, 306 (1995)

Chapter 2

The Nonlinear Schrödinger Equation and Spatiotemporal Coupling

2.1 The Nonlinear Schrödinger Equation

Work on intensity-dependent refractive indices has been extensive both theoretically and experimentally.[1-16] The initial motivation of the research was to explain damage tracks found in laser crystals, later shown to be the result of the self-focusing properties of the crystals.[1-4] The index of refraction of the crystals increased with the intensity of the light. Theoretical investigations into this phenomenon lead to a description of both spatial and temporal solitons,[5,6] the former being a result of the balance between the self-focusing nonlinearity and diffraction while the latter is a manifestation of the time-domain interaction of the nonlinear index and the material dispersion. Both types of solitons are solutions to the one-dimensional nonlinear Schrödinger equation[7] (NSE) which describes a one-dimensional field propagating in a nonlinear medium. A spatially one-dimensional field describes a cw beam propagating in a planar waveguide, whereas a temporally one-dimensional result describes the evolution of pulses in a fiber. Two-dimensional fields, such as for pulses in planar waveguides or a cw beams in bulk media, are described by the two-dimensional NSE. The propagation of pulsed optical fields in bulk nonlinear media is described by the three-dimensional NSE. The derivation of the three-dimensional NSE that follows is intended to be illustrative rather than rigorous.

In general, the proper description of the propagation of light in a nonlinear, dispersive medium requires an analysis of the evolution of the optical field in time as well as in all three spatial dimensions.[8] The behavior of the optical field under the influence of dispersion, diffraction and an intensity-dependent refractive index is described by the three-dimensional NSE. The derivation of the three-dimensional NSE begins with Maxwell's equations for a source-free medium written as (in MKS units):

$$\nabla \cdot \mathbf{D} = 0 \tag{2.1}$$

$$\nabla \cdot \mathbf{B} = 0 \tag{2.2}$$

$$\nabla \times \mathbf{H} = \frac{\partial \mathbf{D}}{\partial t} \tag{2.3}$$

$$\nabla \times \mathbf{E} = -\frac{\partial \mathbf{B}}{\partial t}, \tag{2.4}$$

where **D** and **B** are the electric and magnetic flux density vectors respectively, while **E** and **H** are the electric and magnetic field vectors respectively. In eqns. (2.1-4) densities and fields are related via the constitutive relations:

$$\mathbf{D} = \varepsilon_0 \mathbf{E} + \mathbf{P} \tag{2.5}$$

and

$$\mathbf{B} = \mu_0 \mathbf{H}. \tag{2.6}$$

The constants ε_0 and μ_0 are the electric permittivity and magnetic permeability of free space, respectively. **P** is the macroscopic material polarization induced by the electric field in the medium.

Equations (2.5) and (2.6) can be used to eliminate **D** and **B** from eqns. (2.3) and (2.4):

$$\nabla \times \mathbf{H} = \frac{\partial}{\partial t}(\varepsilon_0 \mathbf{E} + \mathbf{P}) \tag{2.7}$$

$$\nabla \times \mathbf{E} = -\frac{\partial}{\partial t}(\mu_0 \mathbf{H}). \tag{2.8}$$

Taking the curl of eqn. (2.8) and substituting in from eqn. (2.7) results in:

$$\nabla \times \nabla \times \mathbf{E} = -\frac{\partial}{\partial t}\mu_0 \frac{\partial}{\partial t}(\varepsilon_0 \mathbf{E} + \mathbf{P}) \tag{2.9a}$$

or:

$$-\nabla^2 \mathbf{E} + \nabla(\nabla \cdot \mathbf{E}) = -\frac{1}{c^2}\frac{\partial^2}{\partial t^2}\mathbf{E} - \mu_0 \frac{\partial^2}{\partial t^2}\mathbf{P}. \tag{2.9b}$$

Consider for a moment the second term on the left hand side (LHS) of eqn. (2.9). For linear, isotropic source-free media, $\nabla \cdot \mathbf{E} = \varepsilon_0 \nabla \cdot \mathbf{D}$ hence this term vanishes. It is common to assume that this term's, contribution even in the case of nonlinear media, is negligible compared to that of other terms in eqn. (2.9b) hence it is usually neglected. Neglecting this term results in:

$$\nabla^2 \mathbf{E} - \frac{1}{c^2}\frac{\partial^2}{\partial t^2}\mathbf{E} = \mu_0 \frac{\partial^2}{\partial t^2}\mathbf{P}, \tag{2.10}$$

which is in the form of a wave equation for **E** driven by the second derivative of **P**.

The polarization **P** generally consists of a linear part $\mathbf{P}_L$ and a nonlinear part $\mathbf{P}_{NL}$. The linear part is related linearly to the electric field via the linear electric susceptibility of the medium, $\chi^{(1)}$:

$$\mathbf{P}_L(t) = \varepsilon_0 \int_{-\infty}^{\infty} \chi^{(1)}(t-t')\, \mathbf{E}(t')\, dt' \quad . \tag{2.11}$$

In the most general case, $\chi^{(1)}$ is a time-dependent tensor relating all components of either field, but for isotropic media it is simply a time-dependent scalar.

For linearly polarized fields in the slowly varying envelope approximation we can write the polarization and electric fields as follows:

$$\mathbf{P}_L = \frac{1}{2}\hat{x}\{P_L \exp(-i\omega_0 t) + \text{c.c.}\}, \tag{2.12a}$$

$$\mathbf{P}_{NL} = \frac{1}{2}\hat{x}\{P_{NL} \exp(-i\omega_0 t) + \text{c.c.}\}, \tag{2.12b}$$

$$\mathbf{E} = \frac{1}{2}\hat{x}\{E \exp(-i\omega_0 t) + \text{c.c.}\}. \tag{2.12c}$$

Here ω_0 is the assumed central oscillation frequency; P_L, P_{NL} and E are the slowly-varying envelopes of the polarization and electric fields respectively, c.c. is an abbreviation for "complex conjugate", and $\hat{x}$ is the unit vector in the polarization direction. For isotropic media we can then take $\chi^{(1)}$ to be a scalar and rewrite eqn. (2.11) as :

$$P_L(t) = \varepsilon_0 \int_{-\infty}^{\infty} \chi^{(1)}(t-t')\, E(t')\, dt', \tag{2.13}$$

an equation relating the scalar magnitudes of the fields. Then rewriting eqn. (2.10) in terms of the single field component of our linearly polarized field:

$$\nabla^2 E - \frac{1+\chi^{(1)}}{c^2}\frac{\partial^2}{\partial t^2}E = \mu_0 \frac{\partial^2}{\partial t^2} P_{NL} \,. \tag{2.14}$$

In the general case of an intensity-dependent index of refraction, the nonlinear part of the polarization is related to the electric field via the third-order electric susceptibility of the medium by the relation:

$$\mathbf{P}_{NL} = \varepsilon_0 \int_{-\infty}^{\infty}\int_{-\infty}^{\infty}\int_{-\infty}^{\infty} \chi^{(3)}(t-t_1,t-t_2,t-t_3)\, \mathbf{E}(t_1)\mathbf{E}(t_2)\mathbf{E}(t_3)\, dt_1 dt_2 dt_3 . \qquad (2.15)$$

This reduces to a scalar form similar to eqn. (2.13) for isotropic media and linearly polarized fields. Moreover, assuming an instantaneous response the nonlinear polarization component oscillating at the carrier frequency of the input field ω_0 is given by:

$$P_{NL} = \frac{3\varepsilon_0\chi^{(3)}}{4} |E|^2 E . \qquad (2.16)$$

The typical approach to the problem from this point is to treat the nonlinear polarization perturbatively by taking $P_{NL} = \varepsilon_0\varepsilon_{NL}E$, where $\varepsilon_{NL} = 3\varepsilon\chi^{(3)}|E|^2/4$ and neglecting the time-dependence of ε_{NL} for the remainder of the derivation. Thus, substituting eqn. (2.16) into eqn. (2.14) and taking the Fourier transform results in:

$$\nabla^2 \tilde{E} + \varepsilon(\omega) k_0^2 \tilde{E} = 0, \qquad (2.17)$$

where $k_0 = \omega/c$ and the Fourier transform is defined as:

$$\tilde{E}(r,\omega-\omega_0) = \int_{-\infty}^{\infty} E(r,t)\exp[i(\omega-\omega_0)t]dt, \qquad (2.18)$$

and

$$\varepsilon(\omega) = 1 + \chi^{(1)}(\omega) + \varepsilon_{NL} \,. \tag{2.19}$$

Next, the paraxial approximation is made by assuming the field $\tilde{E}$ propagates with propagation constant β_0, thus:

$$\tilde{E} = \tilde{A} \exp(i\beta_0 z) \,. \tag{2.20}$$

Substituting eqn.(2.20) into eqn. (2.17) and dropping the $\partial^2\tilde{A}/\partial z^2$ terms under the paraxial approximation results in:

$$\left(\frac{\partial^2}{\partial x^2} + \frac{\partial^2}{\partial y^2}\right)\tilde{A} + 2i\beta_0\frac{\partial \tilde{A}}{\partial z} + \left[\varepsilon(\omega)k_0^2 - \beta_0^2\right]\tilde{A} = 0 \,. \tag{2.21}$$

Then, taking

$$\beta^2 = \varepsilon(\omega)\, k_0^2 \tag{2.22}$$

and

$$\beta^2 - \beta_0^2 = (\beta + \beta_0)(\beta - \beta_0) \approx 2\beta_0(\beta - \beta_0) \tag{2.23}$$

results in:

$$\left(\frac{\partial^2}{\partial x^2} + \frac{\partial^2}{\partial y^2}\right)\tilde{A} + 2i\beta_0\frac{\partial \tilde{A}}{\partial z} + 2\beta_0(\beta - \beta_0)\,\tilde{A} = -\varepsilon_{NL}\, k_0^2\tilde{A} \,. \tag{2.24}$$

Next, β is expanded in a Taylor series about β_0:

$$\beta = \beta_0 + \beta_1(\omega - \omega_0) + \frac{\beta_2}{2}(\omega - \omega_0)^2 + \ldots \tag{2.25}$$

where $\beta_n = \partial^n\beta/\partial\omega^n$. Putting eqn. (2.25) into eqn. (2.24) results in:

$$\frac{-i}{2\beta_0}\left(\frac{\partial^2}{\partial x^2}+\frac{\partial^2}{\partial y^2}\right)\tilde{A}+\frac{\partial\tilde{A}}{\partial z}-\frac{i}{2}\left[\beta_1(\omega-\omega_0)+\frac{\beta_2}{2}(\omega-\omega_0)^2+\ldots\right]\tilde{A}$$
$$=\frac{i\varepsilon_{NL}k_0^2}{2\beta_0}\tilde{A}\,. \qquad (2.26)$$

Reversing the Fourier transform with the correspondence

$$i\frac{\partial}{\partial t}\leftrightarrow(\omega-\omega_0) \qquad (2.27)$$

and neglecting third and higher-order dispersion terms in the expansion of eqn. (2.25) leaves:

$$i\beta_1\frac{\partial A}{\partial t}+i\frac{\partial A}{\partial z}=\frac{1}{2\beta_0}\left(\frac{\partial^2}{\partial x^2}+\frac{\partial^2}{\partial y^2}\right)A-\frac{\beta_2}{2}\frac{\partial^2 A}{\partial t^2}+\frac{\varepsilon_{NL}k_0^2}{2\beta_0}A. \qquad (2.28)$$

Next, changing variables to a frame moving with the group velocity of the pulse such that $T = t - \beta_1 z$ results in:

$$i\frac{\partial A}{\partial z}=\frac{1}{2\beta_0}\left(\frac{\partial^2}{\partial x^2}+\frac{\partial^2}{\partial y^2}\right)A-\frac{\beta_2}{2}\frac{\partial^2 A}{\partial T^2}+\frac{\varepsilon_{NL}k_0^2}{2\beta_0}A. \qquad (2.29)$$

Then, assuming an input field of the form

$$A(x,y,z,T)=U(x/\sigma,\,y/\sigma,\,z/(\sigma^2\beta_0),\,T/T_0)=U(\xi,\eta,\zeta,\tau), \qquad (2.30)$$

eqn. (2.29) can be rewritten in terms of the normalized transverse coordinates $\xi = x/\sigma$, $\eta = y/\sigma$ (here a cylindrical symmetry is assumed but the approach is readily generalizable to elliptical beams), $\tau = T/T_0$ and the

propagation distance $\zeta = z/L_d = z/(\sigma^2\beta_0)$, normalized to the diffraction length or Rayleigh range of the incident field, leaving

$$i\frac{\partial U}{\partial \zeta} = -\frac{1}{2}\left(\frac{\partial^2}{\partial \xi^2} + \frac{\partial^2 U}{\partial \eta^2} \right) + \frac{\sigma^2\beta_0\beta_2}{2T_0^2}\frac{\partial^2}{\partial \tau^2}U - \frac{\sigma^2\varepsilon_{NL}k_0^2}{2}U. \qquad (2.31)$$

Finally, the field is normalized to its peak input intensity such that $U(\xi,\eta,\zeta,\tau) = U_0 u(\xi,\eta,\zeta,\tau)$ which results in the normalized three-dimensional NSE:

$$i\frac{\partial u}{\partial \zeta} = -\frac{1}{2}\left(\frac{\partial^2}{\partial \xi^2} + \frac{\partial^2}{\partial \eta^2} \right)u + \frac{d}{2}\frac{\partial^2 u}{\partial \tau^2} - \mathrm{sgn}(n_2)\, N^2\, |u|^2 u. \qquad (2.32)$$

Here, the magnitude of the dispersion parameter $d = \mathrm{sgn}(\beta_2)L_d/L_D = \sigma^2\beta_0\beta_2/T_0^2$ is a ratio of the diffraction length to the dispersion length ($L_D = T_0^2/|\beta_2|$) and is a measure of the relative strengths of the influence of dispersion and diffraction on the input field. Here, β_2 is the group velocity dispersion (GVD) parameter and can make d either positive or negative depending on whether the medium is normally or anomalously dispersive respectively. The nonlinearity parameter $N^2 = (2\pi\sigma/\lambda)^2 n_0 |n_2| I_0$ represents the strength of the Kerr nonlinearity with the quantity $|n_2| I_0$ being equal to the magnitude of the maximum nonlinear index change induced by the input field for an input peak intensity I_0. This change can be either positive or negative depending on whether the medium is self-focusing ($n_2 > 0$) or self-defocusing ($n_2 < 0$). Eqn. (2.32) accurately describes three-dimensional optical field propagation under the influences of diffraction, dispersion and an intensity-dependent index of refraction.

2.2 Spatial and Temporal Solitons

The three-dimensional NSE is a cumbersome tool to work with because of its complexity. A logical question to ask is whether or not there exist circumstances under which that complexity can be reduced. The answer is yes. To observe the influence of spatiotemporal coupling on the propagation of ultrashort pulses, we must first understand how light behaves in its absence. There are two ways to reduce the dimensionality of the NSE which will allow us to see the behavior of light in the absence of spatiotemporal coupling.

2.2.1Temporal Solitons

Perhaps the most common condition for which the dimensionality of the NSE is reduced occurs when it is used to describe the propagation of pulses in an optical fiber. In a fiber the maximum index change due to the nonlinearity is typically much less than the index step between the core and the cladding layers of the fiber. Under these conditions the spatial behavior of the field is governed by the linear waveguiding effects of the fiber[7,9] and eqn. (2.17) is solved via separation of variables by assuming a solution of the form:

$$\tilde{E}(\mathbf{r},\omega) = f(x,y)\,\tilde{a}(z,\omega)\exp(i\beta_0 z) \tag{2.33}$$

and substituting into eqn.(2.17) to get:

$$\left(\frac{\partial^2}{\partial x^2} + \frac{\partial^2}{\partial y^2}\right) f + \left[\varepsilon(\omega)k_0^2 - \tilde{\beta}^2\right] f = 0\,, \tag{2.34a}$$

$$2i\beta_0\frac{\partial \tilde{a}}{\partial z} + (\tilde{\beta}^2 - \beta_0^2)\,\tilde{a} = 0\,. \tag{2.34b}$$

Here the $\partial^2\bar{a}/\partial z^2$ term has been dropped in the paraxial approximation to form eqn. (2.34b). Eqn. (2.34a) is an eigenvalue equation for the propagation constant $\bar{\beta}$ of the waveguide mode f(x,y) and can be solved by the usual techniques.[7] Using the solution of eqn. (2.34a) to gain $\bar{\beta}$, eqn(2.33b) is solved via perturbation theory and an approach similar to the one used above to arrive at eqn. (2.31). This results in,

$$i\frac{\partial a}{\partial z} = \frac{\beta_2}{2}\frac{\partial^2}{\partial T^2}a - \gamma|a|^2a. \tag{2.35}$$

Here $\beta = \bar{\beta} + \Delta\beta$, with $\Delta\beta$ is the perturbation to the mode propagation constant, $\bar{\beta}$ caused by the nonlinearity, is used to obtain $\beta_2 = \partial^2\beta/\partial\omega^2$ and $T = t - (\partial\beta/\partial\omega)z$. The nonlinearity parameter $\gamma = n_2\omega_0/cA_{eff}$ contains the waveguide mode structure through the effective area,

$$A_{eff} = \frac{\left[\int_{-\infty}^{\infty}|f(x,y)|^2dxdy\right]^2}{\int_{-\infty}^{\infty}|f(x,y)|^4dxdy}. \tag{2.36}$$

After normalizing the propagation distance to the dispersion length, $\zeta_\tau = z/(T_0^2/|\beta_2|)$, eqn. (2.35) becomes the one-dimensional, temporal nonlinear Schrödinger equation:

$$i\frac{\partial u_\tau}{\partial \zeta_\tau} = \frac{sgn(\beta_2)}{2}\frac{\partial^2 u_\tau}{\partial \tau^2} - sgn(n_2)\,N_\tau^2\,|u_\tau|^2u_\tau, \tag{2.37}$$

where now $N_\tau = \gamma P_0 T_0^2 / |\beta_2|$, with P_0 the peak power of the incident pulse, and N_τ is known as the soliton number.

In the case of a weak nonlinearity, $N_\tau \approx 0$ and eqn. (2.37) reduces to

$$i\frac{\partial u_\tau}{\partial \zeta_\tau} = \frac{\mathrm{sgn}(\beta_2)}{2}\frac{\partial^2 u_\tau}{\partial \tau^2}, \tag{2.38}$$

which can be solved analytically using Fourier transform methods. The solutions allow us to see the effect of dispersion on pulse shape. For an input Gaussian pulse of the form,

$$u_\tau(0,\tau) = \exp\left[-\tau^2(1 + iC)/2\right], \tag{2.39}$$

the parameter C is the chirp parameter and is used to describe the temporal phase distribution of the input field. With a pulse of this form, the solution of eqn. (2.38) is:

$$u_\tau(\zeta_\tau,\tau) = \left[\frac{1}{1 - \mathrm{sgn}(\beta_2)\zeta_\tau(1 + iC)}\right]^{1/2}\exp\left\{-\frac{(1 + iC)\tau}{2\left[1 - \mathrm{sgn}(\beta_2)\zeta_\tau(1 + iC)\right]}\right\}. \tag{2.40}$$

The input pulse and the solutions at $\zeta_\tau = 1$ for several conditions are plotted in fig. (2.1). For the case C = 0, the pulse broadens equally for either type of dispersion, anomalous ($\beta_2 < 0$) or normal ($\beta_2 > 0$). For the case C = 1 and anomalous dispersion, the pulse is compressed at $\zeta_\tau = 1$, while for normal dispersion the pulse broadens more than in the unchirped case. This effect is seen clearly in fig. (2.2) which shows the evolution of the pulse full width at half maximum (FWHM) as a function of ζ_τ for the

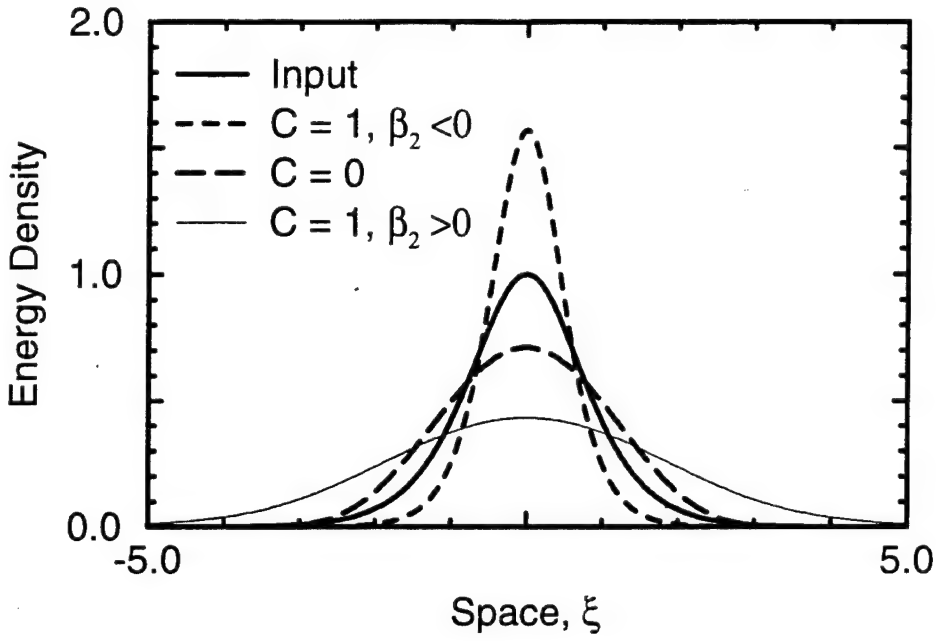

Figure (2.1) In the linear regime the interaction of dispersion and initial temporal phase modulation or chirp affect the pulse shape. The shape of an initially Gaussian pulse with and without chirp after propagating one dispersion length shows that the pulse can be compressed or broadened depending on whether or not the medium is anomalously dispersive ($\beta_2 < 0$) or normally dispersive ($\beta_2 > 0$) respectively.

chirped and unchirped cases. In general, when $C\beta_2 > 0$ the pulse broadens monotonically while for $C\beta_2 < 0$ the pulse is initially compressed before broadening monotonically.

For very high peak powers or long pulses, $N_\tau >> 1$ and the dispersion term in eqn. (2.37) can be neglected,

$$i\frac{\partial u_\tau}{\partial \zeta_\tau} = - \text{sgn}(n_2)\, N_\tau^2\, |u_\tau|^2 u_\tau. \qquad (2.41)$$

This allows study of the affect of the nonlinearity on the optical field as it propagates. Eqn. (2.41) is readily solved to give

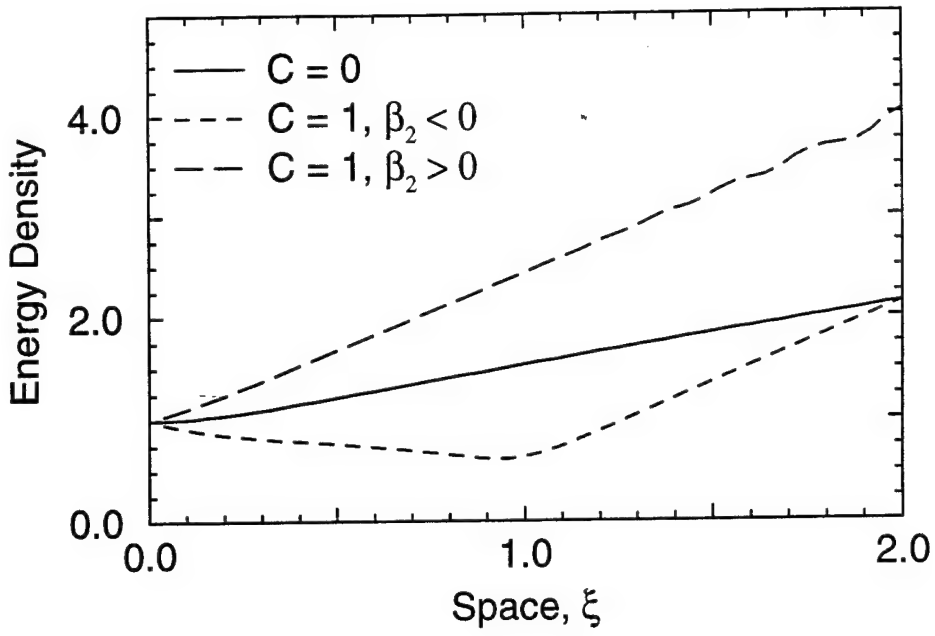

Figure (2.2) The effect of the interaction of dispersion and chirp in a linear medium on the pulse FWHM as a function of propagation distance is plotted. In the anomalous dispersion regime ($\beta_2 < 0$) the pulse is initially compressed while in the normal dispersion regime ($\beta_2 > 0$) the pulse is broadened faster than in the unchirped case.

$$u_\tau(\zeta_\tau,\tau) = u_\tau(0,\tau)\exp\left[\, i\,\mathrm{sgn}(n_2)N_\tau^2\,|\,u_\tau(0,\tau)\,|^2\,\zeta_\tau\right] \qquad (2.42a)$$

$$= u_\tau(0,\tau)\exp(i\phi_{NL})\,. \qquad (2.42b)$$

From this equation we can see that the effect of the nonlinearity on the pulse is to give it a time-dependent phase. Thus the nonlinearity chirps the pulse, in a process known as self-phase modulation (SPM). In the frequency domain, the effect of SPM is to broaden the spectrum of the field, while in the time domain the pulse shape remains unchanged.

Having just seen how dispersion can broaden or compress a chirped pulse it is now time to look at the effect of dispersion on a nonlinearly

chirped pulse. For an initially unchirped Gaussian, the nonlinear phase shift due to SPM is given by,

$$\phi_{NL} = \mathrm{sgn}(n_2) N_\tau^2 \exp(-\tau^2) \zeta_\tau \tag{2.43a}$$

$$\approx \mathrm{sgn}(n_2)\, N_\tau^2\, (1 - \tau^2) \zeta_\tau\,. \tag{2.43b}$$

Thus, SPM induces a chirp approximately given by $C_{SPM} \approx \mathrm{sgn}(n_2)\, N_\tau^2 \zeta_\tau$. From the discussion following eqn. (2.40) we know that this can lead to pulse compression provided $C_{SPM}\beta_2 < 0$ (or broadening for $C_{SPM}\beta_2 > 0$). Thus for an anomalously dispersive medium, a self-focusing nonlinearity will induce a chirp on an input pulse such that it will interact with the dispersion to compress the pulse. The same holds true in a normally dispersive medium for a self-defocusing nonlinearity. The question is, under which conditions will this SPM-induced chirp be strong enough to compete with the tendency of the initially unchirped pulse to dispersively broaden?

This question is answered by returning to eqn. (2.37). Analytic solutions to this equation, known as bright solitons, can be determined via the inverse scattering method.[5] The fundamental bright soliton occurs for $N_\tau = 1$ and represents the perfect balance between the nonlinear SPM and dispersive broadening. The solution,

$$u_\tau(\zeta_\tau, \tau) = \mathrm{sech}(\tau) \exp(i\zeta_\tau/2)\,, \tag{2.44}$$

maintains its shape on propagation and even through collisions with other pulses. Higher-order solitons have more complicated expressions

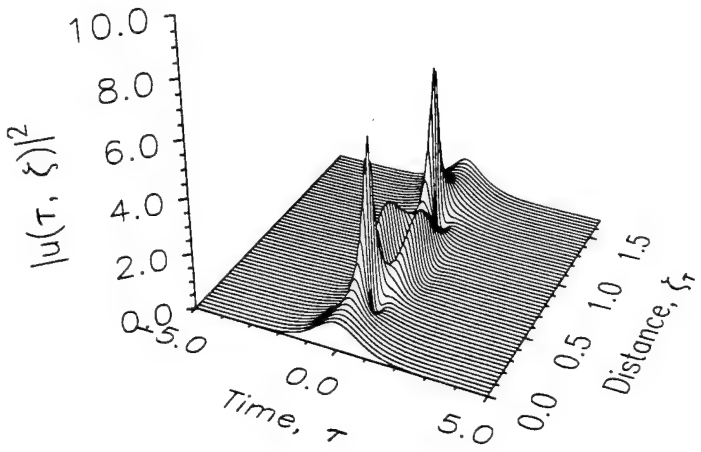

N_τ= 3 Soliton

Figure (2.3) The evolution of a third order (N_τ = 3) bright temporal soliton is illustrated. The input sech(τ) pulse compresses, splits , compresses and recovers its original shape at $\zeta_\tau = \pi/2$.

and behaviors. The behavior shown in fig. (2.3) for an N_τ = 3 or third-order soliton is typical. Numerical simulations have shown the input sech(τ) field is compressed initially reaching its smallest width at $\zeta_\tau \approx 0.5/N_\tau + 1.73/N_\tau^2$ with a compression factor given by $F_c \approx 4.1N_\tau$. The compression is followed by a splitting, then another compression, then at $\zeta_\tau = \pi/2$ the soliton regains its original shape and the process repeats itself.

An interesting issue to consider is the influence of the nonlinearity and dispersion on the pulse shape when $C_{spm}\beta_2 > 0$, i.e. when they are both acting to broaden the pulse. This situation arises in a self-defocusing medium in the anomalous dispersion regime and in a self-focusing medium in the normal dispersion regime. When the two effects are acting in concert we expect the dispersive pulse broadening to be

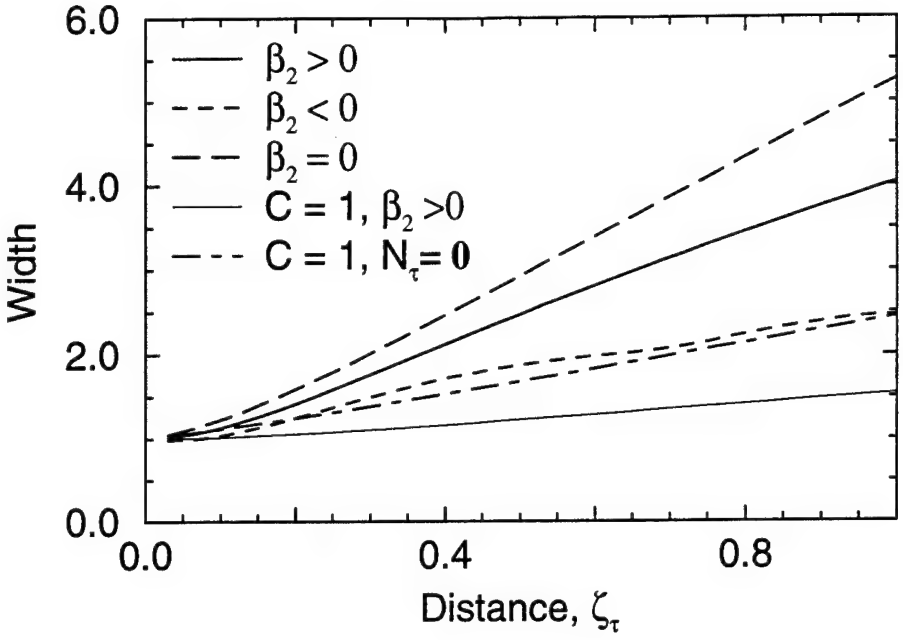

Figure (2.4) The width of a pulse propagating in a self-focusing (N = 3), normally dispersive ($\beta_2 > 0$) medium increases faster than in the linear case. Frequency chirp can either increase or decrease the rate of pulse broadening.

enhanced. As shown in fig. (2.4), where we plot pulse width as a function of propagation distance for these two cases, we see that in fact the nonlinearity does lead to an enhanced pulse broadening. Whether or not the pulse broadens as fast as an initially chirped pulse in a linear medium depends on the strength of the chirp and the strength of the nonlinearity. In any case the linearly chirped input pulse broadens faster initially while the nonlinearly broadening pulse requires more distance to reach the same pulse width since its chirp accumulates as it propagates. More interesting perhaps is the case in which the input pulse is chirped so as to initially linearly compress the pulse. What we find is that because the linear compression increases the peak intensity, the nonlinear phase

accumulation at the pulse peak also increases thereby enhancing the broadening of the pulse after the compression.

2.2.2 Spatial Solitons

A simpler way to reduce the dimensionality of the NSE of eqn. (2.32) is to make the cw approximation. This is done simply by assuming that dispersive effects occur on a much longer distance scale than diffractive effects and is true for weakly dispersive media or long pulses such that d << 1 in eqn. (2.32). In this situation the third term on the right hand side (RHS) of eqn. (2.32) can be neglected, resulting in an equation describing cw self-focusing in bulk media,

$$i\frac{\partial u}{\partial \zeta} = -\frac{1}{2}\left(\frac{\partial^2}{\partial \xi^2} + \frac{\partial^2}{\partial \eta^2}\right)u - \mathrm{sgn}(n_2)\, N^2\, |u|^2 u. \qquad (2.45)$$

There are two situations in which the dimensionality of this equation can be further reduced.

Recall that eqn. (2.32) was derived by assuming a cylindrical symmetry in the transverse coordinate normalizations. If instead we allow the spatial profile of the field to have nonuniform dimensions such that $\sigma_x \neq \sigma_y$ then normalizing the transverse coordinates as $\xi = x/\sigma_x$ and $\eta = y/\sigma_y$ results in the modified two-dimensional NSE,

$$i\frac{\partial u}{\partial \zeta} = -\frac{1}{2}\left(\frac{\partial^2}{\partial \xi^2} + d_y\frac{\partial^2}{\partial \eta^2}\right)u - \mathrm{sgn}(n_2)\, N^2\, |u|^2 u, \qquad (2.46)$$

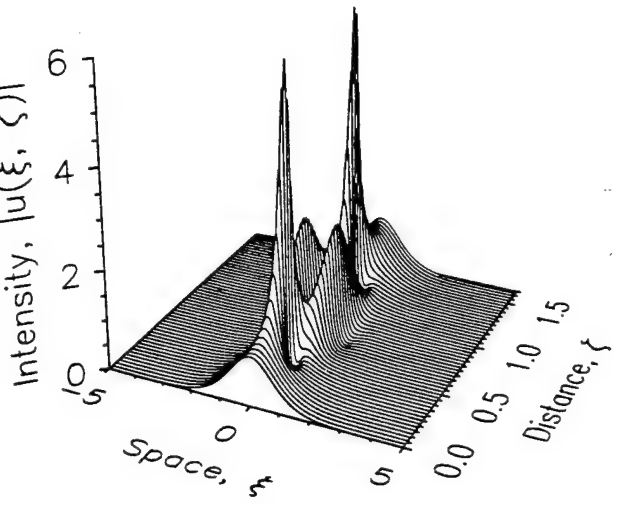

N = 3 Soliton

Figure (2.5) The evolution of a third order (N = 3) bright spatial soliton is illustrated. This is identical to the behavior shown in fig. (2.3) except that it describes spatial rather than temporal field behavior.

where $d_y = \sigma_x^2/\sigma_y^2$. In the case of a highly elliptical beam such that $\sigma_x << \sigma_y$ we know intuitively that diffraction will be much weaker in the y plane than in the x plane. The d_y parameter verifies our intuition since in that case $d_y << 1$ and eqn. (2.46) can be rewritten, after neglecting the second term, as

$$i\frac{\partial u}{\partial \zeta} = -\frac{1}{2}\frac{\partial^2 u}{\partial \xi^2} - \mathrm{sgn}(n_2)\, N^2\, |u|^2 u, \qquad (2.47)$$

the spatial one-dimensional NSE. This equation is isomorphic to equation eqn. (2.37), the temporal one-dimensional NSE, for $\beta_2 < 0$ and so supports bright solitons for $n_2 > 0$.

There are two important distinctions between eqn. (2.47) and eqn. (2.37). First is that eqn. (2.47) describes the spatial evolution of the field

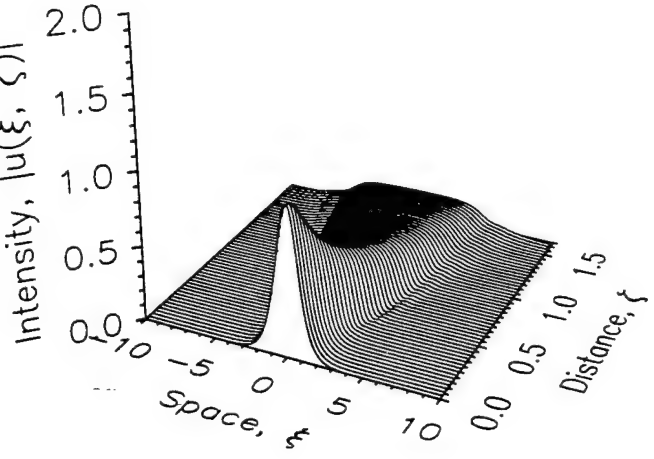

N = 3 Defocusing

Figure (2.6) The evolution of a cw beam in a N = 3 defocusing medium. The field broadens faster than it would in a linear medium under the influence of diffraction alone.

and so the solitons it supports are spatial solitons. Second, given the absence of anomalous diffraction, there are only two regimes to consider: self-focusing and self-defocusing. In the former, bright spatial solitons exist. The behavior of an N = 3 bright spatial soliton is shown in fig. (2.5). Note that the graph is identical to that of fig. (2.3) with the exception of the labels on the horizontal axes. Indeed, spatial solitons behave identically as temporal solitons. Spatial solitons such that N > 1 narrow to a minimum spatial FWHM at $\zeta \approx 0.5/N + 1.73/N^2$ with a compression factor given by $F_c \approx 4.1N$. The narrowing is followed by a splitting then an eventual recovery of the input field shape at $\zeta = \pi/2$.

In the self-defocusing regime, fig. (2.6) shows the behavior typically described by eqn. (2.47). The beam broadens monotonically and faster than it would under the influence of diffraction alone. A lens will produce the

spatial phase curvature analogous to the frequency chirp described earlier with similar effects. In a self-defocusing medium, the effect of focusing the beam with a lens is to initially override the impact of the nonlinearity. The final result, however, is a broader beam in the far field because the initial focusing by the lens increases the nonlinear phase accumulated by the field which enhances the broadening. Conversely, a defocusing lens, because it will reduce the accumulated nonlinear phase, will narrow the far field of a beam propagating through a self-defocusing medium.

The other condition whereby the dimensionality of eqn. (2.45) can be reduced is that of a beam in a planar waveguide. As in the case of an optical fiber, the index step used to create the waveguide is usually more than an order of magnitude greater than any change in the refractive index due to nonlinear effects. Thus we can neglect the nonlinearity when describing the spatial characteristics of the field in the direction perpendicular to the plane of the waveguide. This manifests itself by starting at eqn. (2.32) and assuming a solution of the form,

$$\tilde{E}(\mathbf{r},\omega) = g(y)\tilde{a}(x,z,\omega)\exp(-i\beta_0 z)\,, \tag{2.48}$$

then separating variables to arrive at the pair of equations for the field in the waveguide:

$$\frac{\partial^2 g}{\partial y^2} + (\varepsilon(\omega)k_0^2 - \bar{\beta}^2)\, g = 0\,, \tag{2.49a}$$

$$\frac{\partial^2 \tilde{a}}{\partial x^2} + 2i\beta_0\frac{\partial \tilde{a}}{\partial z} + (\tilde{\beta}^2 - \beta_0^2)\,\tilde{a} = 0\,. \tag{2.49b}$$

Here eqn. (2.49a) is an eigenvalue equation for the propagation constant $\tilde{\beta}$ of the planar waveguide mode g and it can be solved using the usual techniques. In a procedure exactly analogous to the one used to derive the temporal NSE, a perturbative approach is used to arrive at,

$$i\frac{\partial a}{\partial z} = -\frac{1}{2\beta_0}\frac{\partial^2 a}{\partial x^2} + \frac{\beta_2}{2}\frac{\partial^2 a}{\partial T^2} - \gamma|a|^2 a. \tag{2.50}$$

If the propagation distance is now normalized with respect to the diffraction length such that $\zeta = z/(2\pi\sigma^2/\lambda)$, this equation becomes the two-dimensional spatiotemporal NSE,

$$i\frac{\partial u}{\partial \zeta} = -\frac{1}{2}\frac{\partial^2}{\partial \xi^2}u + \frac{d}{2}\frac{\partial^2}{\partial \tau^2}u - \mathrm{sgn}(n_2)\,N^2\,|u|^2 u, \tag{2.51}$$

where d is defined as in eqn. (2.31) with β_2 containing via β the nonlinear perturbation to the propagation constant of the waveguide mode and $N = (2\pi\sigma/\lambda)^2 n_0 |n_2| I_0$ also as in eqn. (2.32). This equation describes the behavior of pulses in a planar waveguide. As in the derivation of eqn. (2.47) in the long-pulse limit or cw approximation $d<<1$. Thus, in this limit the dispersion term can be neglected, resulting in the one-dimensional spatial NSE, eqn. (2.47).

2.3 Spatiotemporal Coupling

The two-dimensional spatiotemporal NSE, eqn. (2.51) enables the investigation of nonlinear spatiotemporal coupling with minimum complexity. The first evidence of spatiotemporal coupling can be obtained

from analyzing the equation itself. In the low-power limit, $N \approx 0$ and eqn. (2.51) reduces to,

$$i\frac{\partial u}{\partial \zeta} = -\frac{1}{2}\frac{\partial^2}{\partial \xi^2}u + \frac{d}{2}\frac{\partial^2}{\partial \tau^2}u\,, \tag{2.52}$$

which can be solved by separation of variables. This techniques necessarily requires that the time-domain and space-domain behaviors evolve independent of one another. When nonlinear effects become significant enough that eqn. (2.51) must be employed, separation of variables can no longer be used to find the solution. Thus, we must conclude that the two behaviors no longer evolve independent of one another, i.e. the space and time behaviors are coupled to one another by the nonlinearity.

Although analytical solutions of eqn. (2.51) exist[11] their stability and applicability to physical problems is limited. We obtain further evidence of spatiotemporal coupling by solving eqn. (2.51) numerically. The details of such work will consume the bulk of this thesis, presently however one example will suffice. In figs. (2.3) and (2.6) we plotted the temporal and spatial evolution of an N = 3 pulse in a self-defocusing, normally dispersive medium in the absence of spatiotemporal coupling. Note that the compression of the pulse reaches a maximum at $\zeta_\tau \approx 0.2$ while at $\zeta = \hat{0}.2$ the beam in fig. (2.6) has merely broadened 18%. Now in fig. (2.7) we plot the spatial and temporal evolution of the same optical field but with spatiotemporal coupling included in the model. In a two-dimensional simulation it is not possible to plot the entire field as in figs. (2.3) and (2.6), instead we look at a slice through the center of the field. Fig. (2.7a) shows the evolution of $|u(0,\tau,\zeta)|^2$, a slice in time through the spatial center of

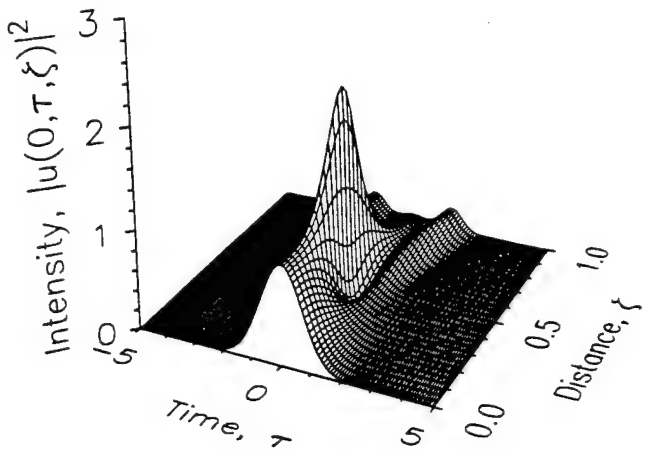

(a)Temporal Profile

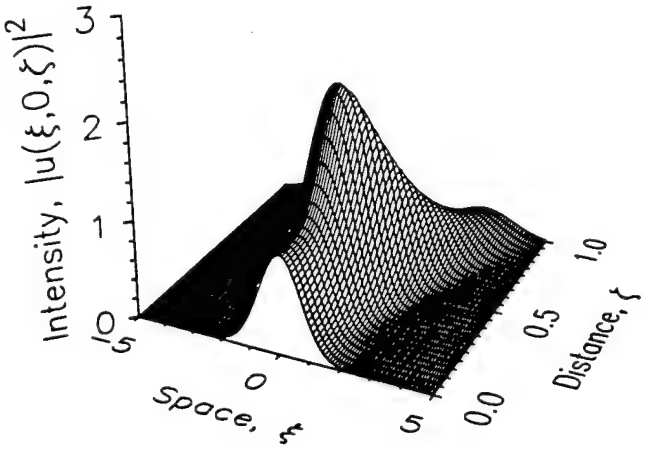

(b)Spatial Profile

Figure (2.7) The effects of spatiotemporal coupling on the beam and pulse shapes as a two-dimensional field propagates in a self-defocusing (N = 3) normally dispersive medium. In (a) the behavior of the field at $\xi = 0$ when compared to fig. (2.3) shows a reduced pulse compression. But in (b) the field at $\tau = 0$ shows a localized beam narrowing which is the opposite of the behavior shown in fig. (2.6).

the two-dimensional field. Note that while the compression still occurs at $\zeta = 0.2$ (When d = 1 the dispersion length and the diffraction length are equal hence $\zeta_\tau = \zeta$) it is reduced from that obtained for the one-dimensional simulation. An even more dramatic change in behavior is observed for the field behavior at the pulse center, $|u(\xi,0,\zeta)|^2$ shown in fig. (2.7b). Here the monotonic broadening is gone, replaced by an initial compression then an enhanced broadening. Thus figs. (2.7) show that a moderate (N = 3) nonlinearity can provide enough spatiotemporal coupling to significantly alter the field behavior in both space and time.

2.4 Numerical Model

While in recent years some significant progress has been made analytically describing the behavior of the field governed by the NSE, the most fruitful avenue of research has been numerical simulations.[7,12-16] There are generally two ways to approach the problem of multidimensional wave propagation simulation: finite difference methods and pseudospectral methods. We use the latter with a technique known as the split-step Fourier method. The basic idea stems from recognizing that the NSE can be written in terms of operators,

$$i\frac{\partial u}{\partial \zeta} = -\frac{1}{2}\left(\hat{D} + \hat{N}\right) u \tag{2.53}$$

where,

$$\hat{D} = \frac{\partial^2}{\partial \xi^2} + \frac{\partial^2}{\partial \eta^2} - d\frac{\partial^2}{\partial \tau^2}, \tag{2.54a}$$

$$\hat{N} = 2N^2 |u|^2. \tag{2.54b}$$

The $\hat{D}$ operator contains the effects of dispersion and diffraction, while the nonlinear operator $\hat{N}$ contains the effect of the nonlinearity. The solution to eqn. (2.53) correct to third-order in the step size h is

$$u(\zeta+h,\xi,\eta,\tau) \equiv \exp\left(\frac{h}{4}\hat{D}\right)\exp\left[\frac{1}{2}\int_{\zeta}^{\zeta+h}\hat{N}\,d\zeta'\right]\exp\left(\frac{h}{4}\hat{D}\right)u(\zeta,\xi,\eta,\tau). \quad (2.55)$$

This describes the propagation of the wave for one half-step under the influence of diffraction and dispersion only, followed by a propagation for a full step under just the influence of the nonlinearity and finally another diffractive-dispersive half-step. The middle step is computed by an approximation to the integral using the trapezoidal rule and an iterative procedure to determine the field at $\zeta + h$. In practice the exponential of the differentials is computed by performing a multi-dimensional fast Fourier transform (FFT) of the field so that the differentiations become multiplications:

$$F\left\{\exp\left[i\frac{h}{4}\left(\frac{\partial^2}{\partial\xi^2}+\frac{\partial^2}{\partial\eta^2}-d\frac{\partial^2}{\partial\tau^2}\right)\right]\right\} = \exp\left[i\frac{h}{4}\left(-k_\xi^2-k_\eta^2+k_\tau^2\right)\right]. \quad (2.56)$$

This makes the evaluation of $\exp(i\,h\,\hat{D})/4)$ much easier in the Fourier domain. Once the multiplication is performed the FFT is reversed so the nonlinear effects may be introduced via a simple multiplication by a field-dependent phase. Finally the first process is repeated for the second dispersive-diffractive half-step. The process extends readily to any number of dimensions by reducing (or increasing) the dimensionality of the FFT employed in the dispersive-diffractive half-step.

For three-dimensional simulations, memory usage and computation time need to be considered. To ensure acceptable frequency resolution over the entire propagation distance, we attempt to ensure that the grid on which the data is stored is a minimum of five times as large as the pulse width. With a wave modeled to a resolution of $\tau_p/20$ (or $\sigma_\xi/20$) this means a grid with a minimum of 100 points in each dimension. Consequently, for accurate three-dimensional modeling a 128x128x128 grid is employed. Storing $2x10^6$ complex data points requires approximately 16 MB (or 32 MB if double precision is used) and processing a data set that large is extremely computationally intensive. As a result, the bulk of the results presented here are for simulations of the field described by the two-dimensional spatiotemporal NSE, eqn. (2.51). These simulations are performed using a 256x256 point grid with step sizes ranging from 0.01 to 0.0001 diffraction lengths depending on the size of the nonlinearity being modeled. In general, the step size is chosen such that $hN^2 | u_{max} |^2 < 0.01$ over the course of the simulation.

2.5 References

1. G. A. Askar'yan, "Effects of the gradient of a strong electromagnetic beam on electrons and atoms," Sov. Phys. JETP **15**, 1088 (1962)

2. R. Y. Chiao, E. Garmire, C. H. Townes, "Self-trapping of optical beams," Phys. Rev. Lett. **13**, 479 (1964)

3. P. L. Kelly, "Self-focusing of optical beams," Phys. Rev. Lett. **15**, 1005 (1965)

4. J. H. Marburger, "Self-focusing as a pulse sharpening mechanism," IEEE J. Quant. Electron. **QE-3**, 415 (1967)

5. V. E. Zakharov, A. B. Shabat, "Exact theory of two-dimensional self-focusing and one-dimensional self-modulation of waves in nonlinear media," Sov. Phys. JETP **34**, 62 (1972)

6. A. Hasegawa, F. Tappert, "Transmission of stationary nonlinear optical pulses in dispersive dielectric fibers. I Anomalous dispersion," Appl. Phys. Lett. **23**, 142 (1973)

7. G. P. Agrawal, *Nonlinear Fiber Optics*, (Academic Press, Boston, 1989)

8. R. W. Boyd, *Nonlinear Optics*, (Academic Press, San Diego, 1992)

9. G. I. Stegeman, "Nonlinear Guided Wave Optics," in *Contemporary Nonlinear Optics*, G. P. Agrawal and R. W. Boyd, eds., (Academic Press, San Diego, 1992)

10. H. Kogelnik, "Theory of Optical Waveguides," in *Guided-Wave Optoelectronics*, T. Tamir, ed., (Springer-Verlag, Berlin Heidelberg, 1988 and 1990)

11. L. Gagnon, "Exact solutions for optical wave propagation effects including transverse effects," J. Opt. Soc. Am. B **7**, 1098 (1990)

12. M. D. Feit, J. A. Fleck, Jr., "Beam nonparaxiality, filament formation, and beam breakup in the self-focusing of optical beams," J. Opt. Soc. Am. B **5**, 633 (1988)

13. G. R. Hadley, "Multistep method for wide-angle beam propagation," Opt. Lett. **17**, 1743 (1992)

14. R. W. Ziolkowski, J. B. Judkins, "Full-wave vector Maxwell equation modeling of the self-focusing of ultrashort optical pulses in a nonlinear Kerr medium exhibiting finite response time," J. Opt. Soc. Am. B **10**, 186 (1993)

15. H. E. Hernandez-Figueroa, "Nonlinear nonparaxial beam-propagation method," Electron. Lett. **30**, 352 (1994)

16. S. Chi, Q Guo, "Vector theory of self-focusing of an optical beam in Kerr media," Opt. Lett. **20**, 1598 (1995)

Chapter 3

Pulse Propagation in Dispersive Nonlinear Media

3.1 Background

It has been well established for many years that, to lowest order, pulse propagation in nonlinear dispersive media is described accurately by the nonlinear Schrödinger equation (NSE).[1] As we discussed in chapter 1, the NSE has helped provide an understanding of a wide variety of effects such as beam steering,[2,3] soliton formation and propagation,[4,5] self-focusing[6-16] and pulse compression.[1,9,17-19] Pulse compression has been a subject of intense interest for many years due to its wide ranging applications in areas such as optical communications and ultrafast phenomena.[1,19] Attempts to fully understand self-focusing began more than 25 years ago and have evolved from analytic approximations for cw beams[6-8] to the moving focus model for the self-focusing of long (>1 ns) or non-dispersive pulses.[9,10] However, it is only recently that the full three-dimensional NSE has been employed for the investigation of self-focusing of ultrashort pulses in normally-dispersive media.[11-15] Moreover because the nonlinearity makes the NSE inseparable, it is only in its multidimensional form that the coupling between the spatial and temporal behaviors can be investigated. The impact of the nonlinearity on both the spatial and the temporal behavior can be investigated with the two-dimensional NSE, eqn. (2.50),

$$i\frac{\partial u}{\partial \zeta} = -\frac{1}{2}\frac{\partial^2}{\partial \xi^2}u + \frac{d}{2}\frac{\partial^2}{\partial \tau^2}u - \mathrm{sgn}(n_2)\,N^2\,|u|^2 u. \qquad (3.1)$$

This equation governs pulse propagation in planar waveguides and in bulk media for highly elliptical beams. For many years, optical pulse propagation in fibers has been an area of intense investigation.[1] Apart from the obvious communication applications, optical fibers are important because they provide a simplified environment in which to study nonlinear effects. Planar waveguides are similar to fibers in that there is still good field confinement. But since the confinement is only one-dimensional, it is possible to study the influence of diffractive effects on the field dynamics in the presence of the Kerr nonlinearity responsible for self-focusing or defocusing. This interplay is particularly interesting when the field is in the form of an ultrashort pulse, in which case not only do the dispersive and diffractive effects occur simultaneously but also the spatial behavior is coupled via the nonlinearity to the temporal behavior. This chapter is devoted to studying the effects of such a spatiotemporal coupling in planar optical waveguides modeled as a dispersive nonlinear medium.

Self-focusing and self-defocusing are well-known nonlinear phenomena[4,7-10,12-16] leading to contraction or expansion of an optical beam as it propagates in a Kerr medium whose refractive index increases or decreases linearly with optical intensity. The interaction of dispersion and self-focusing has been studied extensively. In the first part of this chapter we show how self-focusing and pulse compression are related via spatiotemporal coupling. However, self-defocusing has attracted relatively little attention since it leads to a uniform broadening of the optical beam.

It was pointed out recently that a beam propagating in a self-defocusing medium may actually narrow if it is launched together with an intense pump beam.[20-22] The physical mechanism behind such an induced focusing is spatial cross-phase modulation, a nonlinear phenomena in which an intense pump beam changes the phase front of the signal beam locally in such a way that it leads to beam narrowing in a self-defocusing medium. In the second part of this chapter we show that with a single, pulsed, optical beam the beam-broadening due to self-defocusing can be either enhanced or suppressed through temporal self-phase modulation depending on the nature of group-velocity dispersion inside the nonlinear medium. The physical mechanism in this case is the spatiotemporal coupling occurring when dispersion and diffraction act together on a pulsed optical beam.

3.2 Self-Focusing Nonlinearity

For a narrow beam of ultrashort pulses, dispersion and diffraction have roughly equal influence on the behavior of the optical field and thus $d \approx 1$ in eqn. (3.1). We can then make neither the plane wave nor the cw approximations (discussed in chapter 2) and so must use the two-dimensional NSE [eqn. (3.1)] to describe the field evolution. The question then arises: how does the presence of the added dimension affect the outcome of the simulation, i.e. how does spatiotemporal coupling manifest itself in this situation? One might guess that, since anomalous dispersion and diffraction both lead to field compression in the presence of the self-focusing nonlinearity, when both effects are included the degree of compression would increase. In fact it does, and for nonlinearities such

that $N > \sqrt{2}$, self-focusing eventually leads to wave collapse and a breakdown[23] of our model [in reality the wave collapse is averted by higher-order nonlinearities,[24] higher-order dispersion,[25] non-paraxiality[26,27] and self-steepening[1] terms neglected in eqn. (3.1)]. The dynamics of the catastrophic wave collapse have been investigated by several authors[23-27] and provided many useful insights into a variety of experimentally observed phenomena. The focus of those early investigations was on arriving at an understanding of the damaging effects of the wave collapse rather than spatiotemporal coupling, hence we will not revisit many of these results here.

Spatiotemporal coupling was evident in the results of the wave collapse investigations because it was found that the addition of a third dimension to the simulations resulted in a more rapid collapse, hence the interaction of the dispersion and the nonlinear index provided an additional mechanism for concentrating the field energy. To show how spatiotemporal coupling can be used to advantage we apply a quadratic spatial phase modulation (a thin lens) to the Gaussian input field,

$$u(\xi,\tau,0) = \exp\left[-\frac{(\xi^2 + \tau^2)}{2}\right] \exp[i\,\phi(\xi,\tau)]. \qquad (3.2)$$

by choosing $\phi(\xi,\tau) = -\xi^2/2f$ where f is the focal length of the lens the field passes through prior to entering the nonlinear medium. In fig. (3.1), we plot the spatially-averaged pulse width (FWHM) and the time-averaged beam width (FWHM) as a function of propagation distance for a range of focal lengths f with N = 3 and d = -1. As seen there, a focusing modulation ($f > 0$) can hasten the collapse while a defocusing modulation can either

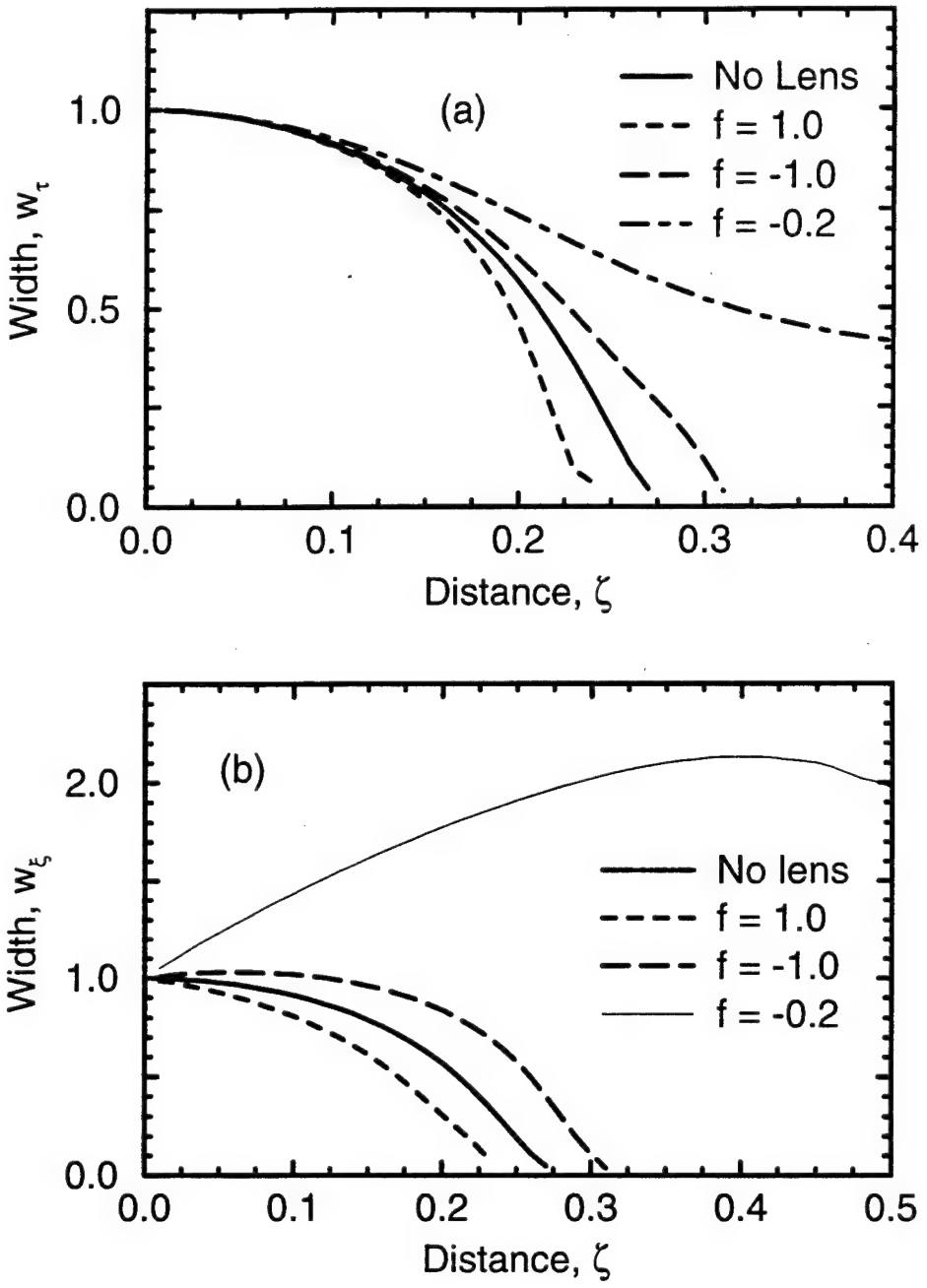

Figure (3.1) To show the influence of spatial phase modulation on the wave collapse occurring for N = 3 and d = -1, the integrated pulse and beam widths as a function of propagation distance are plotted. In (a) the pulse compression can be increased or decreased depending on the type of lens employed and in (b) the beam width behaves in a corresponding fashion.

delay or eliminate it entirely depending on the modulation amplitude and the length of the nonlinear medium, with larger amplitudes (smaller values of f) being required to overcome larger nonlinearities. The noteworthy point here is that the time-domain behavior is altered with a spatial manipulation. The mechanism at work is fairly simple. The spatial phase modulation for $f < 0$ merely spreads energy out (or helps concentrate it for $f > 0$) from the center of the field thereby reducing (or enhancing) the nonlinearity-induced phase curvature of the field which is the cause of the collapse. This result is analogous to that of ref. 23 in which the self-focusing of chirped pulses in the anomalous dispersion regime was numerically and analytically investigated. There, the authors found that the wave collapse could be either hastened or postponed, depending on the type of temporal phase modulation.

In the normal-dispersion regime and negligible diffraction (plane-wave approximation), the interaction of the dispersion and the nonlinearity leads to a monotonic pulse spreading as seen in fig. (3.2a). As we discussed briefly in the previous chapter, however, the inclusion of the diffractive term when $d \approx 1$ can lead to a modest degree of localized pulse compression. We see this in fig. (3.3a) where we plot the pulse width $w_{\tau 0}$ (FWHM) at the beam center $\xi = 0$, normalized to its input value, as a function of propagation distance for a range of dispersion strengths. This effect can be understood by recalling that higher-order ($N > 1$) spatial solitons [see fig. (3.2b)] undergo periodic beam narrowing (and a corresponding increase in intensity) and that the distance to the first minimum decreases as N increases. In the non-dispersive case ($d = 0$), an input pulse with $N > 1$ can be viewed as a continuous series of spatial solitons ranging from zeroth-order at the wings of the pulse to order N at

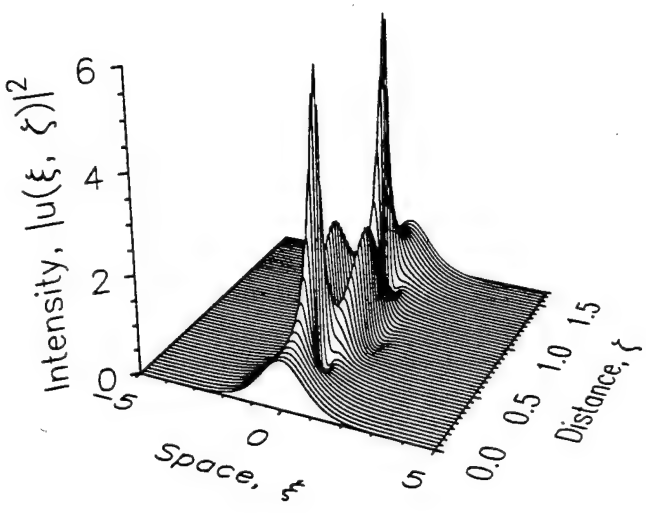

(a) N = 3 Soliton

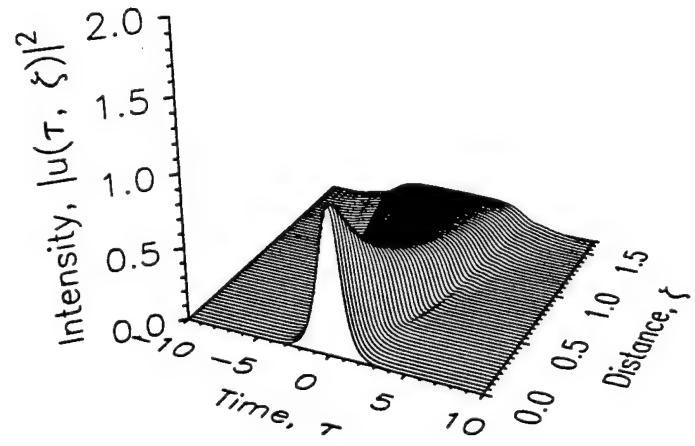

(b) N = 3 Broadening

Figure (3.2) The results of one-dimensional simulations showing the two types of behaviors described by the NSE for a self-focusing nonlinearity. For an input Gaussian field with N = 3 we have (a) the evolution through compression, splitting and recovery of a bright spatial soliton and (b) the monotonic broadening of a pulse in the normal dispersion regime.

its center. Since the center has the highest order, it will spatially narrow at a shorter distance than the wings. As a result, the pulse appears compressed because the center has become more intense while the wings have remained virtually unchanged. As we saw in the previous chapter, when normal dispersion interacts with a self-focusing nonlinearity ($n_2 > 0$), the effect is to spread power from the peak of the pulse to the wings. For weak dispersion ($d \approx 0.1$) this effect is minimal compared to the spatial soliton effects; thus the compression is strongest. As the strength of the dispersion is increased, the effect becomes more important, until at $d = 1$, a large nonlinearity ($N = 5$) is required to achieve even a minimal (3%) reduction in pulse width [fig. (3.3b)] at the beam center.

When we view the entire beam by integrating over ξ before measuring the pulse width we find that if $d > 0$ the average pulse width increases and if $d < 0$ the pulse is compressed provided $|N^2/d| > 1$. This is precisely the result obtained in the previous chapter for the one-dimensional case described by the one-dimensional temporal NSE,

$$i\frac{\partial u_\tau}{\partial \zeta_\tau} = \frac{\mathrm{sgn}(\beta_2)}{2}\frac{\partial^2 u_\tau}{\partial \tau^2} - \mathrm{sgn}(n_2)\, N_\tau^2\, |u_\tau|^2 u_\tau. \qquad (3.3)$$

However, spatio-temporal coupling still plays a role in the field behavior. The spatial self-focusing dominates the field behavior initially, creating the large peak intensity and localized pulse compression of fig. (3.3a). The large peak intensity creates a large nonlinearity-induced phase curvature which fuels the pulse broadening. Consequently, the more dominant the initial self-focusing, the broader the pulse will be at large ζ. To understand the influence of spatio-temporal coupling, we should plot the pulse width

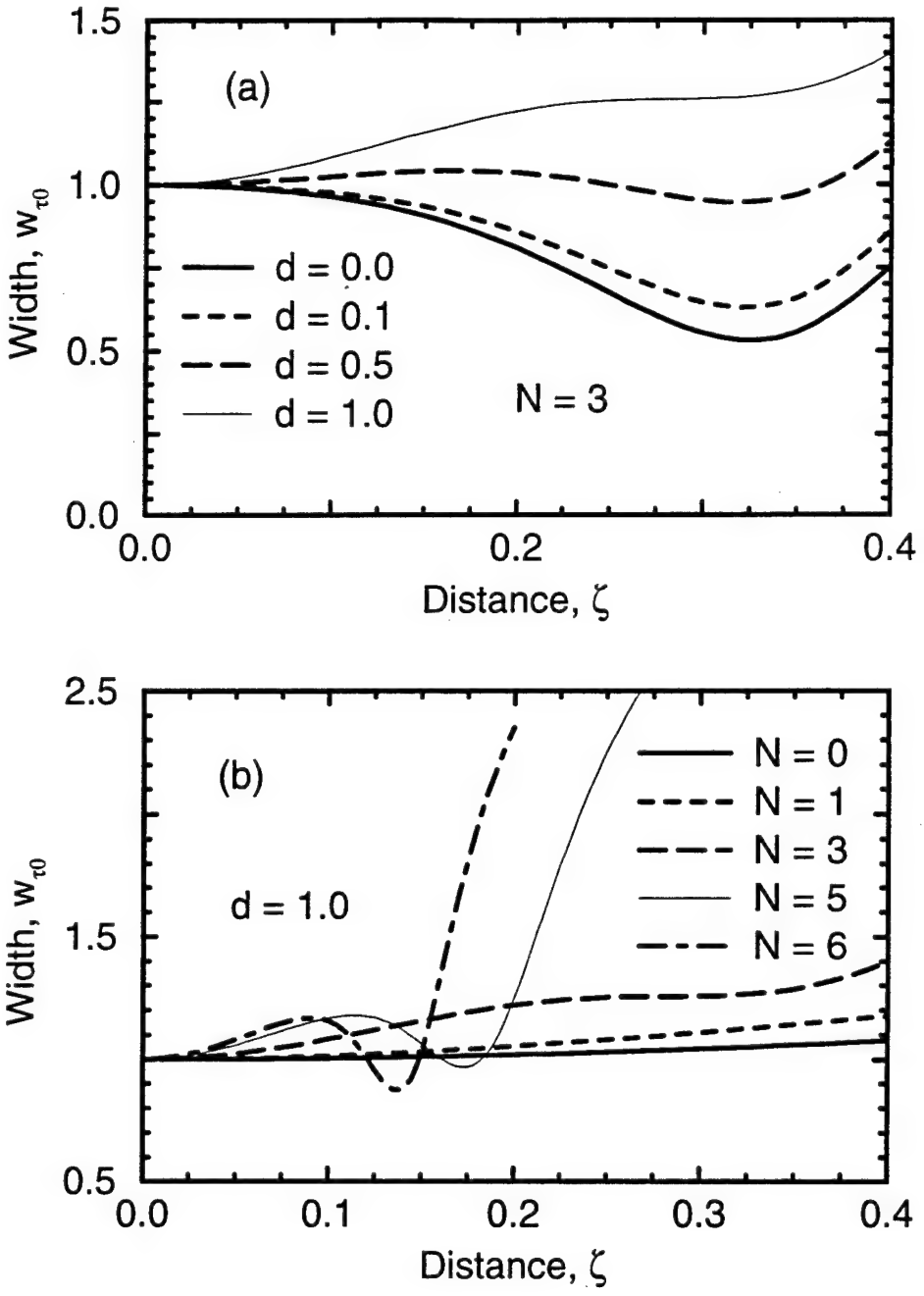

Figure (3.3) The amount of localized pulse compression in the normal dispersion regime depends on both the amount of dispersion and strength of the nonlinearity. The normalized pulse width at $\xi = 0$ is plotted showing that (a) the amount of localized compression decreases as the strength of the dispersion is increased, and (b) for d = 1, a strong nonlinearity (N = 5) is required to compress the pulse below its input width.

as a function of dispersion length for a constant value of N^2/d. Thus in fig. (3.4a), where we plot the spatially averaged pulse width, w_τ, as a function of $\zeta' = \zeta d$ for two dispersion strengths (d = 0.1, 1) and $|N^2/d| = 16$, we see that the pulse is broader at $\zeta' = 0.4$ for the d = 1 case because the spatial self-focusing is initially ten times stronger than in the d = 0.1 case. Similarly, a strong initial dispersion which reduces the peak field strength quickly will in turn reduce the strength of the spatial self-focusing. Referring to fig. (3.4b) where we plot the temporally-averaged beam width, w_ξ, normalized to its input value for N = 3 and a range of dispersion strengths we see that as the strength of the dispersion is increased, the overall beam narrowing influence of the self-focusing medium is first reduced before increasing again. The reason for this is that the strength of the nonlinear pulse broadening depends on N^2/d while the distance over which its effects become important is proportional to d, consequently the beam-broadening influence of the dispersion reaches a minimum at approximately d = 0.5.

We can further exploit the spatio-temporal coupling with spatial phase modulation and either enhance or suppress the pulse compression. As seen in fig. (3.5a), where we plot $w_{\tau 0}$ as a function of ζ, the degree of localized pulse compression for a given nonlinearity can be either increased or decreased depending on the type of lens used to modulate the beam. A focusing lens aids the field compressive action of the self-focusing nonlinearity and hence the localized pulse compression is increased. A diverging lens has the opposite effect. Note that with the f = 1 focusing lens the N = 3 field can be compressed more than the N = 4 field that has passed through an f = -1 lens, thus the degree of maximum local compression is not determined only by the nonlinearity. Hence, with the

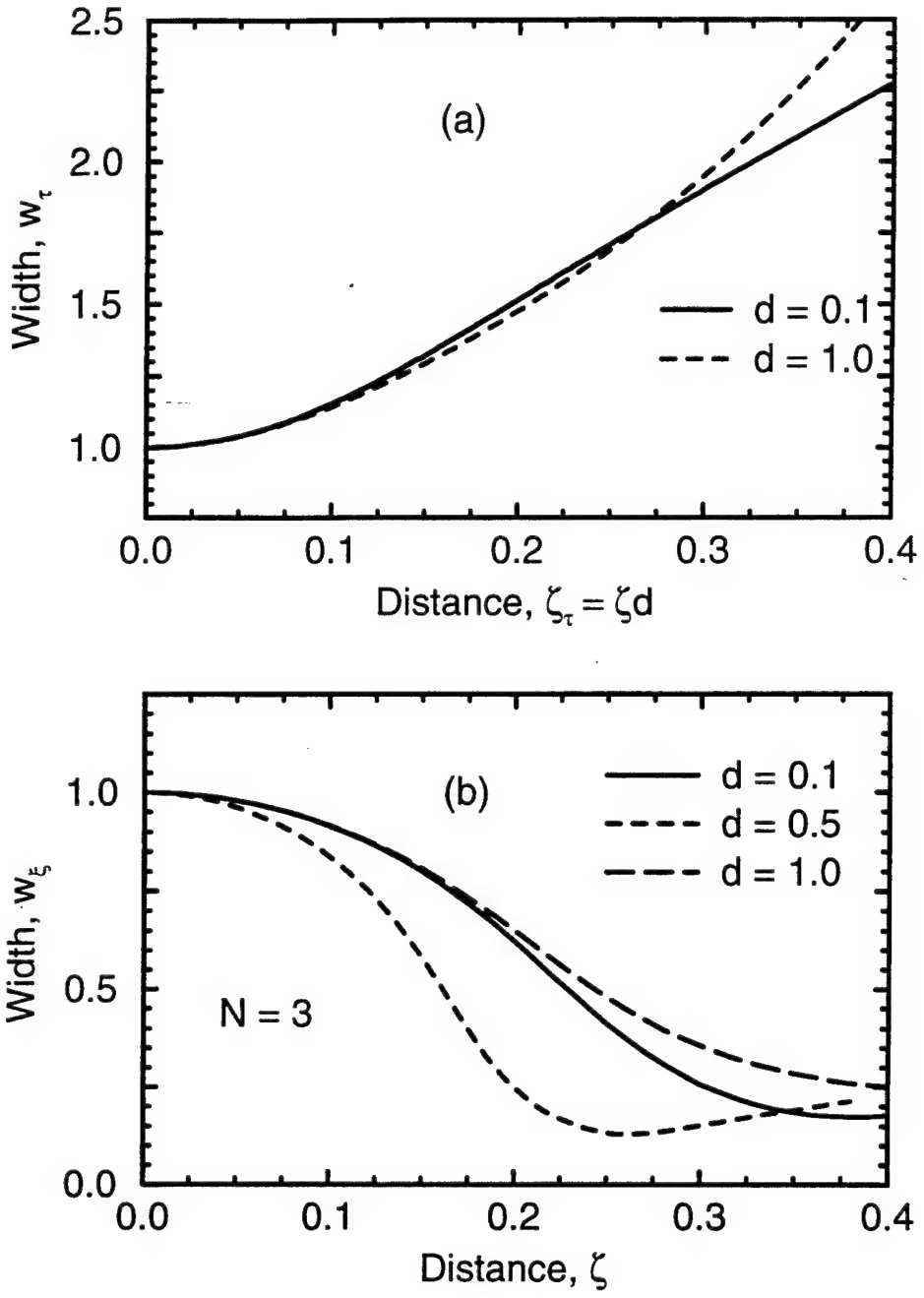

Figure (3.4) The interplay of spatial-self-focusing and dispersive pulse broadening is shown. In (a) for $|N^2/d| = 16$ the integrated pulse width as a function of *dispersion* length the stronger self-focusing (for d = 1) eventually creates a broader pulse. In (b) for N = 3 increasing the strength of the dispersion first enhances (d = 0.5) the self-focusing and then saturates it so that for d = 1 the self-focusing is actually weaker.

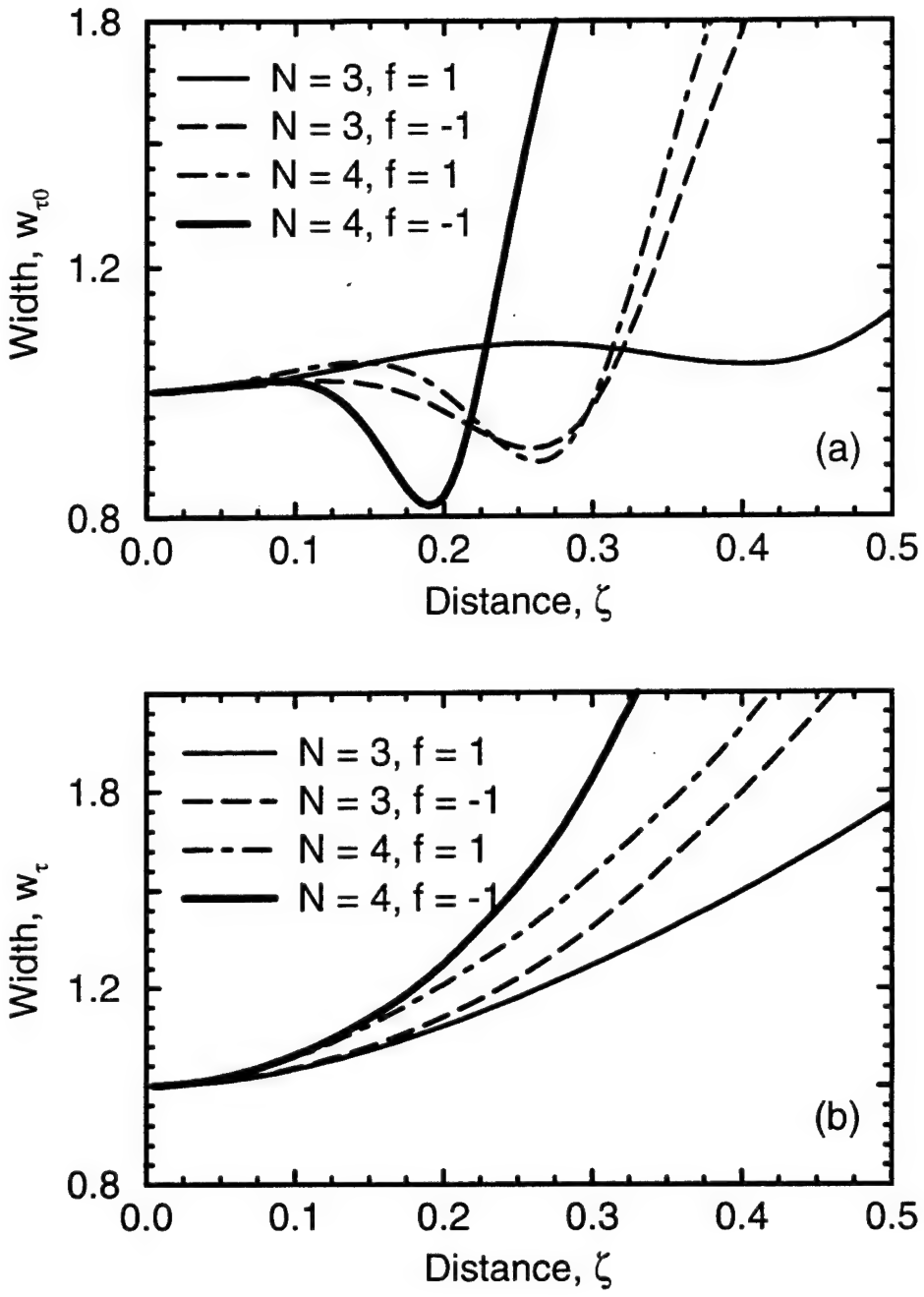

Figure (3.5) The influence of spatial phase modulation on the temporal behavior is shown for d = 0.5 and two different nonlinearities. In (a) the plot of the pulse width at $\xi = 0$ shows that depending on the lens, the localized compression can be either enhanced or compressed with spatial phase modulation, while in (b) the localized compression is seen to enhance the integrated-pulse broadening.

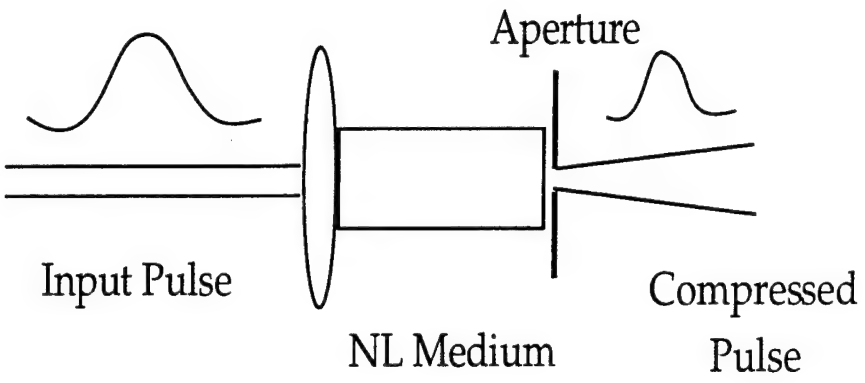

Figure (3.6) A simple filtering scheme for pulse compression. The pulses pass through a lens and enter a nonlinear medium. The action of the nonlinear medium compresses the pulse but only at the beam center. The slit selects the center of the beam and thus the transmitted pulse is compressed.

spatial phase modulation, localized pulse compression can occur over a wide range of nonlinearities where it would not occur at all in its absence. However, even with a large modulation amplitude and a weak positive dispersion (d = 0.1), there is still no spatially averaged pulse compression. In fig. (3.5b), we see that the effect of the modulation on the spatially-integrated pulse width, w_τ, is as expected from the discussion in the preceding paragraph. Whatever enhances (reduces) $w_{\tau 0}$ for small ζ will reduce (enhance) w_τ at large ζ.

From a practical standpoint, it would be useful to be able to capitalize on this localized pulse compression. The most obvious way is the simple filtering scheme illustrated in fig. (3.6). Placing a spatial

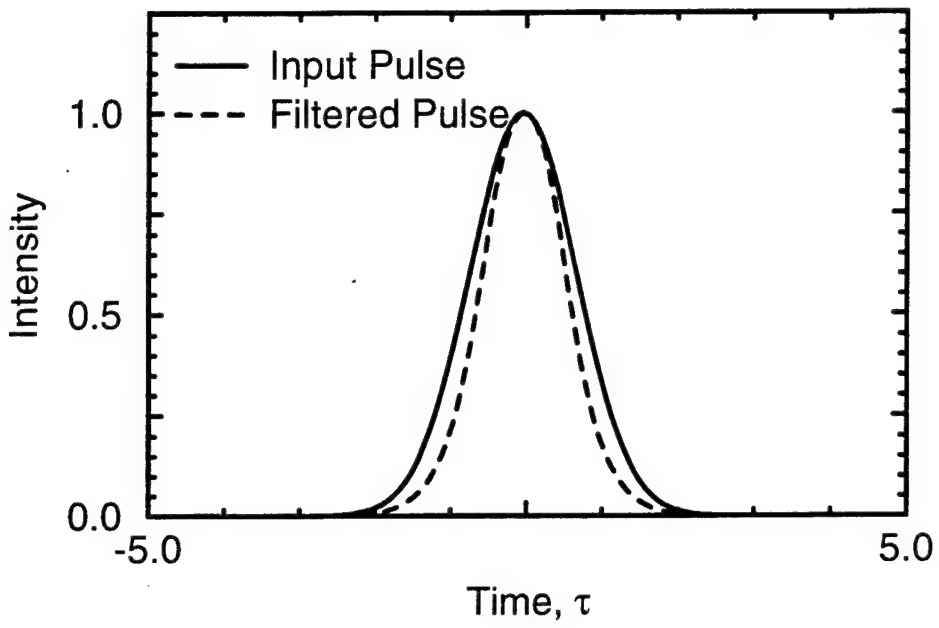

Figure (3.7) The shape in time of a pulse transmitted by the filtering arrangement of fig. (3.6) compared to the input pulse shape. The parameters are N=3, ζ = 0.33, d = 0.1 and chosen to correspond to the point of maximum pulse compression observed in fig. (3.3a). The pulse width is reduced to 78% of its initial value.

aperture or slit at the distance of minimum local pulse width could effectively compress the pulse by selecting that portion of the field that is temporally narrow. The results of such a filter are illustrated in fig. (3.7) where we plot the pulse transmitted by a slit placed at ζ = 0.33 (the point of minimum $w_{\tau 0}$) for the case of an input Gaussian beam with dispersion parameter d = 0.1 and N = 3 at input. When compared to the spatially-integrated input field (dashed line) we see that there is indeed significant pulse compression. We illustrate the drawbacks of such a compression scheme by plotting the instantaneous phase of the field after it has propagated to ζ = 0.33 in fig. (3.8). There are two important points to note about fig. (3.8). First, the spatial curvature of the phase is quite large and

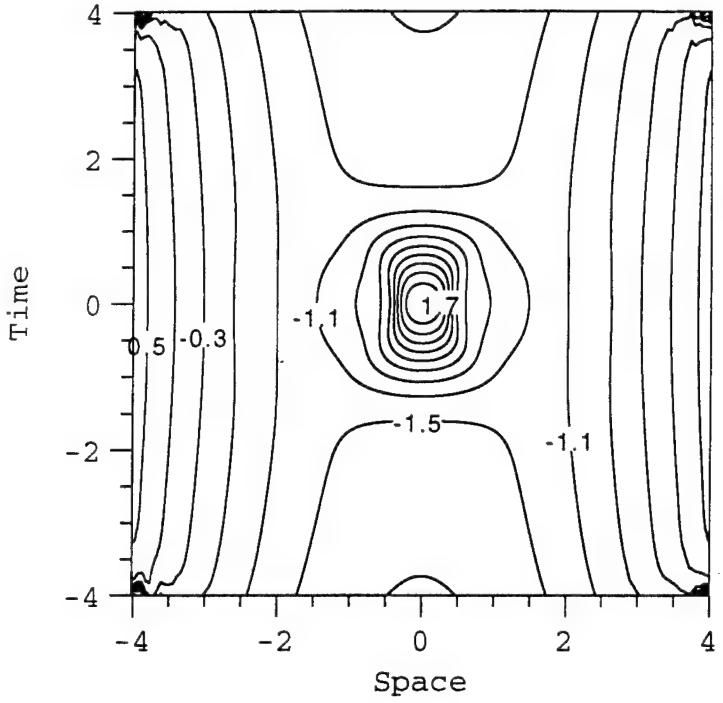

Figure (3.8) The instantaneous phase of the field arriving at the slit in figs. (3.6-7). The contours are equally spaced between -2π and 2π. Note the steep spatial and temporal phase curvatures of that portion of the field that is incident on the slit.

indicates that the pulse once through the slit will spatially diverge quite rapidly. Moreover, the spatial curvature of the phase depends on τ as well, thus time-dependent collection optics would be required to re-collimate the beam. This also brings up the second point: the temporal phase curvature of the center of field in fig. (3.8) is also quite large and hence, as we saw in chapter 2, transmission through a normally dispersive medium (such as the type of which many lenses are made) will result in rapid temporal broadening. Nonetheless, it is conceivable that with anomalously dispersive lenses following the slit the arrangement illustrated in fig. (3.6) could be used to compress pulses into a somewhat collimated beam. We will see in the next chapter that there is a simpler arrangement for compressing pulses using a nonlinear medium and a slit.

However, in both cases it is important to note that the compression occurs in spite of the dispersion rather than as a direct result of it as in the anomalous dispersion case.

3.3 Self-Defocusing Nonlinearity

A self-defocusing nonlinear medium is one in which the index of refraction of the material decreases as the intensity of the optical field increases. In the self-defocusing case with the plane-wave approximation, the roles of the two dispersion regimes are reversed. The nonlinearity now works with anomalous dispersion and the pulse broadens exactly as it does in the normal-dispersion regime of a self-focusing medium [fig. (3.2a)]. Conversely, the normal-dispersion regime with a defocusing nonlinearity supports temporal solitons [fig. (3.2b)]. The picture becomes more interesting when we include diffraction. In the anomalous dispersion case, diffraction and dispersion work together to broaden the field in both dimensions. As illustrated in fig. (3.9a), for small ζ the pulse at the beam center broadens more quickly than in the one-dimensional (plane wave) case. But, as we see in fig. (3.9b) since this reduces the strength of the nonlinearity, the effect for large ζ is a more slowly broadening spatially-averaged pulse. Spatial phase modulation in this case can slow the rate of pulse broadening by broadening the beam spatially (a perhaps undesirable result) effectively reducing the peak power and thus the nonlinearity induced temporal phase curvature which is what broadens the pulse.

In the absence of diffraction, the effect of normal dispersion interacting with the defocusing nonlinearity is to compress the pulse

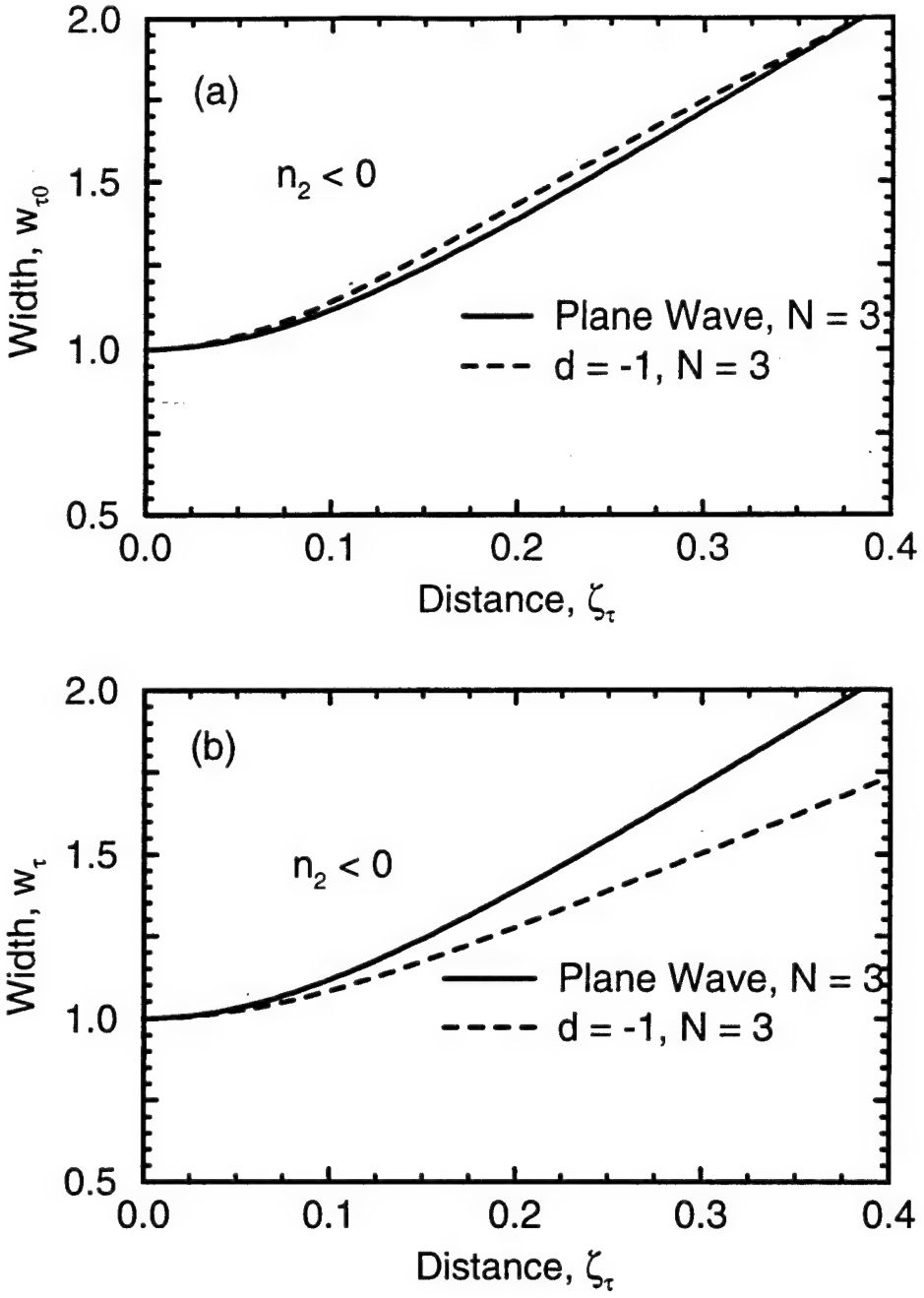

Figure (3.9) In the anomalous dispersion regime with a self-defocusing nonlinearity the pulse and beam broaden monotonically. In (a) including diffraction in the model is seen to initially slightly increase the pulse width at the beam center, while in (b) the effect of diffraction on the spatially integrated pulse width is the opposite: the rate of broadening is decreased.

[fig. (3.2b)], the compression factor getting larger as the nonlinearity is increased. Similarly, cw simulations show that the effect of diffraction interacting with the nonlinearity is to increase the rate of beam broadening. It is therefore not surprising that when the diffractive effects of a waveguide are included with a defocusing nonlinearity, the result is a more moderate pulse compression (rather than a wave collapse) as seen in fig. (3.10a). The reason for this is that although the dispersion and the nonlinearity are acting to bring energy in from the temporal wings of the field, the diffraction is using the nonlinearity to move energy out to the spatial wings thereby reducing the peak field strength and thus the pulse compression. The self-defocusing-induced beam spreading can be counteracted by imposing a focusing spatial phase curvature on the input field which the diffraction must overcome before it can reduce the peak power. Thus, because of the spatio-temporal coupling we are again able to enhance (or reduce) the pulse compression with spatial phase modulation. As seen in fig. (3.10b), with a very tight focus such as f = 0.5 we can achieve even greater pulse compression than that obtained without diffraction. Alternatively, we may eliminate the pulse compression with a very strong diverging lens.

Another interesting aspect of the spatio-temporal coupling occurring in planar waveguides is the counterintuitive result that as the strength of the defocusing nonlinearity is increased, the spatial width of the field at the peak of the pulse can be reduced (the beam can be focused) as evidenced by the data in figs. (3.11). In fig. (3.11a) we plot the beam width (FWHM) at the pulse peak $w_{\xi 0}$ normalized to its input value as a function of the propagation distance for d = 2 and a range of beam intensities. We see that except for the N = 2 case, there is a secondary

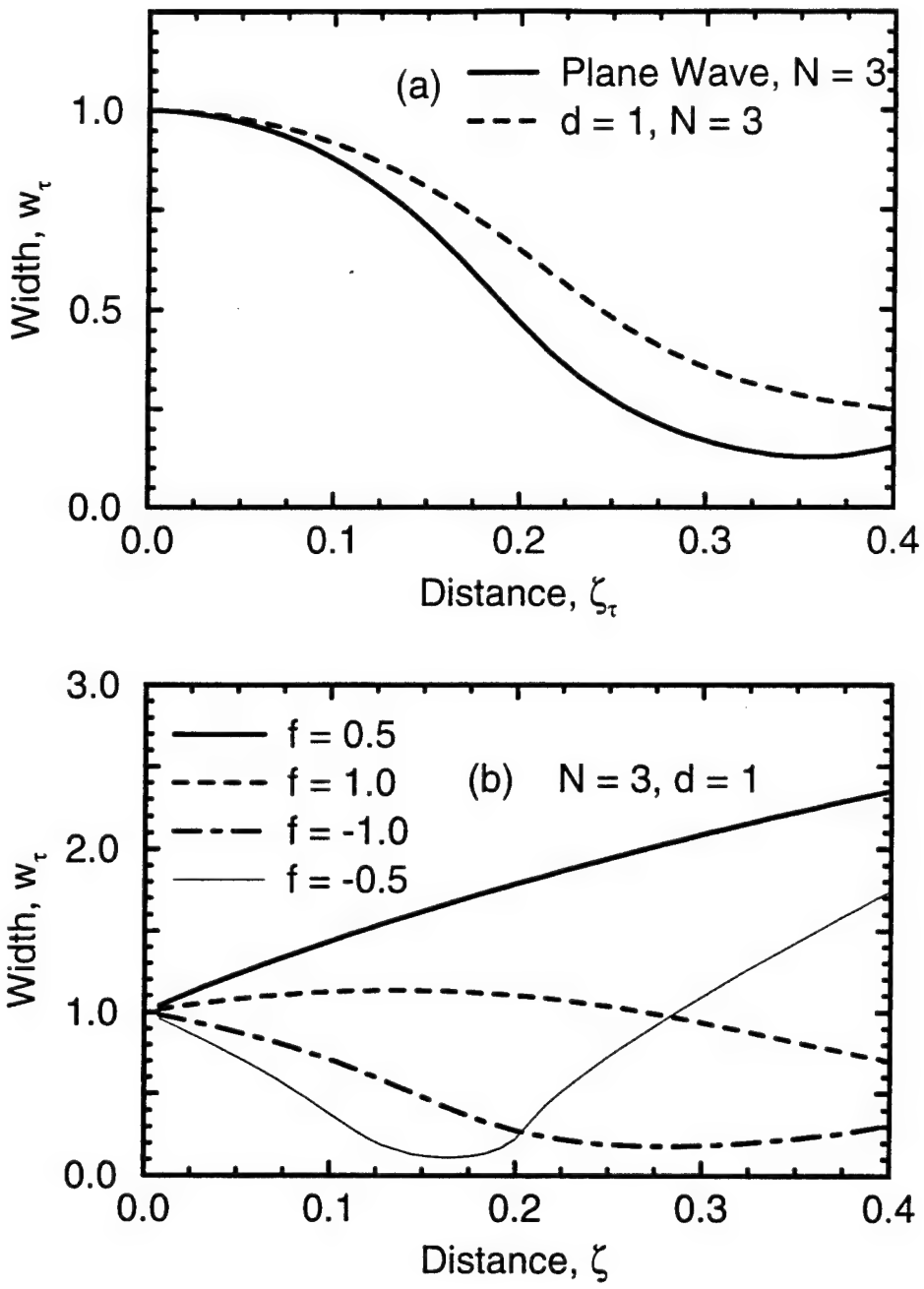

Figure (3.10) In the normal dispersion regime with a self-defocusing nonlinearity the pulse compresses while the beam broadens. In (a) the effect of including diffractive effects on the spatially-integrated pulse is to reduce the broadening, while in (b) spatial phase modulation is employed to enhance the pulse-broadening.

minimum in $w_{\xi 0}$ which gets deeper as the strength of the nonlinearity is increased. Were we to plot the analogous parameter for the temporal FWHM at the beam center, we would find that the (spatial) secondary minima occur at approximately the same position as the point of maximum temporal compression. Of course for d = 2 and N = 2 there is no temporal compression because the distance over which the temporal compression would occur in the absence of spatial effects is larger than the distance necessary for the nonlinearity-induced spatial phase curvature to become significant, as a result, there is no secondary minimum in ξ_0 either. However, since the distance to the point of maximum pulse compression is proportional to $1/N^2$ as the nonlinearity is increased the temporal compression soon dominates the spatial defocusing and the localized minima occur.

The dependence of the spatial width on the pulse compression takes an interesting turn when we consider the effect of increasing dispersion as in fig. (3.11b). Here, we again plot the beam width at the pulse peak $w_{\xi 0}$ as a function of propagation distance, but for a constant nonlinearity (N = 4) and dispersion parameters ranging from 0 to 10. We again see the secondary minima associated with the point of maximum pulse compression. Since the distance to the point of maximum temporal compression is roughly proportional to d, and this is also the distance over which self-defocusing must act to spread the field, one might expect the minimum $w_{\xi 0}$ to decrease as the strength of the dispersion increases. But, since the maximum pulse compression increases as N^2/d, the temporal compression weakens as the strength of the dispersion is increased. Therefore, as we see in fig. (3.11b), the minimum $w_{\xi 0}$ actually occurs at about d = 5 where the pulse is compressed quickly and strongly enough to

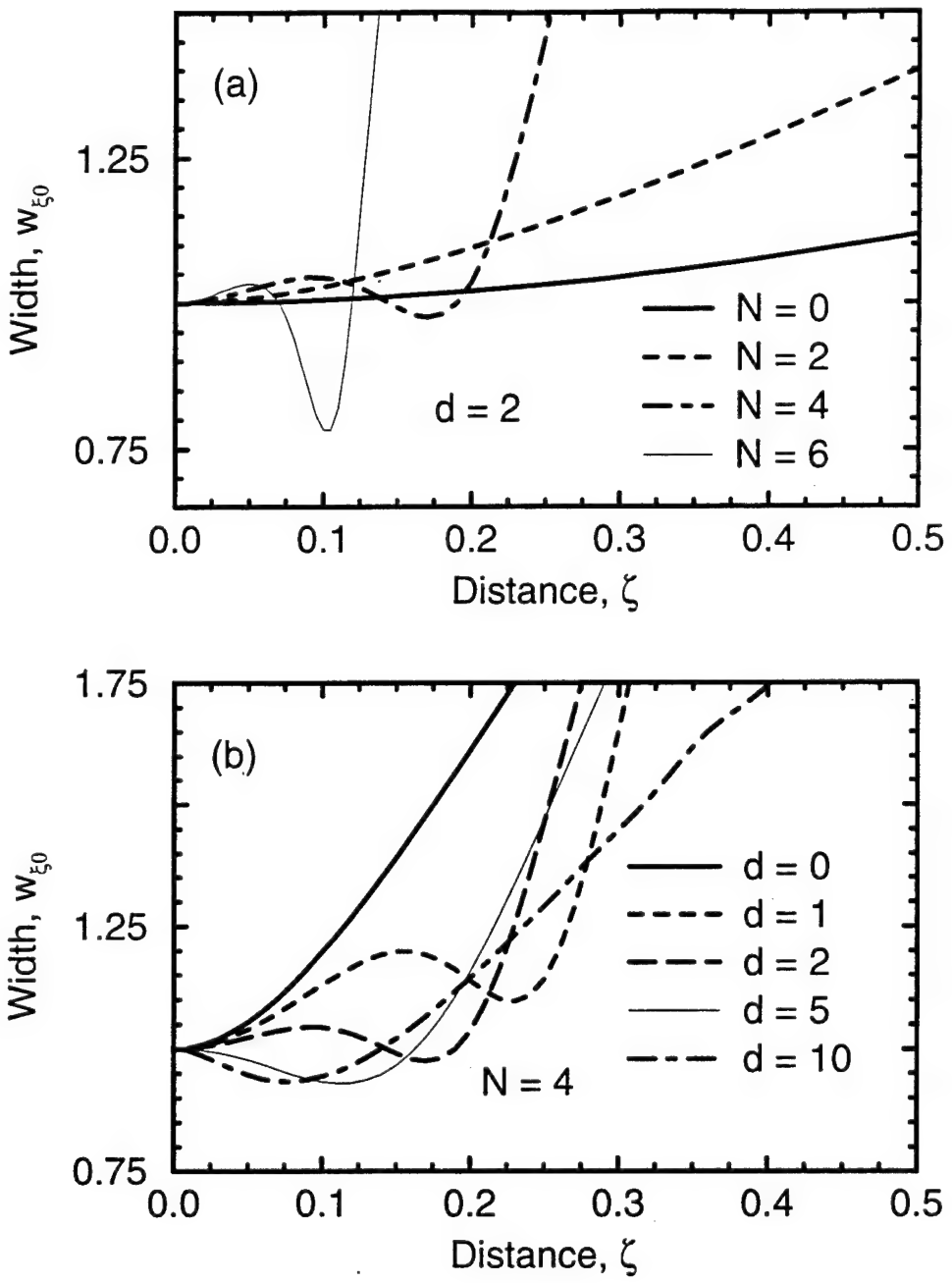

Figure (3.11) To show the impact of the N and d parameters, the width (FWHM) of the spatial intensity distribution through the center of the pulse (τ = 0) normalized to its input value is plotted as a function of propagation distance. In (a) the effect of increasing the strength of the nonlinearity is to increase the localized spatial narrowing, while in (b) the dispersion-induced enhancement of the localized narrowing saturates near d = 5.

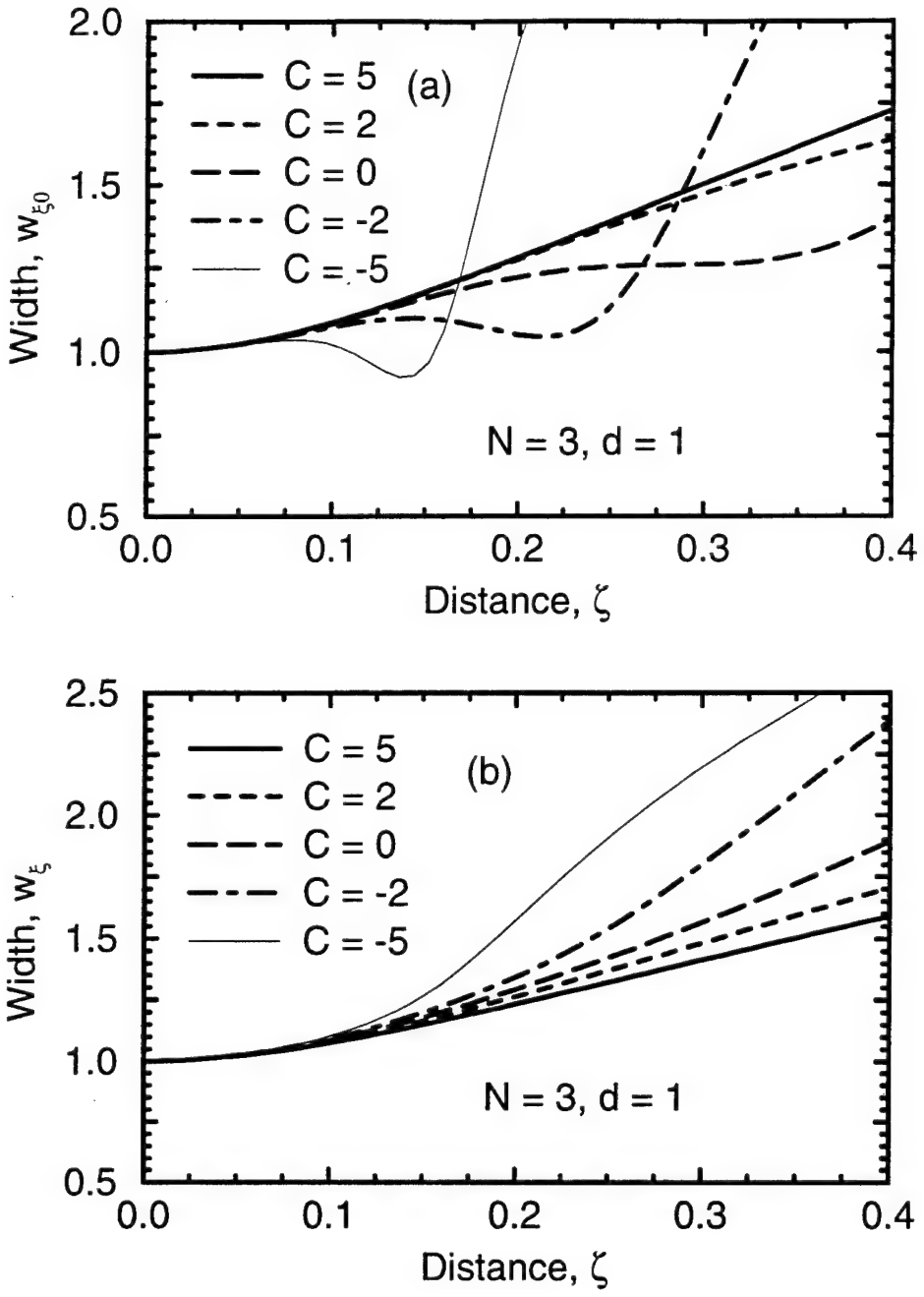

Figure (3.12) Temporal phase modulation can be used to control the beam width in a self-defocusing medium. In (a) an upchirp ($C > 0$) is seen to reduce the localized beam narrowing occurring at $\tau = 0$, while a downchirp ($C < 0$) is seen to enhance it. In (b) the effect of chirp on the time-integrated beam width is such that an upchirp leads to a slower beam broadening while a down chirp increases the beam width. In an anomalously dispersive medium the effects of the upchirp and downchirp would be reversed.

dominate the self-defocusing. This is also the dispersion for which the beam is broadest at large ζ.

By the same reasoning, a temporal phase modulation (frequency chirp) which will enhance (suppress) the pulse compression will also enhance (suppress) the localized beam narrowing at small ζ. This behavior is shown in fig. (3.12a) where we plot the normalized beam width at the pulse peak $w_{\xi 0}$ for N = 3 and a range of chirp parameters, C = -5 to 5. As before, when we observe the effect of modulation on the temporally-integrated beam width at large ζ we see that the effect of the spatio-temporal coupling on the field behavior is the opposite of that observed at the pulse peak for small ζ. In fig. (3.12b) we plot time-integrated beam width, w_ξ for the same parameters as in fig. (3.12a) and we see that at large ζ the effect of positive chirp is to reduce the influence of self-defocusing, while the effect of negative chirp is to enhance it. In neither case, however, does the modulation come close to compensating for the influence of the nonlinearity on the beam width.

3.4 Pulse Propagation in Bulk Media

Although the reduced dimensionality of eqn. (3.1) results in much less computationally intensive simulations, many practical applications require an understanding of pulse propagation in bulk media. In the absence of confining structures (waveguides or fibers) the equation which describes optical pulse propagation in nonlinear dispersive media is the three-dimensional NSE, eqn. (2.32),

$$i\frac{\partial u}{\partial \zeta} = -\frac{1}{2}\left(\frac{\partial^2}{\partial \xi^2} + \frac{\partial^2}{\partial \eta^2}\right)u + \frac{d}{2}\frac{\partial^2}{\partial \tau^2}u - \mathrm{sgn}(n_2)\, N^2\, |u|^2 u. \qquad (3.4)$$

In this form eqn. (3.4) implies a symmetry in the two transverse spatial coordinates, ξ and η, by normalizing them with respect to the assumed input beam width, σ. This symmetry may be broken with an input spatial dependence of the field that is non-symmetric in ξ and η [e.g. $u(\xi,\eta,\tau,0) = \exp(-\xi^2/2)\exp(-\eta^2/4)f(\tau)$]. However, our focus here is on extending the understanding gleaned from the earlier results of this chapter to the three dimensional case. Consequently, our discussion will concern the effects of the added dimension rather than the subtleties associated with elliptical beam propagation.[28]

We already have some information on two-dimensional spatial self-focusing and self-defocusing. The form of the NSE describing these two phenomena in the dispersionless limit is

$$i\frac{\partial u}{\partial \zeta} = -\frac{1}{2}\left(\frac{\partial^2}{\partial \xi^2} + \frac{\partial^2}{\partial \eta^2}\right)u - \mathrm{sgn}(n_2)\, N^2\, |u|^2 u. \qquad (3.5)$$

This equation is isomorphic to eqn. (3.1) for $d < 0$ (anomalous dispersion) thus our earlier two-dimensional results for the anomalous dispersion regime also describe spatial self-focusing and self-defocusing in bulk media. The self-focusing of beams in bulk media leads to wave collapse as does the propagation of pulses in the anomalous dispersion regime in self-focusing planar waveguides. In the self-defocusing case illustrated by fig. (3.9), we saw that the second dimension had the effect of enhancing the nonlinear broadening of the beam. The question we really seek to answer is: how does dispersion effect the propagation of pulses in nonlinear

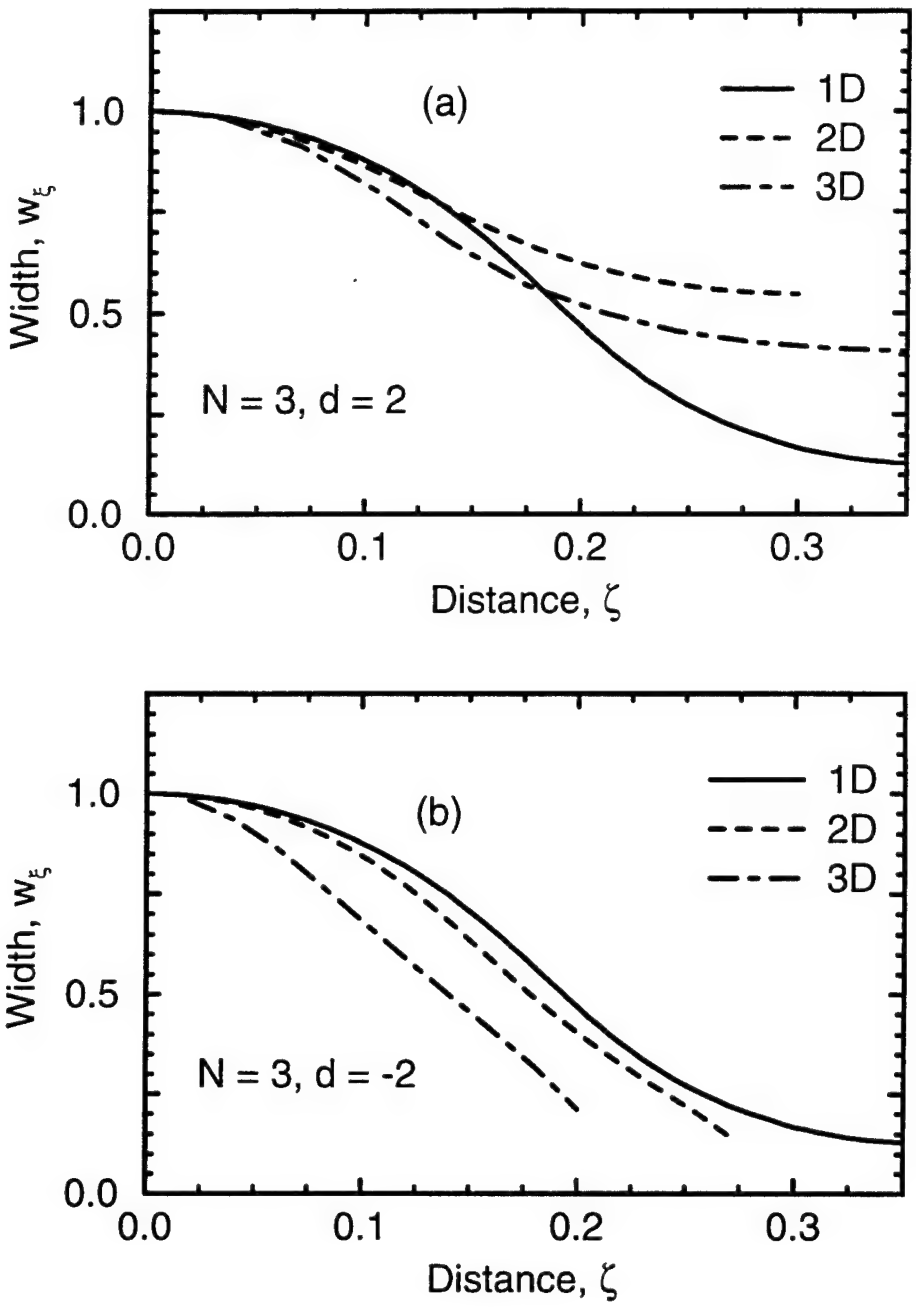

Figure (3.13) The results of propagation in bulk media are compared to those of lesser dimensionality for a self-focusing nonlinearity. In (a) the normal dispersion regime the second dimension is dispersion which spreads the field energy which leads to a broader beam than in the 1D case, while the third dimension is diffraction which works with the nonlinearity to compress the beam making the field spatially narrower again. In (b) anomalously dispersive media the dispersion and the diffraction both work to contract the field energy leading to a more rapid wave collapse as the dimensionality is increased.

media? As before the answer depends on the type of dispersion and the sign of the nonlinear index.

In figs. (3.13) we seek to distinguish the behavior of pulses propagating in bulk self-focusing media from those propagating in media of lower dimensionality. In this as well as the next plot the 1D case refers to cw propagation in a planar waveguide, the 2D case refers to pulse propagation in the presence of dispersion in a planar waveguide and the 3D case refers to pulse propagation in bulk media. In the normal dispersion regime [fig. (3.13a)] the dispersion reacts to the nonlinear index in a manner opposite to that of diffraction in that it spreads energy away from the center of the field. Thus the difference in the 1D and 2D cases, a reduced narrowing of the beam, is because the inclusion of dispersion reduces the peak field strength which in turn reduces the nonlinear phase accumulation. Adding the third dimension increases the beam narrowing because the third dimension is diffractive which, when combined with a self-focusing nonlinearity, provides another mechanism for energy concentration. In the anomalous case the dispersion also provides a mechanism for field compression hence addition of the second and then third dimension [fig. (3.13b)] both increase the beam narrowing and lead to a more rapid wave collapse.

For a self-defocusing nonlinearity the roles of the two dispersion regimes are reversed in the sense that now the anomalous dispersion works to broaden the field and the normal dispersion works to compress it. We illustrate the two cases in figs. (3.14). In normally dispersive media [fig(3.14a)] the addition of the temporal dimension (the 2D case) results in an initially more compressed field which, because it results in a higher peak intensity and thus higher nonlinear phase curvature, leads to a

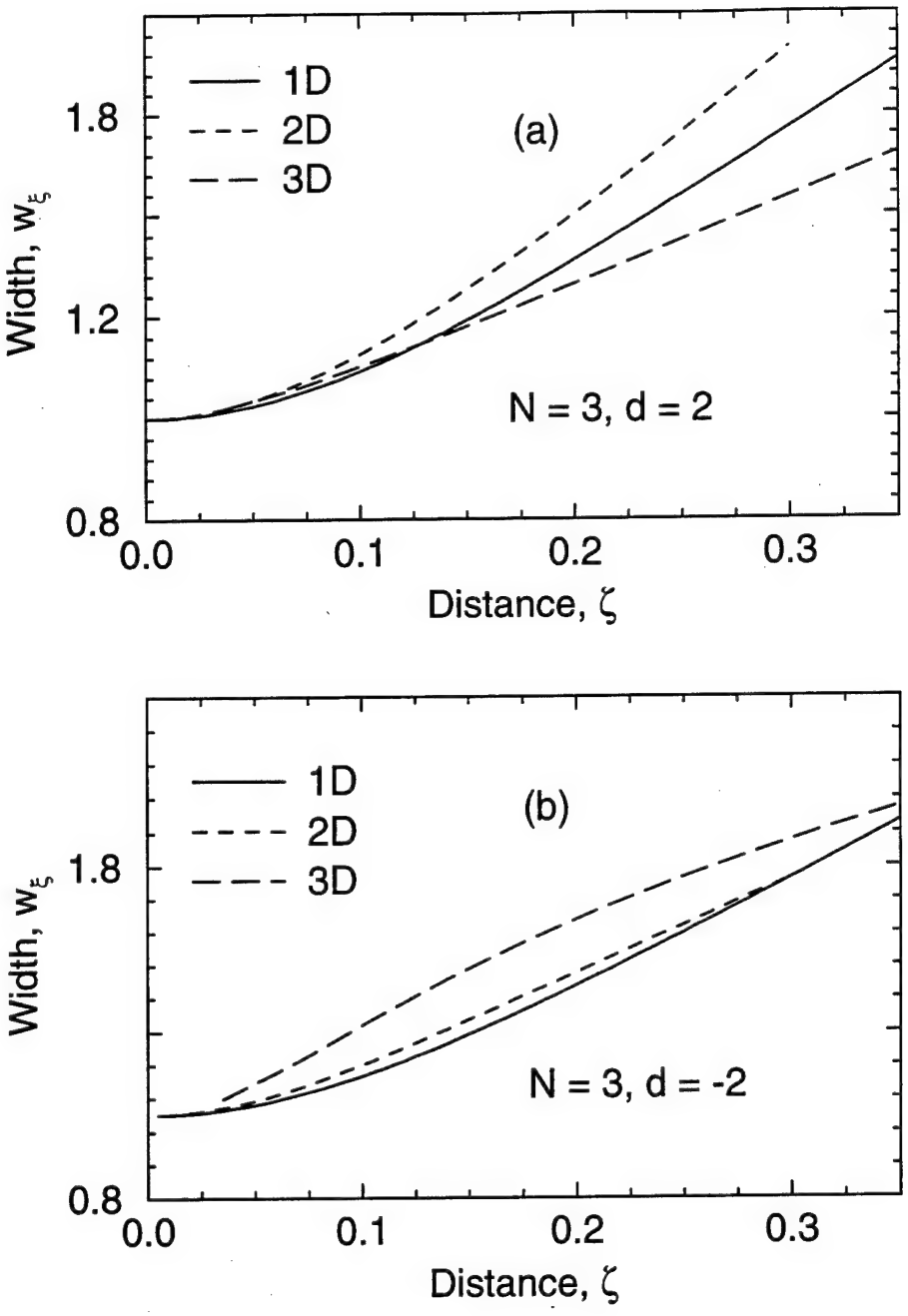

Figure (3.14) For a self-defocusing nonlinearity the third dimension provides another avenue to deplete the strength of the nonlinearity. In (a) the normal dispersion regime the temporal compression enhances the broadening in the 2D case while in the 3D case the field is initially broadening faster spatially than temporally which quickly reduces the nonlinear contribution to the beam size. In (a) the anomalous case all dimensions work to broaden the field which leads to broader beams at small ζ and smaller beams at large ζ as the dimensionality is increased.

greater broadening than the 1D case. In the 3D case the temporal compression has the effect of spatially flattening the field so that the rate of broadening is even less than in the 1D case. For the case of anomalous dispersion [fig. (3.14b)] the three dimensions all provide broadening mechanisms thus as the dimensionality is increased the initial broadening of the field increases. As a result the intensity at the center of the field drops so rapidly that the nonlinear contribution to the phase accumulation soon becomes negligible. This leads to the somewhat counterintuitive result that as the dimensionality is increased the broadening of the beam is reduced at large ζ.

3.5 Conclusions

In this chapter we have presented an overview of the effects of spatio-temporal coupling on the behavior of ultrashort pulses traveling in nonlinear planar optical waveguides. We have seen that in a waveguide with $n_2 > 0$ and $\beta_2 > 0$, a strong nonlinearity can bring energy in from the spatial wings of the field faster than the normal dispersion can move it to the temporal wings, thus making a localized pulse compression possible in the normal dispersion regime. This initial compression at the center of the beam, however creates an enhanced pulse broadening at larger propagation distances. Further, since the initial compression is driven by spatial self-focusing, a focusing spatial phase modulation will enhance both the initial compression and eventual pulse broadening occurring at large ζ. Conversely, a defocusing spatial phase modulation will reduce both the initial compression and the later broadening. We have also seen that with $n_2 < 0$ and $\beta_2 > 0$ a strong nonlinearity can bring energy in from

the temporal wings faster than the diffraction can spread it to the spatial wings, making a localized beam narrowing in a self-defocusing medium possible. This initial narrowing at the peak of the pulse fuels an even greater self-defocusing at large distances which may be enhanced or reduced with temporal phase modulation (frequency chirp). In both cases the mechanism is the same: a strong compressive effect initially overpowers a broadening effect which in turn strengthens the eventual broadening occurring at larger propagation distances.

There are a variety of materials and devices in which nonlinearity-induced spatio-temporal coupling plays an important role. This coupling will also be important in materials which exhibit Kerr-like nonlinearities such as the resonant nonlinearities of semiconductors and semiconductor-doped glasses. As discussed in chapter 1, spatio-temporal coupling is behind the self-mode-locking[29-31] of the new generation of ultrafast solid-state lasers (Ti:Al_2O_3, Cr:$LiSrAlF_6$ etc.) and further developments in this area necessarily require a clear understanding of this mechanism. A proposed ultrafast pulse-shaping technique also exploits the spatio-temporal coupling provided by the Kerr nonlinearity. Another application where spatio-temporal coupling should be important is in Z-scan measurements of the nonlinearity of dispersive materials using ultrashort pulses, particularly for thicker samples. Both of these techniques will be discussed in the chapters to follow.

3.6 References

1. G. P. Agrawal, *Nonlinear Fiber Optics*, 2nd ed. (Academic Press, San Diego, 1995)Chaps. 2 and 6.

2. A. T. Ryan and G. P. Agrawal, "Steering of optical beams in nonlinear Kerr media by spatial phase modulation," Opt. Lett., **18**, 1795 (1992).

3. X. D. Cao, D. D. Meyerhofer, G. P. Agrawal, "Optimization of optical beam steering in nonlinear Kerr media via spatial phase modulation," J. Opt. Soc. Am. B **11**, 2224 (1994).

4. V. E. Zakharov and A. B. Shabat, "Exact theory of two-dimensional self-focusing and one-dimensional self-modulation of waves in nonlinear media," Sov. Phys. JETP **34**, 62 (1972).

5. A. Hasegawa and F. Tappert, "Transmission of stationary nonlinear optical pulses in dispersive dielectric fibers. I Anomalous dispersion," Appl. Phys. Lett., **23,** 142 (1973).

6. R. Y. Chiao, E. Garmire, C. H. Townes, "Self-trapping of optical beams," Phys Rev. Lett., **13**, 479 (1964).

7. P. L. Kelley, "Self-focusing of optical beams," Phys. Rev. Lett., **15**, 1005 (1965).

8. W. G. Wagner, H. A. Haus, J. H. Marburger, "Large-scale self-trapping of optical beams in the paraxial ray approximation," Phys. Rev., **175**, 256 (1968).

9. J. H. Marburger, "Self-focusing as a pulse sharpening mechanism," IEEE Journal of Quantum Electronics, **QE-3**, 415 (1967).

10. Y. R. Shen, *The Principles of Nonlinear Optics*, (Wiley, New York, 1984) Chap. 17.

11. N. A. Zharova, A. G. Litvak, T. A. Petrova, A. M. Sergeev and A. D. Yunakovskii, "Multiple fractionation of wave structures in a nonlinear medium," JETP Lett., **44**, 13 (1986).

12. P. Chernev and V. Petrov, "Self-focusing of light pulses in the presence of normal group-velocity dispersion," Opt. Lett. **17**, 172 (1992).

13. P. Chernev and V. Petrov, "Self-focusing of short light pulses in dispersive media," Opt. comm. **87**, 28 (1992).

14. J. E. Rothenberg, "Pulse splitting during self-focusing in normally dispersive media," Opt. Lett. **17**, 583 (1992).

15. G.G. Luther, A.C. Newell, and J.V. Moloney, "The effects of normal dispersion on collapse events," Physica D, **74**, 59 (1994).

16. R. W. Boyd, *Nonlinear Optics*, (Academic Press, San Diego, 1992), Chaps. 6 and 7.

17. L. F. Mollenauer, R. H. Stolen and J. P. Gordon, "Experimental observation of picosecond pulse narrowing and solitons in optical fibers," Phys. Rev. Lett., **45**, 1095 (1980).

18. L. F. Mollenauer, R. H. Stolen, J. P. Gordon and W. J. Tomlinson, "Extreme picosecond pulse narrowing by means of soliton effect in single-mode optical fibers Opt. Lett., **8**, 289 (1983).

19. P.P. Mamyshev in *Optical Solitons - Theory and Experiment*, J. R. Taylor, ed. (Cambridge University Press, Cambridge UK, 1992), Chap. 8.

20. G. P. Agrawal, "Induced focusing of optical beams in self-defocusing nonlinear media," Phys. Rev. Lett., **64**, 2487 (1990)

21. A. J. Stentz, M Kauranen, J. J. Maki, G. P. Agrawal, and R. W. Boyd, "Induced focusing and spatial wave breaking from cross-phase modulation in a self-defocusing medium," Opt. Lett., **17**, 19 (1992)

22. S Dinev, A. Dreischuh, and I. Ivanova, "Induced deflection of optical beams in an off-axis geometry," J. Mod. Opt., **39**, 667 (1992)

23. X. D. Cao, G. P. Agrawal and C. J. McKinstrie, "Self-focusing of chirped optical pulses in nonlinear dispersive media", Phys. Rev. A 49, 4085 (1994)

24. V. M. Malkin, "On the analytic theory for stationary self-focusing of radiation," Physica D **64**,251 (1993)

25. V. I. Karpman, "Influence of high-order dispersion on self-focusing. I. Qualitative investigation," Phys. Lett. A **160**, 531 (1991); V. I. Karpman and A. G. Shagalov, "Influence of high-order dispersion on self-focusing. II. Numerical investigation," Phys. Lett. A **160**, 538 (1991)

26. M. D. Feit, J. A. Fleck, Jr., "Beam nonparaxiality, filament formation, and beam breakup in the self-focusing of optical beams," J. Opt. Soc. Am. B **5**, 633 (1988)

27. G. Fibich, "Small beam non-paraxiality arrests self-focusing of optical beams," Phys. Rev. Lett. **76**, 4356 (1996)

28. R. E. Bridges, "Multi-dimensional effects of intensity-dependent optical nonlinearities on the propagation of light," Ph. D. Thesis, University of Rochester, 1995, and references therein.

29. H.A. Haus, J. G. Fujimoto and E. P. Ippen, "Analytic Theory of Additive Pulse and Kerr Lens Mode Locking", IEEE J. Quantum Electron., **28**, 2086 (1992)

30. I. Androsch and P. Glas, "Influence of Spatio-temporal refractive index changes in a GaAs etalon on the generation of ultrashort pulses in a Nd-phosphate glass laser", Opt. Comm., **105**, 126 (1994)

31. G. W. Pearson, C. Radzewicz and J. S. Krasinski, "Use of ZnS as a self-focusing element in a self-starting Kerr lens modelocked Ti:Sapphire laser", SPIE Proc. Vol. 2116, 76 (1994)

Chapter 4

Spatiotemporal Coupling in Spatial Soliton Beam Steering

4.1 Background

In both the spatial and temporal domains, the nonlinear Schrödinger equation (NSE) has long been a useful tool in describing the behavior of optical fields in nonlinear dispersive media. In recent years the NSE has proven useful in describing some of the new innovations in beam steering.[1-7,11-15] One technique uses spatial intensity modulation of a second beam to induce a temporal prism in the nonlinear medium which then deflects the beam.[1] Others have employed single beams with asymmetric power profiles which resulted in self-bending on propagation.[2-4] Also, both bright[5,6] and dark[7] spatial solitons have been suggested as tools for creating steerable optical waveguides in nonlinear media. There are also a variety of techniques for steering beams in linear media. Some recent innovations include microlens arrays,[8] integrated gratings,[9] and photorefractive holograms.[10]

The results we discuss here have their beginnings in the work of Stentz et al.[11] In their experiment, quasi-cw (100 ns) pulses from a dye laser were tuned to the defocusing side of the sodium D_2 resonance. A pump-probe arrangement was then used to steer the probe pulses by exploiting the phase curvature created by cross-phase modulation from the pump beam propagating in the nonlinear medium. They showed that the presence of the pump beam altered the position of the probe beam by

several beam widths after propagating through the medium. A similar result was achieved by Barthelemy and co-workers[12] who used 30 ps pulses shaped into a highly elliptical beam to produce spatial solitons in a CS_2 cell. To stabilize the solitons, they propagated two beams of equal intensity at a small angle (0.0532 rad) and discovered that the position of the two beams in the far-field was different by as much as 0.61 mrad from that expected from simple linear propagation. Moreover, the deflection was peak-intensity dependent so they were able to shorten their pulses by a factor of five by employing a slit in the far-field to spatially filter the beam. Later, a group in Sofia[13] showed that a pump-probe arrangement could be used as an extension of this technique to shape pulses when both the pump and probe beam are pulsed. Because the deflection via cross-phase modulation is dependent on the power of the pump beam, when the pump beam is pulsed the angle of deflection of the probe is nonuniform in time. A slit in the far-field is then used to shape the probe pulse by selecting only that portion of the pulse that is of interest.

The technique discussed here employs a sinusoidal spatial phase modulation of the beam entering a nonlinear medium as depicted in fig. (4.1).[14,15] Spatial phase modulation splits the input beam into multiple sub-beams while the nonlinear medium traps several of the sub-beams into a spatial soliton in such a way that most of the beam power appears in a narrow beam whose direction can be controlled by changes in the modulation parameters. Moreover, because of the nonlinear cross-phase-modulation among the sub-beams, the direction of the steered soliton depends on the input power of the beam. Thus, when the steered beam is pulsed, we find that spatial filtering with a slit provides a mechanism for pulse shaping in a manner analogous to that achieved by the authors[12,13]

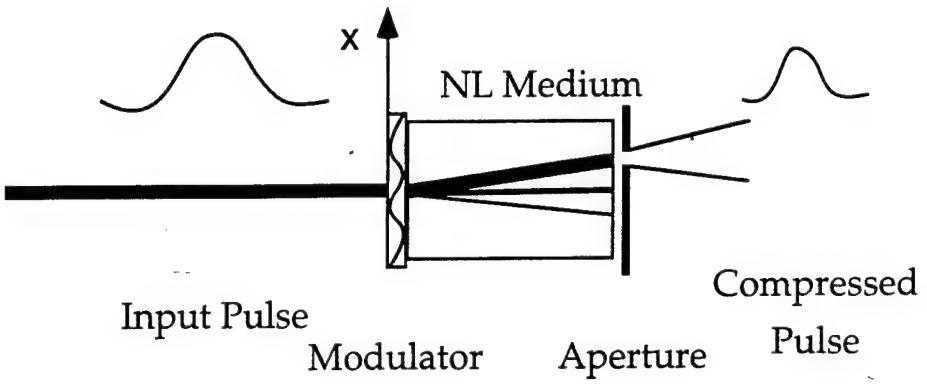

Phase Modulation: $\phi(x) = \phi_0 \sin(2\pi p_x x + \delta)$

Figure (4.1) The beam steering and pulse shaping apparatus we are discussing is similar to the one proposed in chapter 3. A beam of pulses passes through a sinusoidal phase grating prior to entering a nonlinear medium. At the exit of the medium a slit is positioned to select that portion of the field that is of interest.

discussed above. We first study the dynamics of cw beam steering with one-dimensional simulations, then look at the influence of spatiotemporal coupling on the situation by simulating the steering of pulsed beams.

4.2 CW Beam Steering

We focus first on the case of spatially one-dimensional beam steering, i.e. beam steering in nonlinear planar waveguides. The spatial one-dimensional NSE, eqn. (2.46) is solved for a phase-modulated Gaussian input beam having an input spatial profile,

$$u(\xi,0) = \exp(-\xi^2/2)\exp[i\,\phi(\xi)]. \tag{4.1}$$

For the case of sinusoidal phase modulation, $\phi(\xi)$ has the form,

$$\phi(\xi) = \phi_0 \sin(2\pi\, p\xi + \delta), \tag{4.2}$$

where ϕ_0 is the amplitude of the modulation, p is the spatial modulation frequency, and δ is a constant phase shift. In our normalized coordinates, the $p = \sigma p_x$ where p_x is the actual modulation frequency of the system we are attempting to model and σ is the width of the input beam in non-normalized coordinates. The parameters of the physical system depicted in fig. (4.1) also determine the modulation amplitude through $\phi_0 = 4\pi\Delta nL/\lambda$, where L the thickness of the modulator and Δn the amplitude of its index variation. When the modulator is thin enough that phase-matching considerations are unimportant we may treat the effect of the modulation as a simple multiplicative phase factor as in eqn. (4.1). This process is known as Raman-Nath scattering.[16]

By using a standard Bessel-function expansion of the modulation term,[16] we see that phase modulation breaks up the input beam into multiple sub-beams propagating at different angles,

$$u(\xi,0) = \exp(-\xi^2/2)\sum_{-\infty}^{\infty} J_m(\phi_0)\exp[im(2\pi\, p\xi + \delta)]\,. \tag{4.3}$$

Here $J_m(\phi_0)$ is the m^{th} order Bessel function of the first kind evaluated at ϕ_0. With the expression for the input field in this form it is clear that the amplitude of each sub-beam is determined through the modulation

amplitude ϕ_0 and that the steering angles are determined from the modulation frequency p. Thus our numerical simulations attempt to model the interaction and evolution of these initially intersecting sub-beams as they propagate through a Kerr medium. We show that with the proper choice of modulation parameters we can steer most of the power into a single direction.

4.2.1 Linear Beam Steering

As with our discussion of self-phase modulation and solitons in Chapter 2, in order to fully understand the effect of the nonlinearity on the field behavior it is important to first understand the field behavior in its absence. We begin by looking at the evolution of just one of the beamlets in the summation of eqn. (4.3). At the entrance of the modulated beam into the medium, the qth beamlet is described by

$$u_q(\xi,0) = J_q(\phi_0)\exp(-\xi^2/2)\exp(i\,2\pi pq\xi)\,\exp(i\,q\delta), \tag{4.4}$$

(q is an integer). The field behavior is governed by the one-dimensional spatial NSE, eqn. (2.46), which for linear evolution (N ≈ 0) becomes

$$i\frac{\partial u}{\partial \zeta} = -\frac{1}{2}\frac{\partial^2 u}{\partial \xi^2}. \tag{4.5}$$

Eqn. (4.5) can be solved with the initial condition of eqn. (4.4) with the Fourier transform method. The solution is,

$$u_q(\xi,\zeta) = \frac{J_q(\phi_0)\exp(iq\delta)}{\sqrt{1+i\zeta}} \exp\left[-\frac{(\xi - 2\pi pq\zeta)^2}{2(1+\zeta^2)}\right] \exp\left\{i\,\frac{\left[\xi^2 - (2\pi pq)^2\right]}{2(1+\zeta^2)}\right\} \cdot \exp\left(i\,\frac{2\pi pq\xi}{1+\zeta^2}\right) \tag{4.6}$$

Eqn. (4.6) describes a wave propagating at an angle $\theta_q = \arctan(2\pi pq)$ with respect to the original propagation direction. Thus, after propagating a distance ζ the beamlet still has a Gaussian distribution, but it is centered at $\xi = 2\pi pq\zeta$ and broadened to $\sqrt{1+\zeta^2}$ times its original width. In other words, the modulation frequency, p, determines the steering angle of the beamlet. In order for the paraxial approximation (with which the NSE was derived) to remain valid we will choose $p < 1$. From both eqn. (4.6) and eqn. (4.3) we can see that the amount of power initially in a sub-beam also depends critically on the modulation amplitude, ϕ_0, through the factor $J_q(\phi_0)$. Indeed, for $\phi_0 < 1$, there are only five ($q = 0, \pm 1, \pm 2$) beamlets with any significant power. But the ideal choice of modulation depth is $\phi_0 = 2.405$, the first zero of J_0. For this choice of modulation depth, phase modulation leaves no power in the central, undeflected portion of the beam and hence all of the power in the original beam is steered into beamlets moving away from the original propagation direction. For higher modulation amplitudes, not only will some power creep back into the central sub-beam, but more power will leak into the higher-order sub-beams at the wider deflection angles. For low modulation amplitudes, the effect of the modulation is merely to shed some of the power from the central sub-beam.

The absence of power in the $q = 0$ beamlet (for $\phi_0 = 2.405$) does not, however, imply that the input beam is steered off-axis. In figs. (4.2), we see

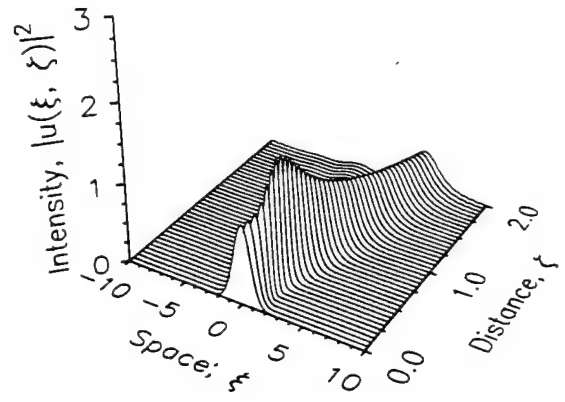

(a) $\delta = 0$

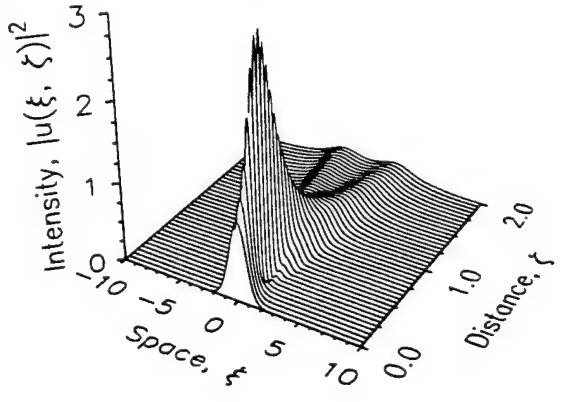

(b) $\delta = \pi/2$

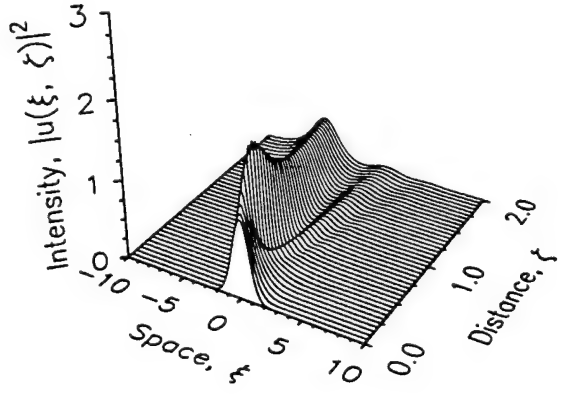

(c) $\delta = \pi$

Figure (4.2) To show the effect of the modulation phase shift δ we plot the intensity of a modulated beam as a function of ξ and ζ for an N = 1 Gaussian input field and the modulation parameters of eqn. (4.2) given by $\phi_0 = 2.405$ and p = 0.2. With (a) $\delta = 0$ the bulk of the beam power is steered to $\xi > 0$; (b) $\delta = \pi/2$ the beam remains symmetric with respect to the original propagation direction; (c) $\delta = \pm\pi$ the beam is steered to $\xi < 0$.

the effects of the modulation phase shift, δ, on the beam steering. The resultant beam can still be centered at $\xi = 0$ even with $\phi_0 = 2.405$ provided $\delta = \pm \pi/2$. It would appear that the role of the modulation phase shift, δ, is more subtle than that of the modulation amplitude or frequency. At first glance, δ merely appears as a relative phase factor for each beamlet. The different phases of the beamlets, however, ultimately determine the direction of power flow. As shown in fig. (4.2b), for $\delta = 0$ all the beamlets have the same phase, but because $J_{-q}(\phi_0) = (-1)^q J_q(\phi_0)$ (for integral $q > 0$) only the beamlets steered to $\xi > 0$ ($q > 0$) are in phase, while the beamlets steered to $\xi < 0$ have alternating sign and thus interfere destructively. As a result most of the input beam power is steered to $\xi > 0$. Conversely, when $\delta = \pm \pi$ as in fig. (4.2c) the situation is reversed and much of the power is steered to $\xi < 0$. This behavior can be understood by referring to fig. (4.3) where we plot the input field with the input phase modulation on the same horizontal scale for $\delta = \pi/2$ and π for the modulation parameters used to create figs. (4.2). When $\delta = \pm \pi/2$ the phase modulation is nearly equivalent to placing a lens in the beam path, as it produces a nearly quadratic variation of the phase front. By contrast, for the phase shift $\delta = 0$ or π, the phase modulation is nearly linear and therefore nearly equivalent to placing a prism in the beam path, resulting in beam deflection.

Perhaps the most important aspect of linear beam steering in terms of its influence on the nonlinear beam steering problem is the overlap of the sub-beams. Returning to eqn. (4.6) we can obtain an estimate of the overlap distance. If we define the sub-beams as overlapped provided the peak of adjacent sub-beams are separated by less than twice the $1/e^2$ halfwidth of the beamlets, then this is equivalent to requiring,

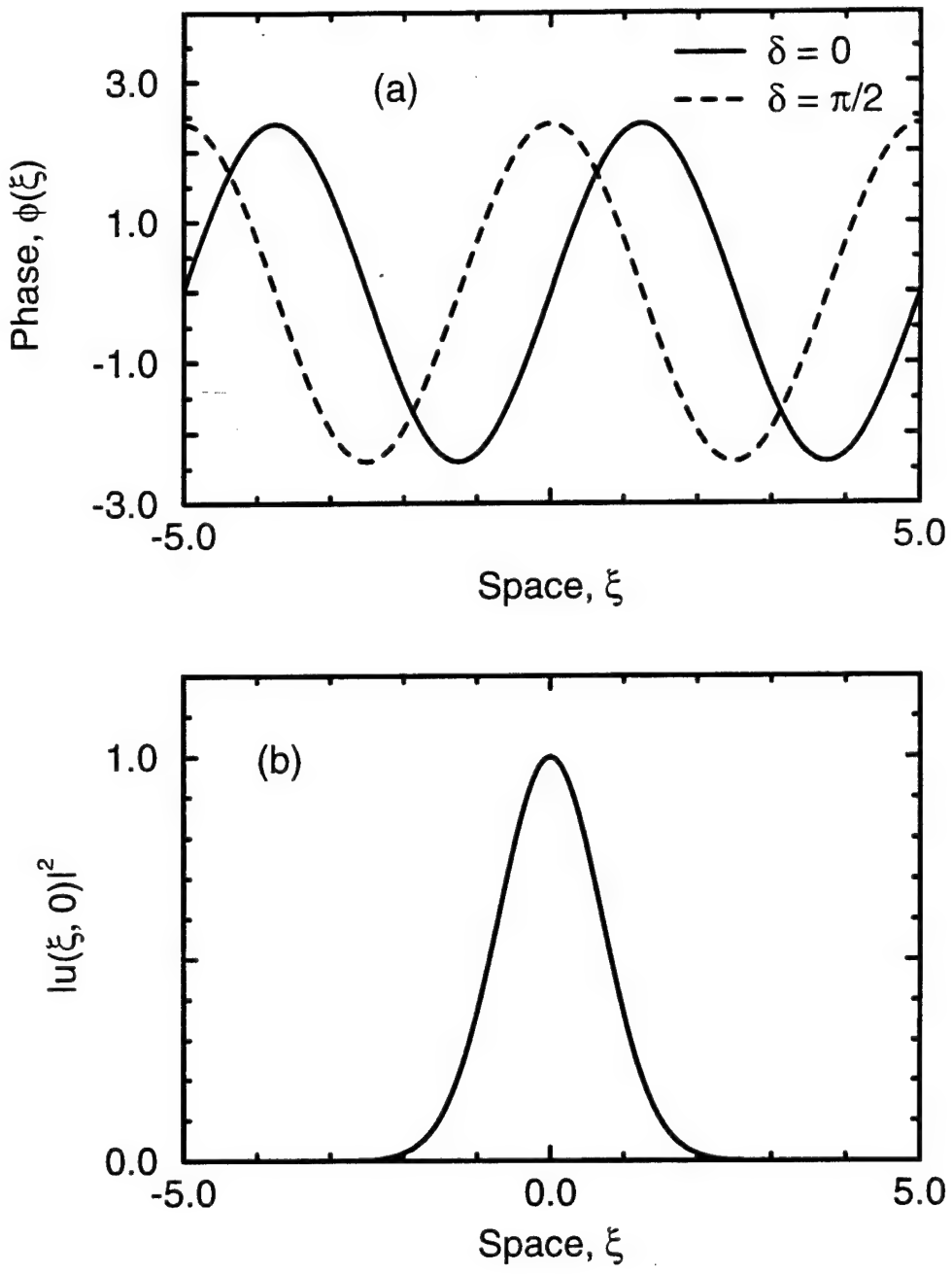

Figure (4.3) Spatial phase modulation function for the parameters of fig. (4.2) on the same horizontal scale as the Gaussian input field. For $\delta = 0$ the phase modulation varies nearly linearly across much of the beam, while for $\delta = \pi/2$ the phase modulation is nearly quadratic.

$$\zeta < (\pi^2 p^2 - 1)^{-1/2} \tag{4.7}$$

for overlap. Notice that when $p \leq \pi^{-1}$, this condition cannot be met which simply means that sub-beams broaden faster than they diverge and hence are always overlapped. Consequently small modulation frequencies do not truly separate the input beam into series of sub-beams as suggested by eqn. (4.3). The result is that most of the power of the beam steered with such a modulation frequency in a linear medium is contained in a central peak with oscillatory wings as seen in figs. (4.2). Contrary to what occurs in a linear medium, a nonlinear medium may either enhance or suppress the broadening of the sub-beams, hence changing the distance over which the sub-beams overlap. More importantly however, the nonlinearity also provides a mechanism for the sub-beams to interact, consequently the overlap of the sub-beams has an enormous influence on the quality, shape and even power of a beam steered in a nonlinear medium. The behavior of the deflected beam as it propagates in a nonlinear medium is the topic of the next section.

4.2.2 Nonlinear Beam Steering

When the peak power of the incident beam is such that $N \approx 0.1$ or higher, eqn. (4.5) is no longer adequate for describing the field behavior and we must return to eqn. (2.46),

$$i\frac{\partial u}{\partial \zeta} = -\frac{1}{2}\frac{\partial^2 u}{\partial \xi^2} - \mathrm{sgn}(n_2)\, N^2\, |u|^2 u, \tag{4.8}$$

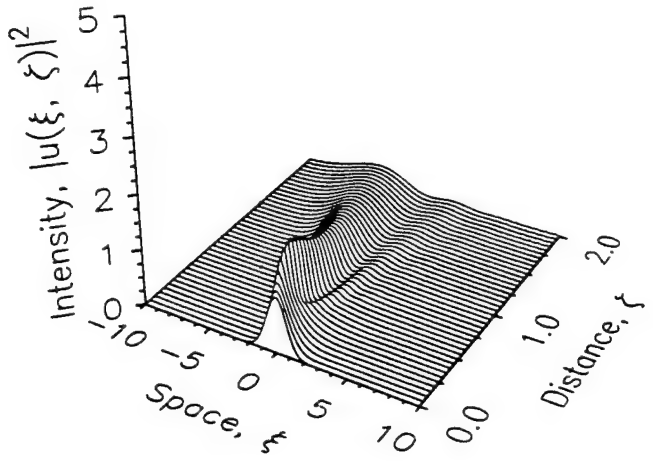

(a) N = 0

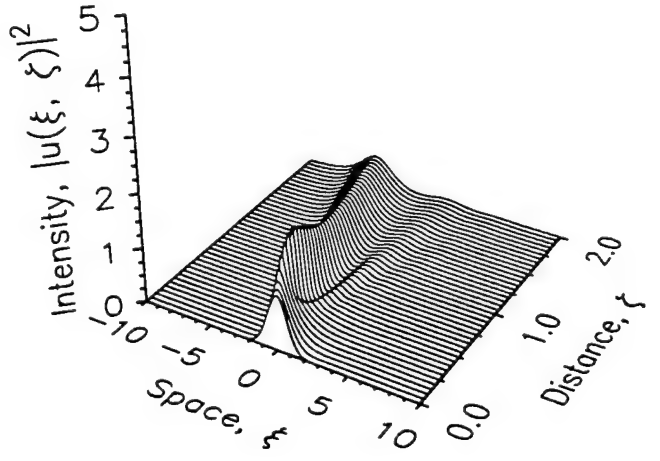

(b) N = 1

Figure (4.4) To show the effect of a nonlinearity on the beam steering we plot the intensity of a beam steered with modulation parameters $\phi_0 = 2.405$, $p = 0.2$ and $\delta = 0$ for several different intensities. For (a) N = 0 we see the steered beam diverges; (b) N = 1 the divergence of the steered beam is

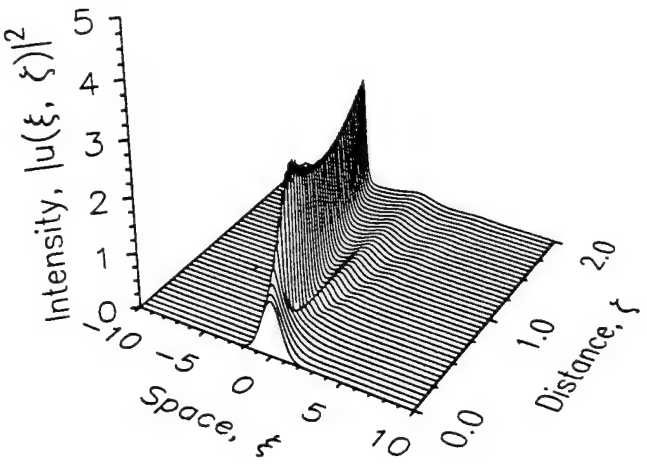

(c) N = 2

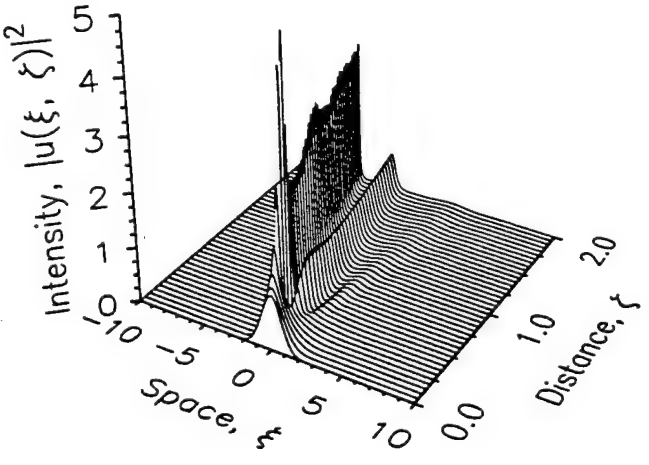

(d) N = 3

suppressed; (c) N = 2 the steered beam forms a fundamental spatial soliton which does not diverge as it propagates beyond the initial overlap region; (d) N = 3 the phase modulation creates two spatial solitons steered to $\xi > 0$ via soliton dragging.

and numerical simulations to study the field behavior. In fig. (4.4) we see the effect of a self-focusing nonlinear medium on Raman-Nath beam steering. Fig. (4.4) compares the beam evolution in a nonlinear medium for several values of N (or peak intensity). As seen in fig. (4.4a), for low powers the steered beam diverges on propagation since the medium is nearly linear. But as the power is increased for figs. (4.4b-d), the primary part of the beam exhibits soliton propagation, whereas the remaining low-power sections of the beam merely diverge. At still higher powers, as in fig. (4.4d), a secondary steered spatial soliton is formed.

To determine the value of N for which the steered beam propagates as a soliton, a clearer understanding of the dynamics is necessary. One might naively think that the soliton condition is satisfied only whenever the amplitude of the beamlet with the greatest power exceeds that required to form a soliton. With this assumption and the modulation parameters in fig. (4.4) we would estimate the soliton condition for the first sub-beam to be, $N > 0.5/J_1(2.405) = 0.96$. Unfortunately, this neglects the nonlinear interaction of the overlapping sub-beams. It is possible to obtain information about the field behavior using analytical methods. Cao et al.[15] used some assumptions about the shape of the field and exploited the conservation laws associated with the NSE to obtain,

$$N^2 > \frac{1}{(\sqrt{2} - \sqrt{\pi}/W)}\left[1 - 2(\theta_d)^2 + \frac{2}{\sqrt{\pi}}\int\left(\frac{d\phi}{dx}\right)^2 \exp(-x^2)\,dx\right], \qquad (4.9)$$

as a condition for soliton propagation with an arbitrary phase modulation $\phi(x)$. Here W is the width of the region within which it is assumed the beam energy is confined and θ_d is the beam deflection angle. For $W >> 1$

and a sinusoidal phase modulation such as is proposed here, this condition becomes,[15]

$$N^2 > \frac{1}{\sqrt{2}}\{1 + 4\pi^2 p^2 \phi_0^2 [1 + \cos(2\delta)\exp(-4\pi^2 p^2) - 2\cos^2\delta \exp(-2\pi^2 p^2)\}. \quad (4.10)$$

Note the strong dependence of this soliton condition on the modulation frequency and thus the overlap of the sub-beams. It is also important to note however, that this is a condition for soliton formation for the entire field, not just one particular sub-beam. Indeed the derivation of this condition, as well as an estimate for the steering angle and the optimum modulation frequency are all obtained[15] without reference to the sub-beams described by eqn. (4.3). The analytical methods employed in ref. 15 are useful because they produce such results as eqns. (4.9) and (4.10) yet limited because they do not produce explicit solutions. For more information on the behavior of the steered sub-beams we must resort to our intuition and numerical simulations.

An important insight into the dynamics of the overlapping sub-beams comes from the paper of Stentz et al.[11] in which was plotted the instantaneous nonlinear phase shift and the resulting contribution to the transverse wave vector due to the presence of a Gaussian beam in a self-defocusing nonlinear medium. In fig. (4.5) we reproduce the plot for a self-focusing nonlinearity such as we model here and we see that for $\xi < 0$ there is a positive contribution to the transverse momentum from the nonlinear phase and a negative contribution for $\xi > 0$. The key point is that the presence of a beam changes the transverse momentum of any beam passing through it in such a fashion that the second beam is steered closer to the direction of the first and vice-versa. Thus after the initial

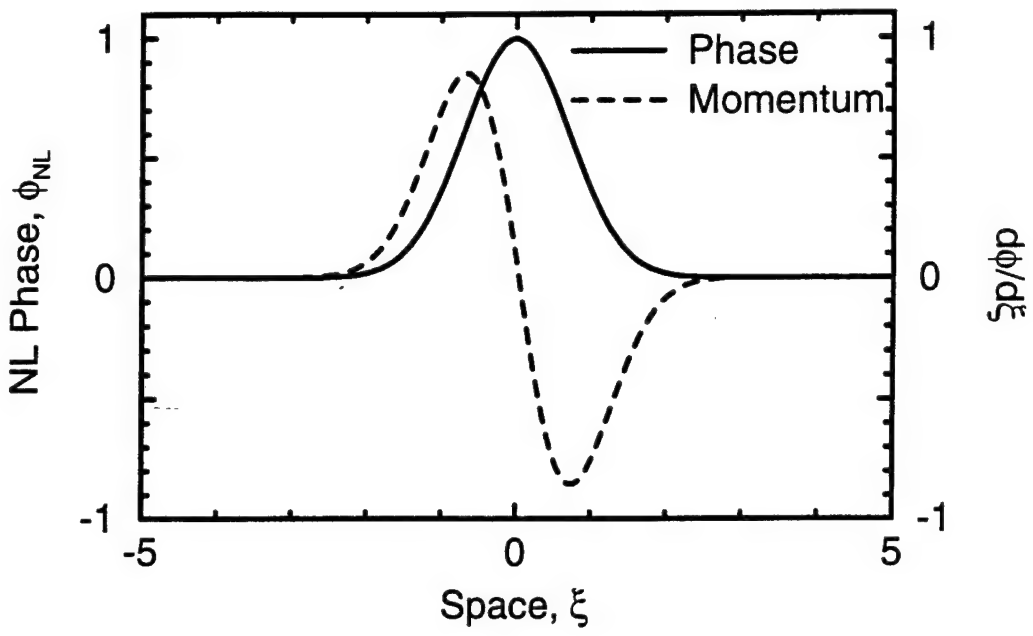

Figure (4.5) The overlapping sub-beams influence one another through cross phase modulation. Here we plot the (solid line) instantaneous nonlinear phase shift due to the presence of a Gaussian beam in a self-focusing nonlinear medium and the (dashed line) contribution to the transverse momentum that results from such a phase shift.

phase modulation provided by the modulator, the interacting sub-beams begin to steer one another. The second way in which the sub-beams interact is through power transfer. By definition, a spatial soliton will not lose power during a collision with another soliton. However, during the initial interaction phase described here, the sub-beams have neither the required shape nor power to be true solitons. Consequently, dispersive wave coupling leads to a transfer of power among the sub-beams. The analogy of this type of sub-beam interaction to temporal soliton trapping is summarized concisely by the authors of ref. 15: "Just as the Kerr nonlinearity can negate the modal dispersion between the fast and slow modes and fuse two subpulses propagating along the fast and the slow axes

of a birefringent fiber to form a single solitary wave (so-called soliton trapping), the same nonlinearity can also negate the spatial dispersion (of diffraction) between several sub-beams. The physical meaning of this analogy is that it is possible to divert power from various sub-beams and form a single spatial soliton."

In the preceding discussion we described how the medium nonlinearity causes the interaction among the overlapping sub-beams. As shown in figs. (4.4) the presence of the nonlinearity can also significantly affect the quality of the steered beam, changing it from a broad, dispersing beam in the linear case to a more confined distribution as the power is increased. A more subtle effect of increasing the nonlinearity is that it can

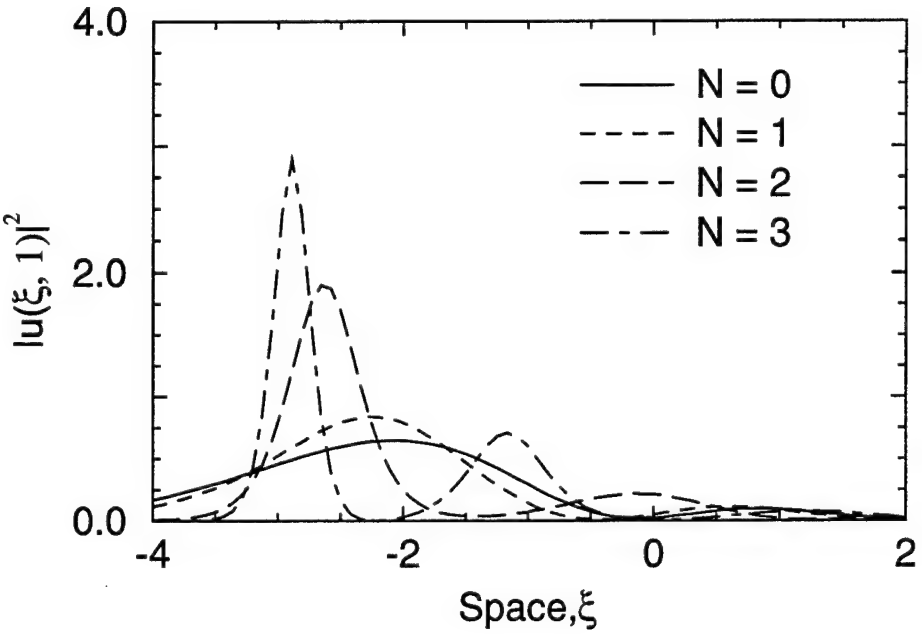

Figure (4.6) The steering angle of the peaks of the beam are dependent on the strength of the nonlinearity. We plot the intensity distribution at $\zeta = 1$ for a modulated beam and nonlinearities N = 0,1,2, and 3.

change the steering angles of the spatial solitons generated by the interaction. This is simply because the magnitude of the nonlinear phase contribution, and hence the contribution to the transverse momentum [as in fig. (4.5)] of one sub-beam to another passing through it, increases with the strength of the nonlinearity. This affect is not noticeable using the methods of ref. 15 simply because the results therein apply to the entire field, whereas the effect we are about to discuss concerns the behavior of only parts of the field. In figs. (4.6-7) we demonstrate the change in steering angle with increasing nonlinearity by plotting in fig. (4.6) the intensity as a function of ξ of steered beams after propagating one diffraction length ($\zeta = 1$) and in fig. (4.7) we plot the ξ position of the peaks at $\zeta = 1$ as a function of N^2 for a large range of nonlinearities. Several

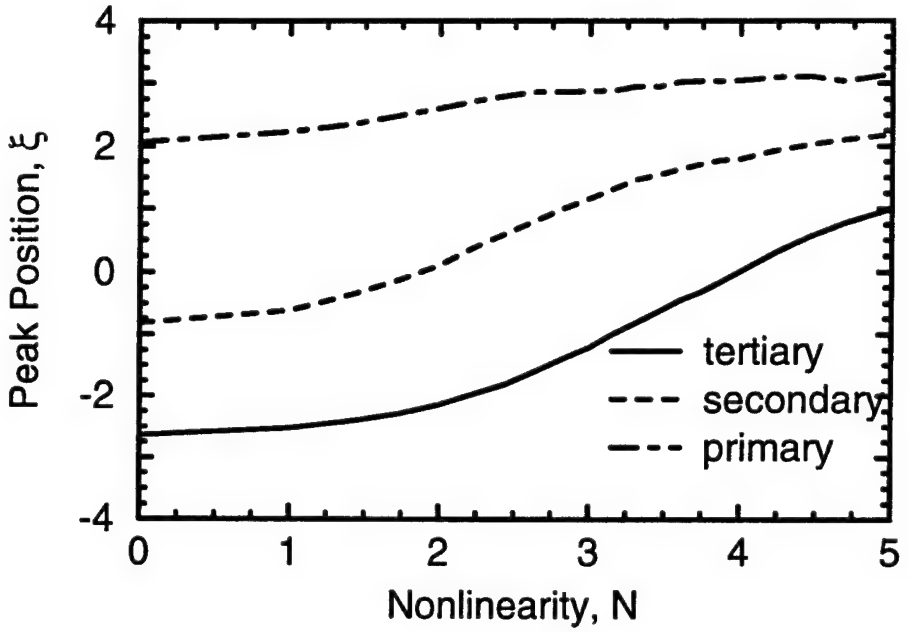

Figure (4.7) The shape of the beam and position of its peaks are intensity dependent. We plot the position of the peaks of the modulated beam at $\zeta = 1$ as a function of N.

observations can be made from this data. First, the lateral position of the peak of the primary steered beam increases slowly with N. Second, the secondary peak position increases quite rapidly as the strength of the nonlinearity increases and the position of the tertiary peak also changes rapidly. These dramatic changes in steered beam direction as the nonlinearity is increased are a result of cross phase modulation among the sub-beams discussed above.

Another interesting feature of nonlinear beam steering is the transfer of power among the beamlets. When the intensities of fig. (4.6) are integrated to obtain the power carried in each of the peaks we find that there is a change in the power carried by each peak as well. In fig. (4.8) we plot the normalized power carried in each of these peaks under the same

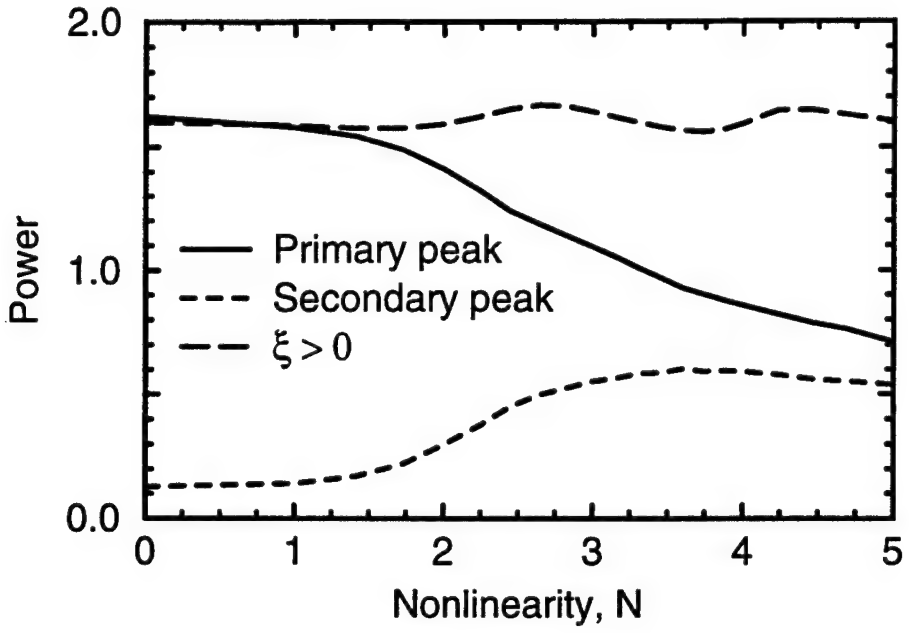

Figure (4.8) The power carried in each of the peaks created by the modulation changes as the nonlinearity changes because of the changing strength of the dispersive wave coupling. The power steered to $\xi > 0$ (upper curve) remains roughly constant.

conditions as in fig. (4.7). One interesting feature is that the primary beam power decreases immediately with increasing N, while the secondary beam power increases immediately with N, reaches a maximum then begins a slow decay. Yet the total power deflected to $\xi > 0$ is roughly constant (the fluctuations arise as the sub-beams cross the $\xi = 0$ axis and so contribute to the integral without actually being steered off-axis). It is interesting to note that the position of the center of the beam $<\xi>$, also a measure of the steering angle,[15] given by

$$<\xi> = \frac{\int_{-\infty}^{\infty} \xi \, |u(\xi,\zeta)|^2 \, d\xi}{\int_{-\infty}^{\infty} |u(\xi,\zeta)|^2 \, d\xi}, \tag{4.10}$$

remains unchanged regardless of the value of N. Thus energy is passed from sub-beam to sub-beam during the initial interaction in such a fashion that although the shapes and peak intensities of the sub-beams may change, the steering angle remains the same. This is merely the conservation of momentum[15] and can be employed as a check on the accuracy of the simulations.

Since the secondary and tertiary peaks initially arise on the $\xi < 0$ side of the initial propagation direction, questions arise as to what extent these peaks are related to the sub-beams of eqn. (4.3). To resolve the questions we must recall that, with these modulation parameters, in the linear regime the sub-beams are always overlapped. Indeed, even in the far-field intensity distribution shown in fig. (4.9) the individual sub-beams

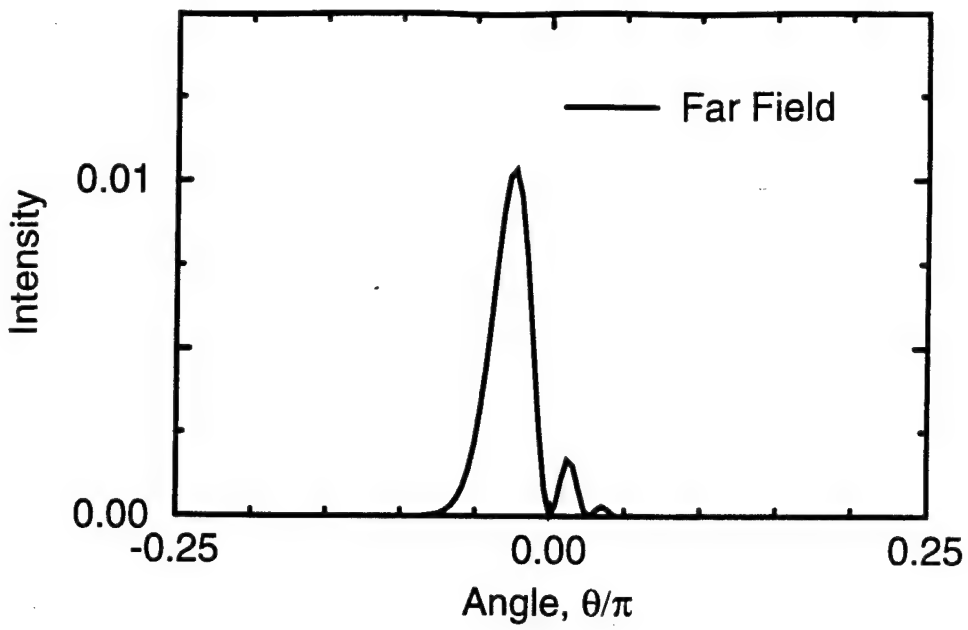

Figure (4.9) Far-field intensity distribution of a phase modulated Gaussian beam after propagating in a linear medium.

cannot be distinguished. Nonetheless the multi-peaked structure of fig. (4.9) is a result of their interference. Moreover, we can see that this structure consists of one large peak on the $\theta < 0$ side and two smaller ones on the $\theta > 0$ side. The primary peak is due to the constructive interference of all the sub-beams of positive order [$m > 0$ in eqn. (4.4)]. The two largest peaks on the $\theta > 0$ side are due essentially to the interference among the m= -1,-2 and -3 sub-beams. It is these three peaks, a result of the interference among the sub-beams not the sub-beams themselves, that evolve into the steered beams described by figs. (4.6)-(4.8). As the nonlinearity is increased the dispersive wave coupling among those interfering beamlets allows the peaks to coalesce into spatial solitons.

4.3 Pulsed Beam Steering and Pulse Shaping

The study of the behavior of pulsed optical fields can be broken into regimes based on the width of the pulse and the dispersion of the medium. For an 800-nm, 10-ps pulse in fused silica, the dispersion length is on the order of 2500 meters. For beam widths much less than 0.5 cm such pulses may be treated as dispersionless without introducing significant error due to pulse broadening or reshaping. For shorter pulses, the dispersion term of eqn. (2.50) must be included in the analysis.

4.3.1 The Dispersionless Limit

Now that we understand cw beam steering, the special features of pulsed beam steering become more accessible. In the dispersionless limit eqn. (4.8) describes the behavior of a two-dimensional field without the longitudinal transfer of energy within the pulse. Consequently the results of figs. (4.6)-(4.9) can provide us with a complete understanding of pulse behavior in this regime. In this limit a pulse may be regarded as a continuous series of cw beams of varying intensity. Then according to figs. (4.6-7) the center ($\tau = 0$) of the pulse should get deflected further than its tails but because of the energy transfer among sub-beams the center should also get flattened somewhat. As discussed earlier, it is difficult to concisely depict the evolution of a two-dimensional field graphically. In fig. (4.10) we plot the two-dimensional analog to fig. (4.6) for the $N = 3$ case. In this contour plot, the contours are logarithmically spaced such that each successive contour represents an intensity two times higher than the previous contour with the outermost contour corresponding to an

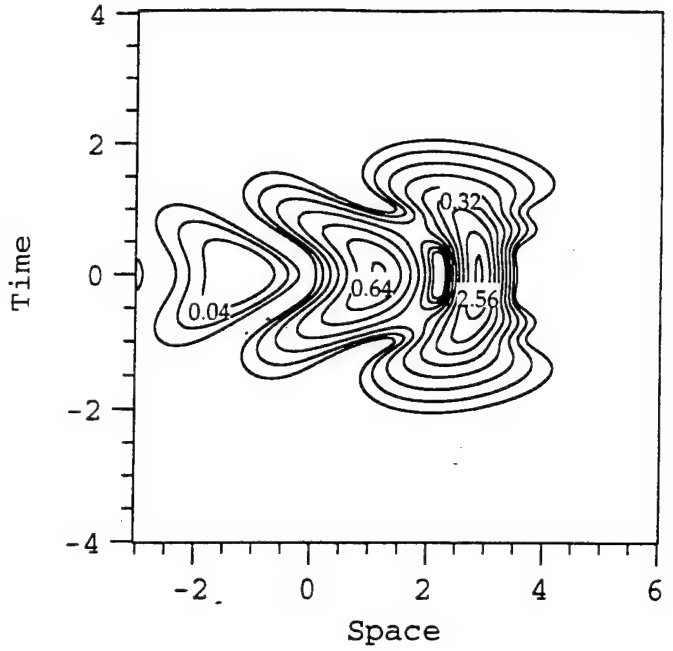

Figure (4.10) A contour plot of the intensity distribution of an initially Gaussian two-dimensional (ξ and τ) field after spatial phase modulation and propagation to $\zeta = 1$ in a nonlinear medium such that $N = 3$ at the pulse peak at $\zeta = 0$ demonstrates the steering of pulsed beams in the dispersionless [$d = 0$ in eqn. (4.11)] limit. The power dependence of the steering angle results in crescent-shaped peaks.

intensity of 0.01. This is the intensity distribution as a function of ξ and τ at $\zeta = 1.0$ of a pulse that is initially Gaussian in both space and time. We see that the center of the pulse is indeed deflected further than the tails thus producing a crescent-shaped structure in both of the large spatial peaks. The energy transfer also flattens the peak of the pulse as expected but the primary mechanism for shaping the pulse is the power dependence of the deflection angle.

If the field of fig. (4.10) were spatially integrated we would find that the initial Gaussian temporal energy distribution would be retained simply because there is no dispersion in the model to change it, hence

there is no actual change in pulse shape when the entire field is considered. However, as in the work of Barthelemy[12] and Dreischuh,[13] spatial filtering of the output beam can be used to select that portion of the field in which there is pulse shaping. In figs. (4.11-13) we show the effects on pulse shape produced by deploying a slit at several ξ positions at a propagation distance of $\zeta = 1.0$ for the field in fig. (4.10). We choose a slit width equal to 0.2 of the incident beam width. Concentrating first on the primary deflected peak we see in fig (4.11a) that centering the slit at $\xi = 2.9$ results in the modestly flattened and compressed pulse discussed previously. Depending on the slit width, the pulse width may be reduced to 70% of its initial value with this set of parameters. As we move the slit inward to $\xi = 2.75$ we find a pulse with a two peaked structure which grows more pronounced until we get the split pulse of fig. (4.11d) at $\xi = 2.3$. Moreover each of the sub-pulses of fig. (4.11d) are shorter than the input pulse by nearly a factor of 3. The higher compression is due to the fact that the change in deflection angle of the primary peak changes more rapidly at lower powers as indicated in fig. (4.7) thus the slit selects a smaller range of intensities. Unfortunately the compression of the pulse is obtained at the cost of a considerable reduction in the pulse energy. The energy in each of the split pulses is approximately 1/11 of the energy in the pulse obtained by filtering at the peak of the field at $\xi = 2.9$.

If we next focus on the effect of spatially filtering the secondary spatial peak of fig. (4.10), we find that a greater pulse compression is possible than that obtained by filtering the primary peak. When the slit is positioned at $\xi = 1.35$ as in fig. (4.12a) the pulsewidth coming out of the slit is just 42% of the pulsewidth incident on the nonlinear medium. This is

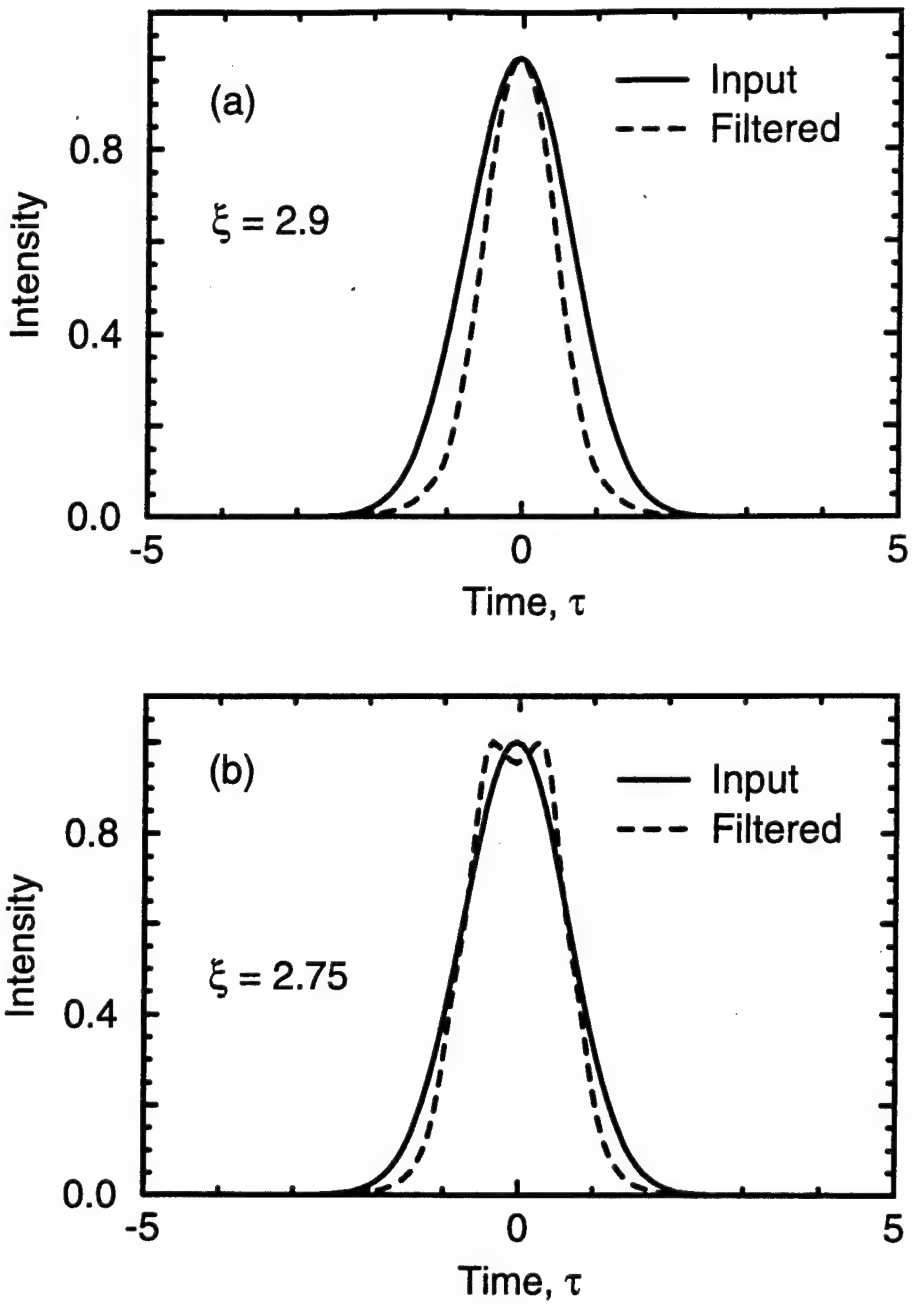

Figure (4.11) A slit may be used to select a portion of the field in fig. (4.10) and so produce pulse shaping. The spatially integrated pulse shape of the entire field, normalized so the peak intensity is unity, is shown for comparison with the pulse shape transmitted through a slit at $\zeta = 1$, also normalized. With a slit placed at (a) $\xi = 2.9$ the transmitted pulse is slightly compressed and flattened; (b) $\xi = 2.75$ the slit now selects a two-

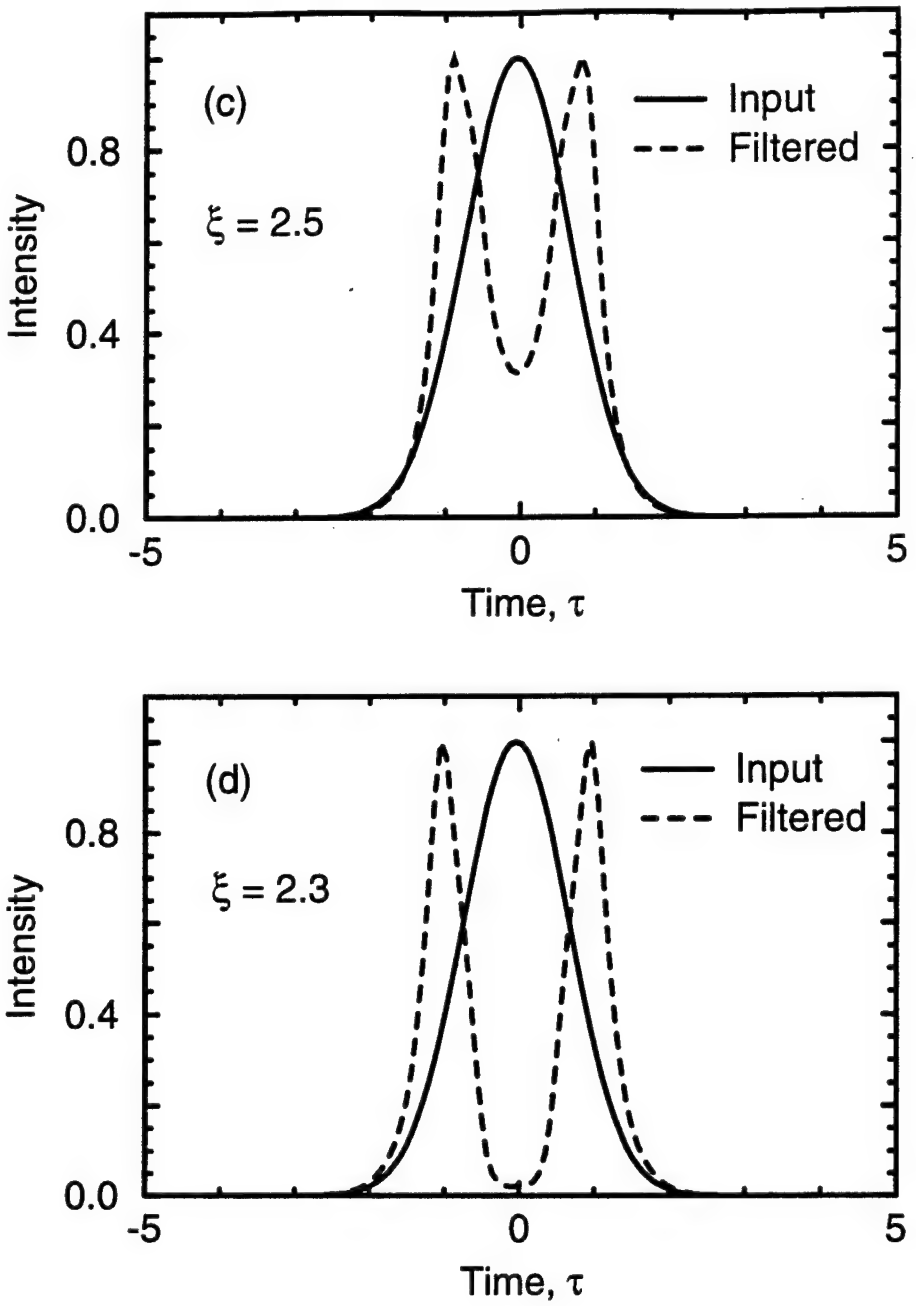

peaked pulse; (c) $\xi = 2.5$ the pulse begins to split; (d) $\xi = 2.3$ the phase modulation and filtering produces a pulse pair.

again the result of the stronger dependence on intensity of the deflection angle of the secondary beam as indicated by the steeper slope of the lower curve of fig. (4.7). Although this is an improvement over the compression observed in the primary peak, much of the input field energy remains in the primary peak where it is weakly compressed. Also, with the lower powers the field is less spatially confined and as a result the spatial spreading of the peak obscures the splitting of the pulse. But, as with the primary peak, the split pulses are compressed further still to less than 1/3 of the input pulse width at $\xi = 0.1$.

The results of filtering the field of fig. (4.10) are summarized in fig. (4.13) where we plot the temporal FWHM of the field transmitted through the slit. In cases where the filtering results in a split pulse, the program automatically calculates the width of the peak at the earliest (most negative) τ. The jumps in the graph occur as the field transmitted by the slit evolves from a single, splitting pulse to two separate pulses. There are six distinct features in fig. (4.13) corresponding to the different structures in the field. The slowly increasing curve from ξ -3 to -0.8 is a result of the slit transmitting the weak tertiary peak discussed previously. The pulses transmitted by the slit in this region have such little energy as to be of no immediate practical interest. As the slit passes through the region from ξ -0.7 to 0.3 it transmits the split pulses produced by the curvature and tails of the secondary peak. It is here that the maximum pulse compression is achieved as indicated by the minimum at $\xi = 0.1$. The next region, from ξ 0.5 to 1.6, corresponds to transmission of the unsplit section of the secondary peak. The split and unsplit portions of the primary peak are transmitted by the slit in the regions ξ 1.7 to 2.5 and

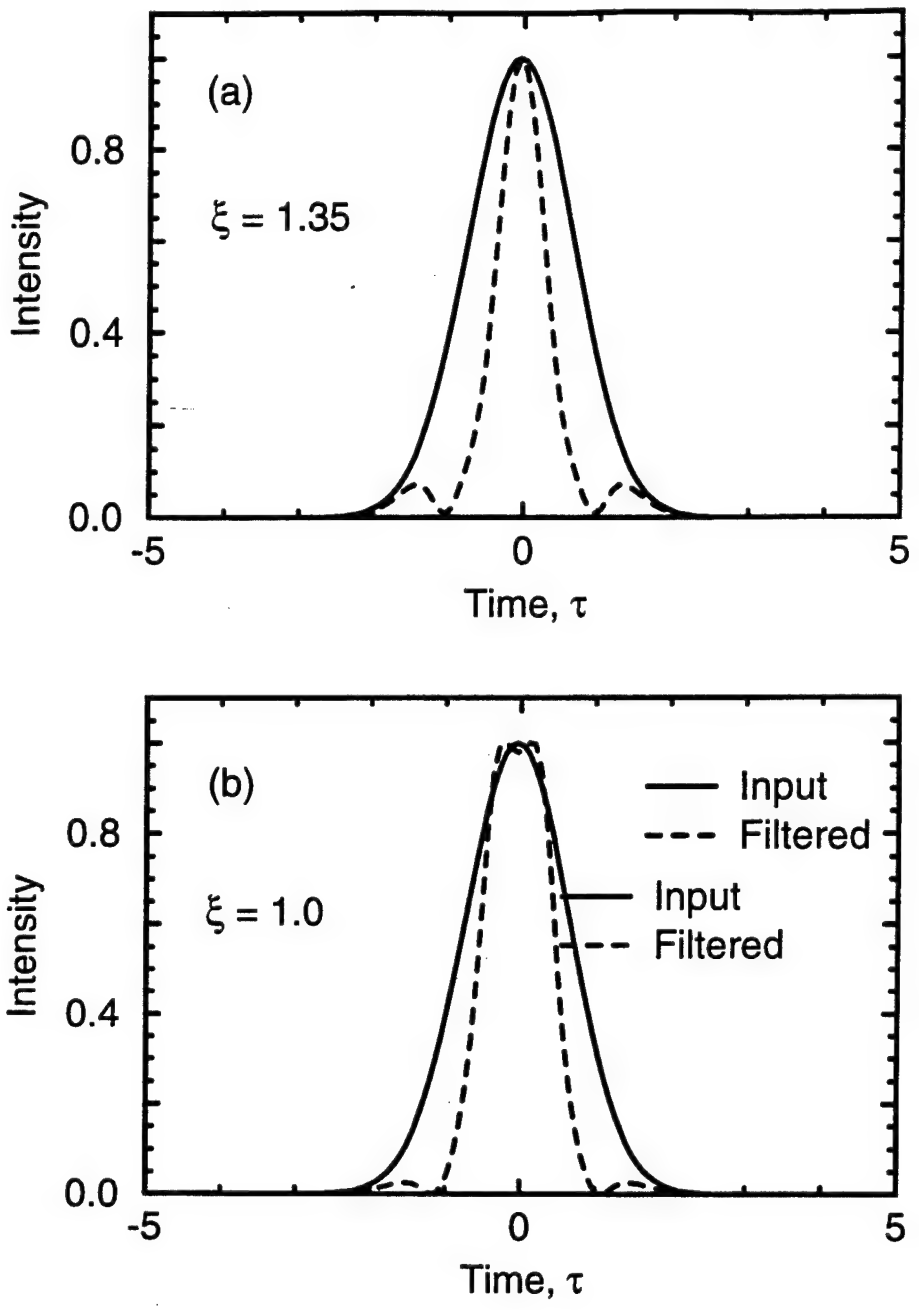

Figure (4.12) Spatially filtering the secondary peak of fig. (4.10) produces similar results to those of fig. (4.11). With a slit placed at (a) $\xi = 1.35$ the pulse is compressed by more than a factor of 2; (b) $\xi =$ the pulse begins to

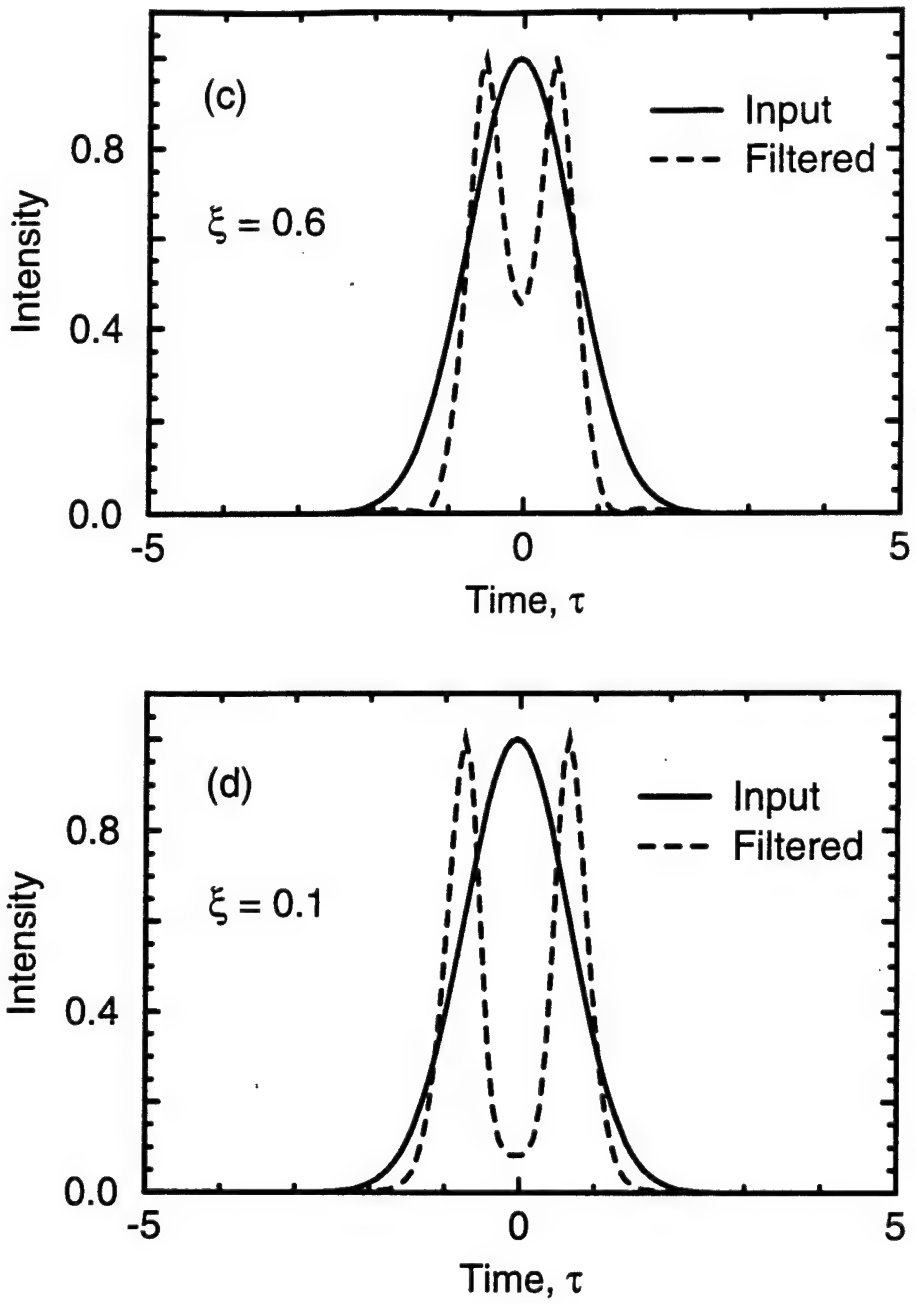

split; (c) $\xi =$ the splitting is more pronounced; (d) $\xi = 0.1$ the split pulses transmitted are compressed by more than a factor of three from the input field.

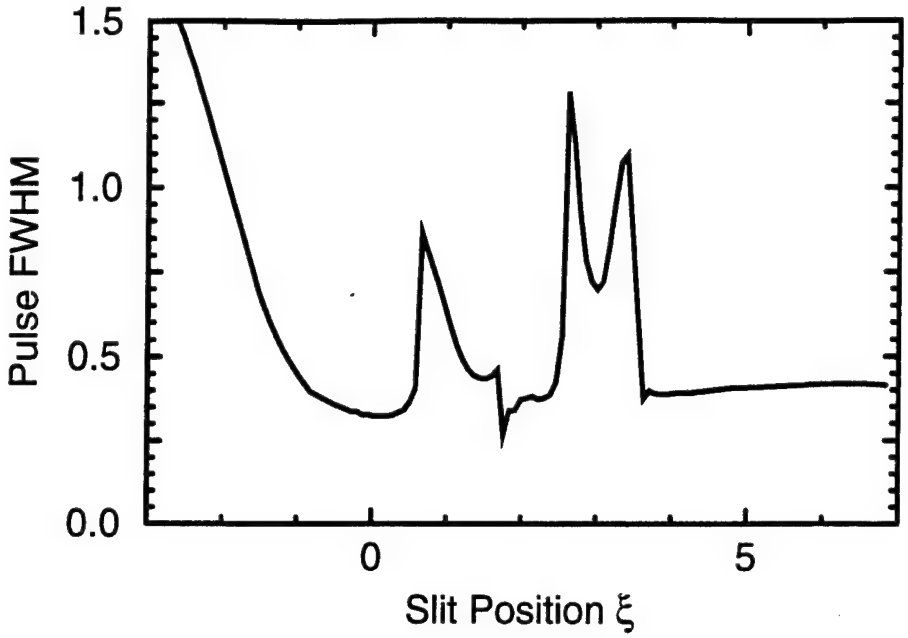

Figure (4.13) We plot the temporal FWHM of the pulse as a function of slit position. The slit is 0.2 times as wide as the input field. As the pulse changes from a single to split pulse there are jumps in the FWHM.

ξ 2.6 to 3.2 respectively. The extreme temporal edges of the input field are so weak that the self-focusing nonlinearity does little to alter their behavior from that described by linear beam steering. Consequently, the diffraction of the field results in a very weak pair of pulses transmitted through the slit in the region ξ >3.4.

Because the pulse compression of the lower power peak is greater, the question arises if it might be more useful to explore spatially filtering a less intense beam and so take advantage of the steeply sloped portion of the upper curve in fig. (4.7). The results of such efforts are shown in fig. (4.14) where we plot the logarithmic intensity countours in ξ and τ at ζ = 1.0 for N = 2 and the same modulation parameters as in figs. (4.11-13). As

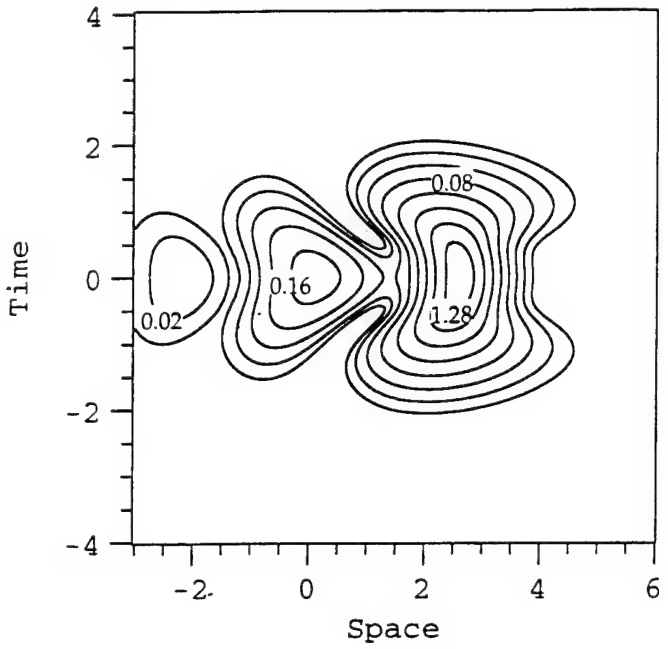

Figure (4.14) A contour plot of the intensity distribution of an initially Gaussian two-dimensional field after spatial phase modulation and propagation to $\zeta = 1$ in a nonlinear medium such that $N = 2$ at the pulse peak at $\zeta = 0$ demonstrates the steering of pulsed beams in the dispersionless [$d = 0$ in eqn. (4.11)] limit. The power dependence of the steering of pulsed beams is observed by comparison with fig. (4.10).

expected from the one-dimensional results, the lower nonlinearity results in a weaker deflection of the secondary peak and more energy in the primary peak. The crescent shape of each peak is also noticeable. In figs. (4.15-16) we see that the effects of propagation and filtering on this field are not as pronounced as in the $N = 3$ case. In particular, the compression of the transmitted pulse is reduced in nearly all cases and the splitting of the pulse is considerably obscured as well. Both effects occur because the lower energy spatial solitons are not as spatially confined as those produced by phase modulating an $N = 3$ beam. The energy at the temporal center of the primary peak may be steered at a greater angle on average than the

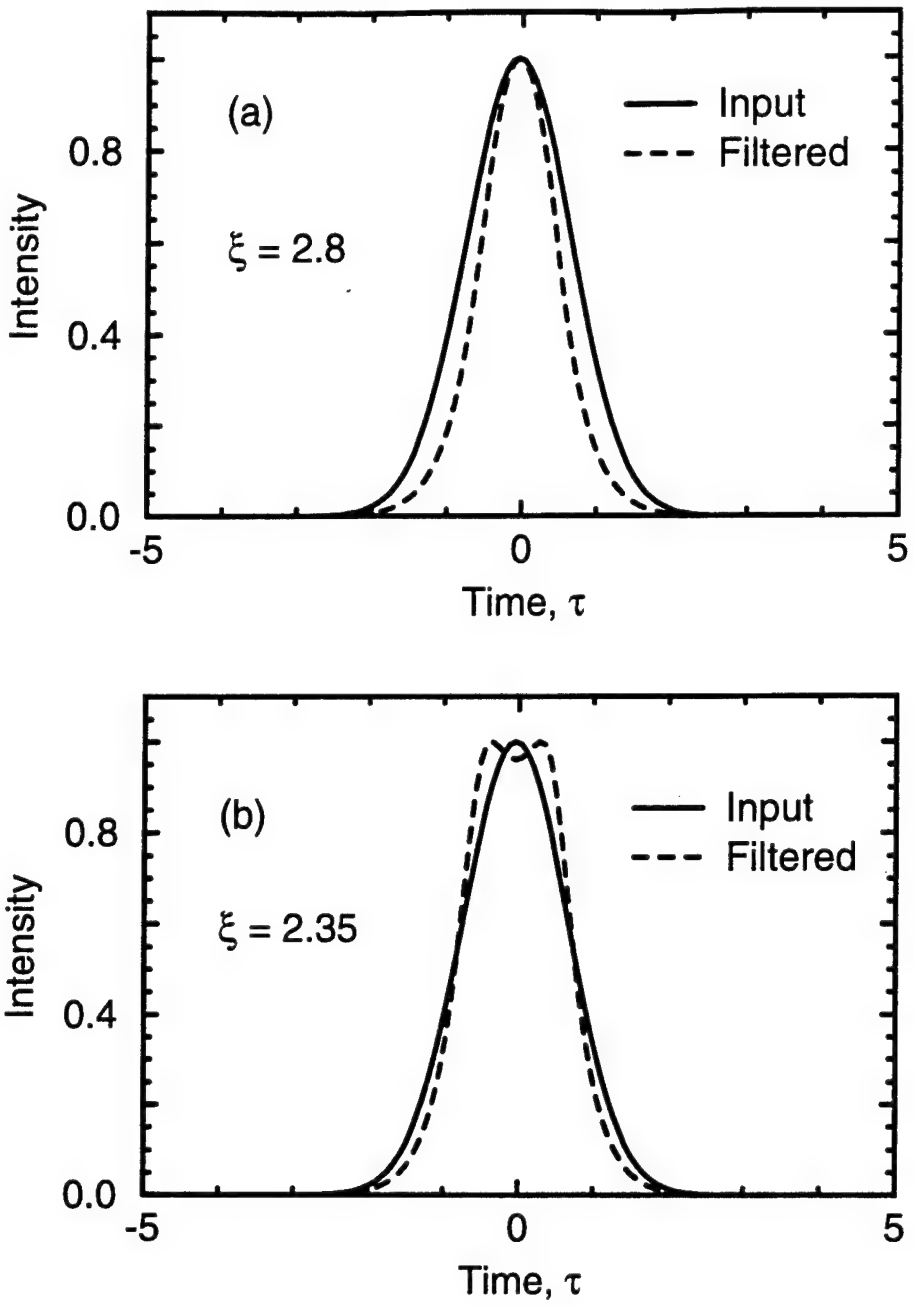

Figure (4.15) The effects on pulse shape of spatially filtering the field of fig. (4.14) with a 0.2 wide slit at the positions indicated. At (a) $\xi = 2.8$ the pulse is compressed to 70% of its input width; (b) $\xi = 2.35$ the pulse begins

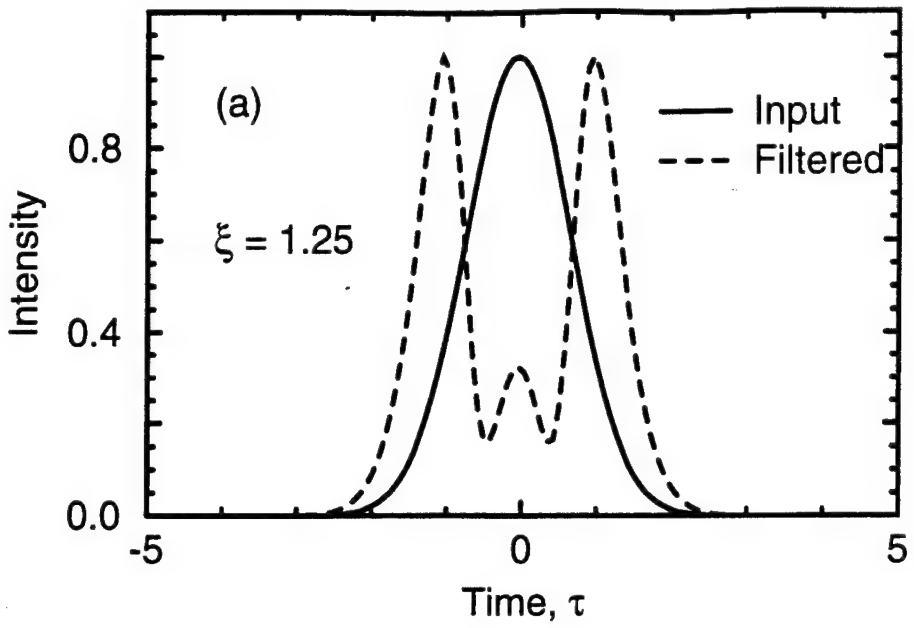

to split; (c) ξ = 1.25 the pulse is completely split and the two pulses are 40% of the input width.

energy in the temporal wings of the peak, but the spatial spreading due to the weaker nonlinearity causes energy from the temporal center to leak through the slit when it is centered in a position designed to capture the split pulse of the tails and vice versa. The former effect results in the splitting being less pronounced, as in fig. (4.15b-c), and the latter results in the center of the pulse being less compressed, as in fig. (4.15a), than in the N = 3 case. These results are summarized in fig. (4.16) where we plot the FWHM of the pulse transmitted by the slit. The tertiary peak is deflected towards $\xi < -3$ consequently its behavior does not affect fig. (4.16), the remaining five regions correspond to those of fig. (4.13) with differences in position and size due to the weaker nonlinearity in this simulation. The results of figs. (4.10-16) are consistent with the general conclusion that

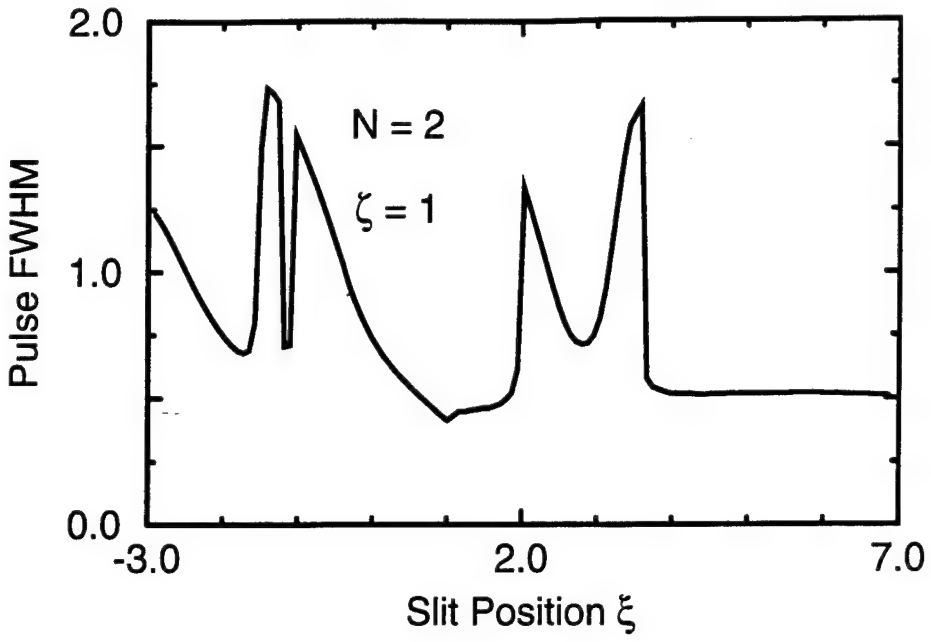

Figure (4.16) We plot the temporal FWHM of the transmitted pulse as a function of slit position. The pulse is produced by spatially filtering the field of fig. (4.14)

greater pulse shaping and shortening is possible as the strength of the nonlinearity is increased.

There are several other parameters affecting pulse shape that are worthy of investigation in the beam steering experiment. The slit width affects the results by blurring the lines between the regions of figs. (4.13) and (4.16) as it is increased. A larger slit width also generally transmits a broader pulse. The distance of propagation in the nonlinear medium also plays an important role. A greater propagation distance affects the transmitted pulse in two ways. First, since the intensity determines the steering angle, the greater the propagation distance the smaller range of intensities transmitted by a given slit position and width. We illustrate this in fig. (4.17) where we plot the field of fig. (4.10) after it has propagated

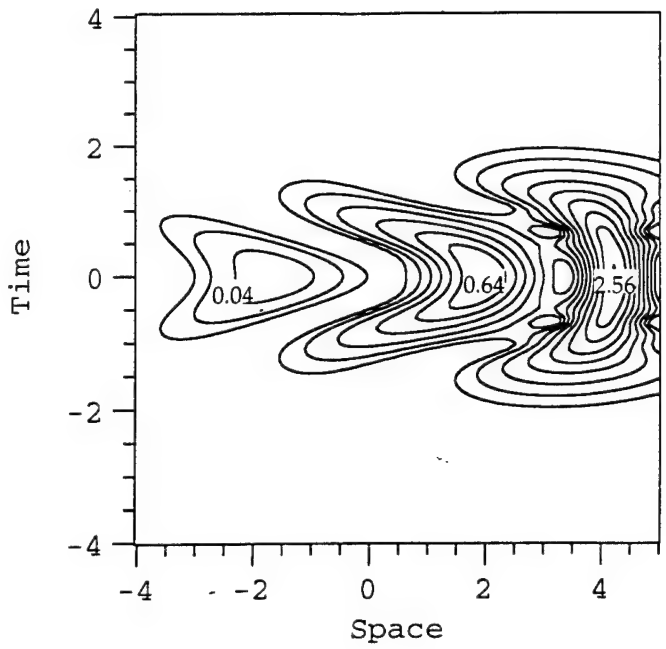

Figure (4.17) The field of fig. (4.10) (N = 3, ϕ_0 = 2.405, p = 0.2, δ = 0) after propagating to ζ = 2. The different steering angles produced by the interaction of the sub-beams after the reaction has had a more dramatic effect on the field structure than in fig. (4.10).

an additional diffraction length. Note that the curvature of the peaks, the secondary peak in particular, are now much more pronounced. Filtering of this field with the same slit used to produce fig. (4.13) produces fig. (4.18) which indicates a general improvement in pulse compression over the range of slit positions. There is again a trade-off with less energy being transmitted in proportion to the improved compression. The second effect of the increased propagation distance is more subtle and only applies to higher intensity (N > 3) fields. Spatial solitons of greater than fundamental (N > 3/2) order undergo oscillations in their spatial width as they propagate. When the peak intensity of the input pulse is such that some portion of the primary steered peak is intense enough to support

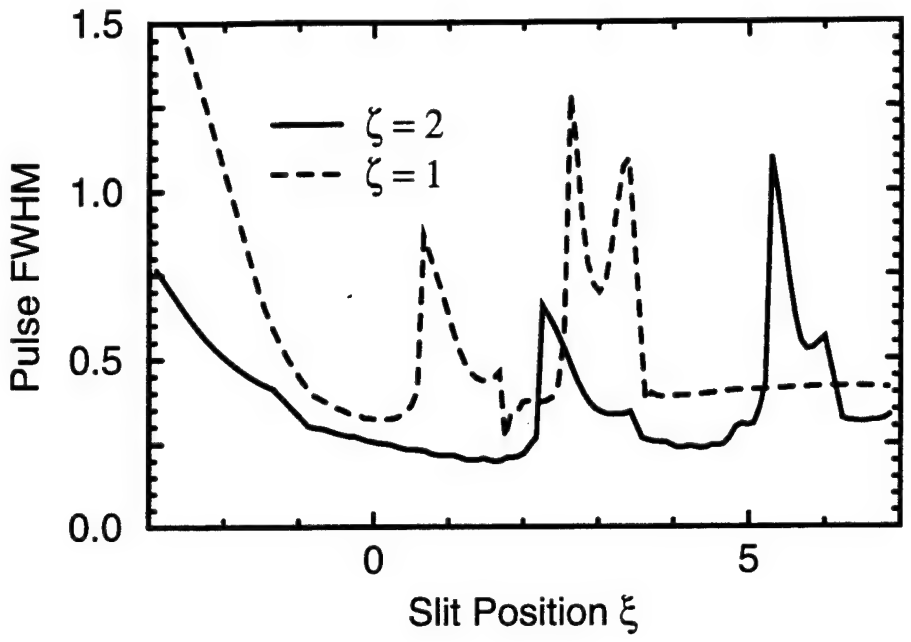

Figure (4.18) The temporal FWHM of the field produced by filtering the field of fig. (4.17) with a slit, as a function of slit position. The result is a greater pulse compression throughout when compared to fig. (4.13).

greater than fundamental order solitons, the oscillations in the spatial width of the temporal center of the primary steered peak will produce nonuniform changes in the pulse width transmitted by a slit placed near the primary peak. These oscillations are responsible for the fluctuations near $\xi = 2.0$ in fig. (4.13) as well as the ripples visible near $\xi = 6$ in fig. (4.18).

The improvement of the pulse compression with increased nonlinear propagation speaks to the reliability of this scheme versus one using only the nonlinear medium to shape the pulse (as discussed in chapter 3). This is further borne out by an investigation of the instantaneous optical phase of the wave as it propagates. In fig. (4.19) we plot the phase of the wave of fig. (4.10). There are several points to be

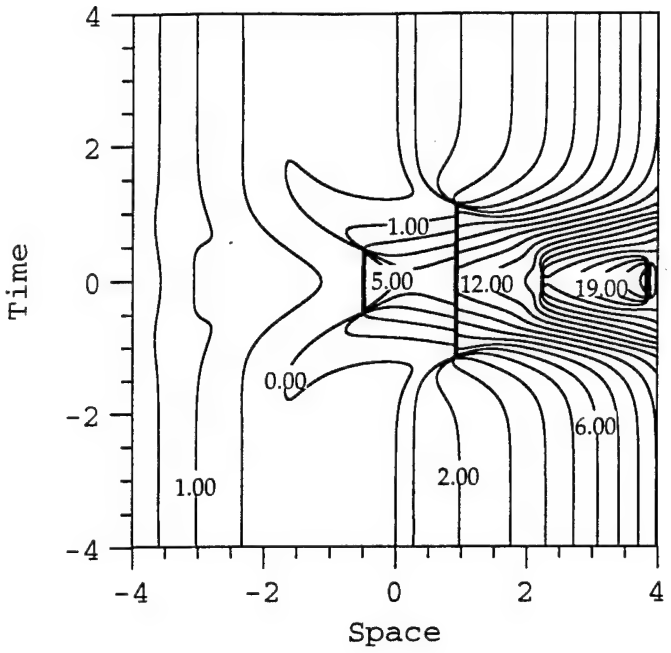

Figure (4.19) The phase distribution of the field of fig. (4.10). The range of the function has been extended from (-π,π) to (-2, 23) for the data shown here. The contours are equally spaced 1 radian apart. The discontinuities occur when the field of fig. (4.10) passes through zero.

made about fig. (4.19). First, to improve readability the range of the phase has been extended to (-2, 23). Nonetheless there are still several discontinuities [at $(\xi, \tau) = (0.9, \pm 1.2)$ e.g.] in the phase at the points where the field strength passes through zero. Second, although there are several regions with both large spatial and temporal phase curvatures, there are also several in which the spatial phase variation is nearly linear. If we plot the derivative of the phase with respect to position ξ along the line $\tau = 0$, as in fig. (4.20) we see that these regions which have nearly linear phase variation ($\partial\phi/\partial\xi \approx$ constant) coincide with some of the optimum slit positions for pulse compression. Moreover, if we repeat the process and plot $\partial\phi/\partial\xi$ at several τ positions, we find that there are regions of nearly

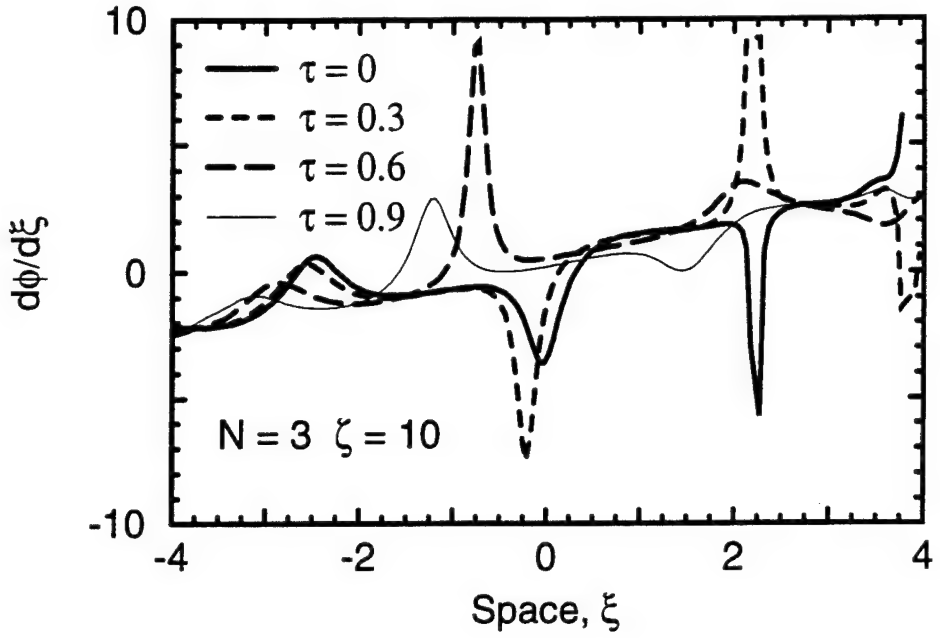

Figure (4.20) To demonstrate the quality of the steered and filtered pulse we plot the spatial derivative of the phase, $\partial\phi/\partial\xi$, at several values of τ. Note that in the region near $\xi = 2.9$ the derivative is nearly constant at all values of τ.

linear spatial phase which do not change position significantly with local time, τ. Thus, with this arrangement, no special (i.e. non-physical) collection optics are required to recollimate the beam after steering and compression. The pulses are, however, temporally phase modulated as indicated in fig. (4.21) which shows the phase of a pulse transmitted by a slit positioned at $\xi = 2.9$ for the field of fig. (4.10). For a dispersionless medium, the transmitted pulse will always be upchirped so with the addition of a linear yet anomalously dispersive medium following the slit the pulses could be further compressed.

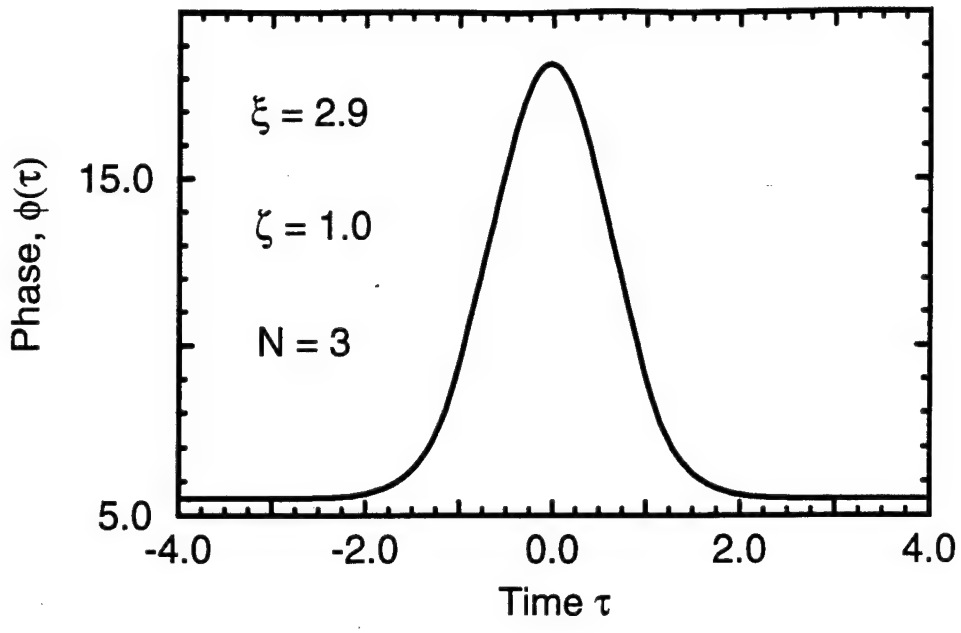

Figure (4.21) The temporal phase distribution of a pulse transmitted by filtering the field of fig. (4.10) with a slit placed at $\xi = 2.9$. The pulse is upchirped.

The modulation parameters can also be expected to change the pulse shaping effects of the proposed arrangement. The influence of the modulation parameters on the pulse shaping is best understood by considering their influence on the sub-beams of the expansion of eqn. (4.3). As we showed in the discussion of linear beam steering, a smaller modulation frequency will result in greater overlap and thus greater interaction among the beamlets which should increase the dependence of the steering angle on the nonlinearity. But since the steered angle is smaller with the smaller frequencies, a greater propagation distance is required to take full advantage of the greater sub-beam interaction. Conversely, a higher modulation frequency will result in a

weaker sub-beam interaction but a greater steered angle which in turn requires a smaller propagation distance for effective pulse shaping. Changes in the modulation amplitude have a related effect. A low modulation amplitude excites only a few sub-beams with small transverse momenta, which necessarily have a large percentage of the field power. The effect is similar to that produced by using a small modulation frequency. Conversely, large modulation amplitudes excite beamlets with larger transverse momenta thus directing the steered peaks at greater angles and producing a weaker interaction, all of which is similar to the effect produced by a higher modulation frequency. At present the complexities of the problem have frustrated attempts to arrive at an analytical determination of the optimum modulation parameters for pulse compression and shaping. Determination of the optimum parameters is then left to continued numerical exploration of the parameter space or laboratory experimentation.

4.3.2 Pulsed Beam Steering with Dispersion

The next issue to address is how the pulse behavior changes due to the presence of dispersion. Dispersion must be considered in the model when we are considering pulses less than 10 ps in beams narrower than a few millimeters. To describe pulsed beam steering in the presence of dispersion, we must resort to the two-dimensional NSE, eqn.(2.50),

$$i\frac{\partial u}{\partial \zeta} = -\frac{1}{2}\frac{\partial^2}{\partial \xi^2}u + \frac{d}{2}\frac{\partial^2}{\partial \tau^2}u - \mathrm{sgn}(n_2)\,N^2\,|u|^2 u\,. \qquad (4.11)$$

We can perhaps combine the understanding created in the previous section with that of Chapter 3 to predict the behavior of the optical field under these conditions. We expect that anomalous dispersion will enhance the pulse compression and pulse shaping somewhat while normal dispersion will suppress them. The most important issue is the extent of the change produced by the nonlinear spatiotemporal coupling. Cao et al.[15] have also produced some interesting results for the behavior of the entire field when it is governed by this equation, however the clearest picture of the pulse/sub-beam dynamics comes from continued numerical simulations.

The most illustrative way to investigate the influence of dispersion on the pulse shaping effects of Raman-Nath beam steering is to measure how a small amount perturbs the dispersionless results. As observed in chapter 3, two-dimensional pulse propagation in a self-focusing anomalously dispersive medium can lead to wave collapse. Consequently, when we model beam steering in this regime we are limited to either shorter propagation distances or very small amounts of anomalous dispersion. Conversely, a significant amount of normal dispersion interacting with a self-focusing nonlinearity leads to a rapid broadening of the pulse. The pulse-compression technique proposed here is not strong enough to overcome significant broadening. We will thus limit our discussion to regimes of pulse propagation best described as weakly dispersive, such that $|d| < 0.5$ in eqn. (2.50).

In the previous section we demonstrated just how important the lateral transfer of energy can be to the temporal shape of the field. Although the dispersion is weak, working in concert with the nonlinearity, it provides a mechanism for the longitudinal transfer of

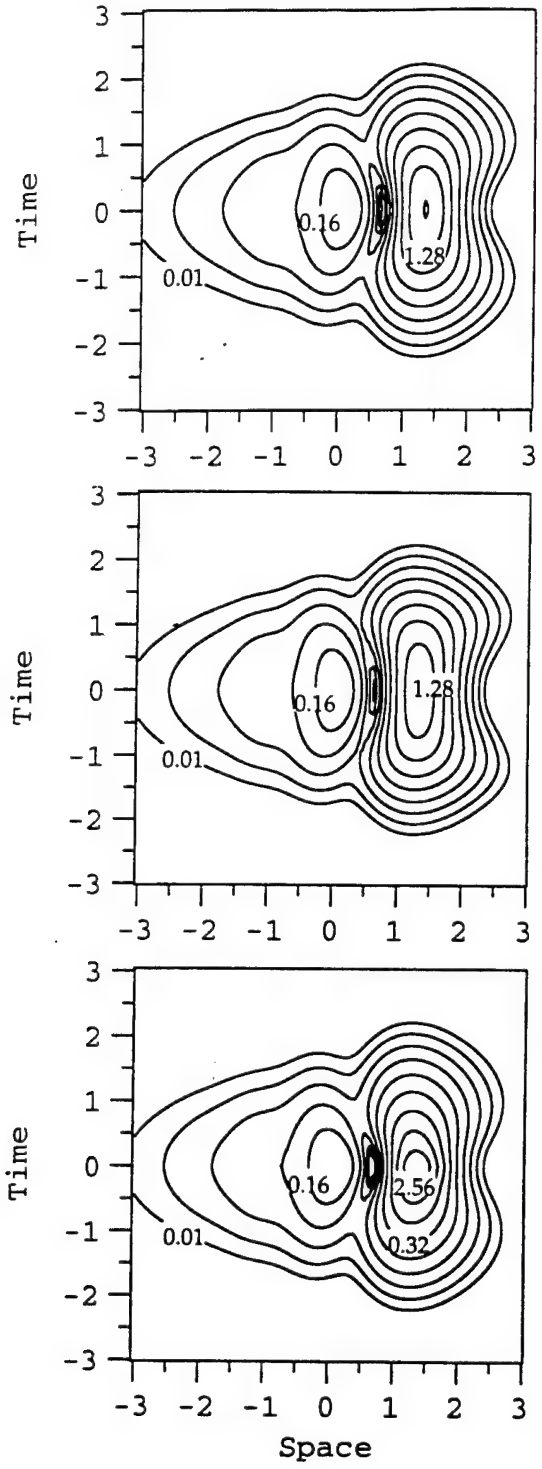

Figure (4.22) We illustrate the effect of dispersion on the pulse shaping with contour plots of the field at $\zeta = 0.5$ for an initially N = 2 input Gaussian field. In (a) we show the dispersionless limit for comparison to (b) the weakly normally dispersive case [d = 0.2 in eqn. (4.11)] and (c) the weakly anomalously dispersive case (d = -0.2). The compression is reduced in the former and enhanced in the latter.

energy within the wave in much the same fashion as the diffraction provides for lateral transfer. In figs. (4.22) we see how much stronger the influence of dispersion is on the pulse shape. In fig. (4.22a-c) we plot the intensity of the field as a function of ξ and τ at $\zeta = 0.5$ for an initially Gaussian field with an input intensity such that N = 2 in eqn. (2.50) and dispersion parameters d = -0.2,0.0 and 0.2 respectively. As we might infer from chapter 3, in the normally dispersive case (d = 0.2) the pulse splitting is enhanced and in the anomalously dispersive case (d = -0.2) the pulse compression is enhanced. What is most astonishing about these plots is the degree to which this relatively weak dispersion qualitatively affects the outcome of the simulation. The quantitative differences are significant as well. In fig. (4.23) we plot the temporal FWHM as a function of slit position for the three cases in fig. (4.22) and two more intermediate cases ($d = \pm 0.1$). We find that these results bear out our intuition. In the region $\xi = 0.7$ to 1.7 the pulse compression is enhanced due to the anomalous dispersion and suppressed due to the normal dispersion. When the slit is positioned slightly closer to the initial propagation direction at $\xi = 0.7$ to 0.8, we find that the split pulses produced by spatial phase modulation and filtering will be roughly equal in duration for both types of media at this propagation distance. The compressive behavior of the primary peak is repeated in the secondary peak (selected by the slit positioned at $\xi = -0.6$ to 0.6) where again the pulses in the anomalous medium are more compressed than in the normal medium. The variation in pulse widths at this peak is much smaller than in the primary peak because the lower power leads to less nonlinear temporal compression (anomalous) or broadening (normal).

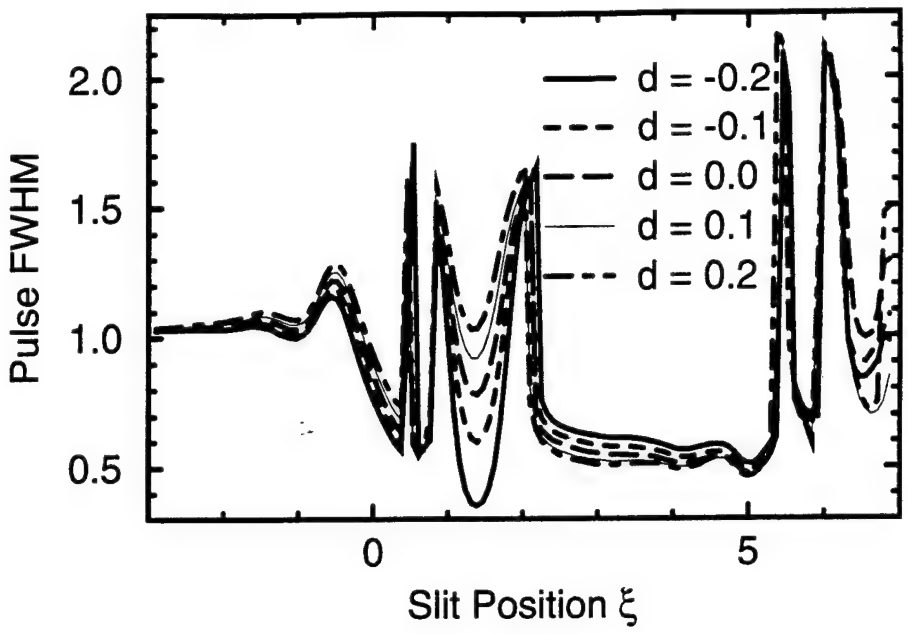

Figure (4.23) To quantify the effect of dispersion on the pulse compression we plot the temporal FWHM of the field transmitted by a slit as a function of slit position for the fields in fig. (4.23) and for the d = ± 0.1 cases as well. The compression is enhanced for the anomalous dispersion and the regions of pulse splitting are made broader by the normal dispersion.

In figs. (4.24a-c) we repeat the above investigation at a higher nonlinearity and a weaker dispersion. The input field intensity is chosen such that N = 3 in eqn. (2.50) and the dispersion parameters are set to d = -0.05, 0.0 and 0.05 respectively. This weak dispersion is necessary because with a nonlinearity this high combined with the focusing influence of the spatial phase modulation the model breaks down in the anomalous dispersion regime due to wave collapse at propagation distances on the order $\zeta = 0.5$ for $d > 0.1$. But even with the weak dispersion used to obtain figs. (4.24a-c) we can observe significant qualitative differences in the field at $\zeta = 0.5$ based on the sign of the dispersion. Again, the anomalous

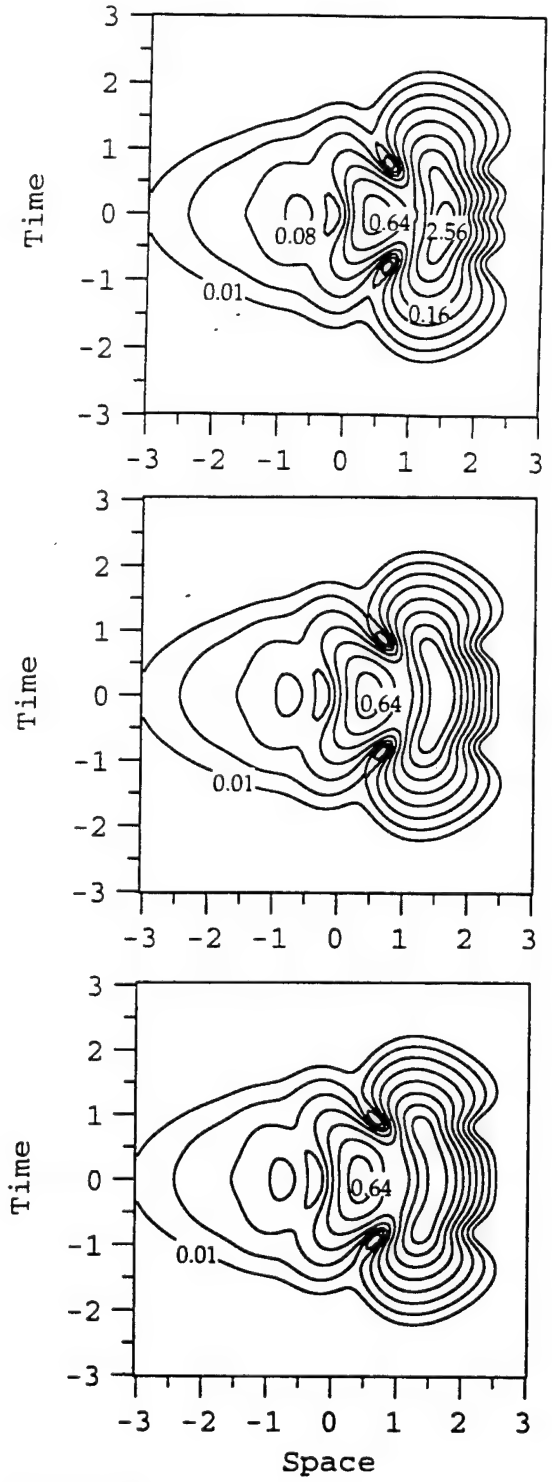

Figure (4.24) To illustrate how the strength of the nonlinearity changes the influence of the spatiotemporal coupling on the pulse shaping we show contour plots of a Gaussian input field with an initial intensity such that N = 3 and dispersion parameters (a) d= -0.05, (b) d = 0 and (c) d = 0.05 after propagating to $\zeta = 0.5$.

dispersion enhances and the normal dispersion suppresses the pulse compression in both the primary and secondary peaks of figs. (4.24). Moreover, the pulse splitting in the normal dispersion regime is more pronounced than in the anomalous dispersion regime. The latter point is more apparent in fig. (4.25) where we plot the FWHM of the pulse transmitted by a slit for the fields of figs. (4.24). We see that the split-pulse compression regime between $\xi = 1.0$ and $\xi = 1.4$ for the $d = 0.05$ case narrows for the $d = 0.0$ case and then disappears when $d = -0.05$. The reason may be inferred from figs. (4.24) but is apparent in fig. (4.26) where we plot the pulses transmitted by a slit at $\xi = 1.2$ in the three cases. As we can see the compressed pulse at the primary spatial peak in the anomalous medium has broad enough spatial wings that they leak energy through the

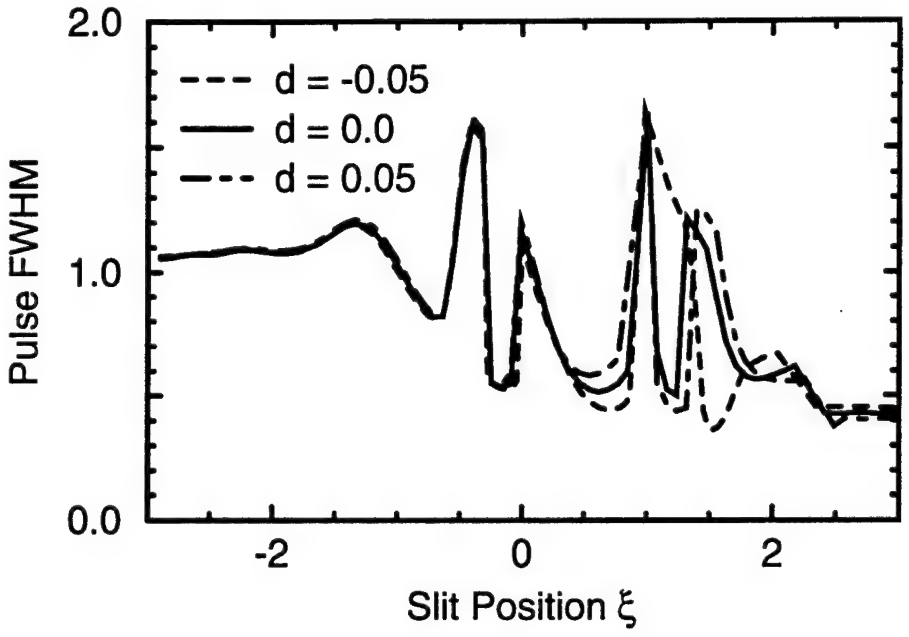

Figure (4.25) The temporal FWHM of the pulse produced by spatially filtering the fields of fig. (4.24) with a slit as a function of the slit position. The anomalous dispersion enhances and the normal dispersion reduces the pulse compression.

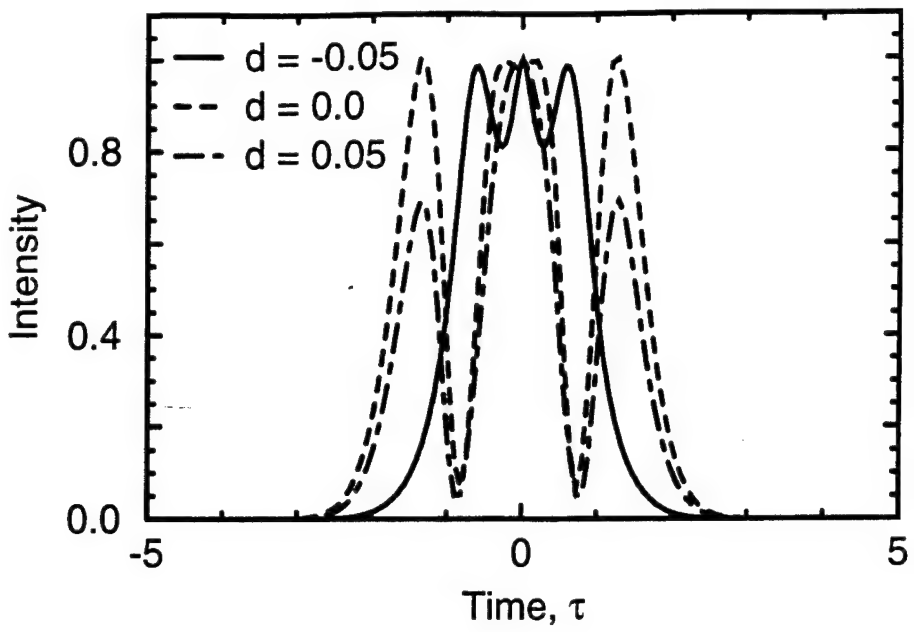

Figure (4.26) The pulses produced by spatially filtering the fields of fig. (4.24) with a slit at $\xi = 1.2$ show the effect of dispersion on the pulse shaping.

slit when it is positioned to capture only the split tails of the pulse. This leakage prevents a complete splitting of the pulse in the anomalous dispersion regime. In the normal dispersion regime, the nonlinear phase accumulation that would split the pulse in the absence of phase modulation moves energy from the temporal peak into the tails as it is deflected. These results are due to the fact that the normal dispersion works with the pulse splitting mechanism created by the spatial phase modulation and slit, whereas the anomalous dispersion works against it.

4.4 Experimental Considerations

In order to translate an optical wave manipulation scheme, such as discussed in the preceding pages, from numerical simulations to laboratory verification, several issues need to be considered. First, we need to consider that in a laboratory there is no savings in experimentation time associated with beam steering in a waveguide or with elliptical beams versus experimentation in bulk media. Indeed, it is generally easier to not have to couple light in and out of a waveguide. Consequently, a question that needs to be addressed is: how will propagation in bulk media affect the beam steering and pulse shaping results discussed here? We can get some idea from our attempts to steer beams in the anomalous dispersion regime. The added dimension of self-focusing implies that the distance of propagation in the nonlinear medium needs to be shortened considerably in order to avoid catastrophic wave collapse. But the same forces driving the wave collapse also drive a stronger interaction of the sub-beams, consequently lengthy nonlinear propagation may not be required for effective beam steering and pulse shaping. We illustrate this with the results of a simulation of beam steering in bulk media in figs. (4.27) in the dispersionless limit. In fig. (4.27a) we plot the two-dimensional slice of the field through $\eta = 0$ after modulation in the ξ-direction with the usual modulation parameters [i.e. $\phi(\xi,\eta,\tau) = 2.405 \sin(0.2\xi)$] and $N = 3$ at the input to the nonlinear medium and propagation to $\zeta = 0.2$. The collapse distance in this case is $\zeta_c \approx 0.3$, consequently the field at this point is dominated by two-dimensional self-focusing. A very compressed pulse could be obtained with a circular aperture centered at $\eta = 0$ and $\xi = 1.2$, but the problems with the output spatial behavior due to the nonlinear phase accumulation discussed in chapter 3 are present as indicated by the far-

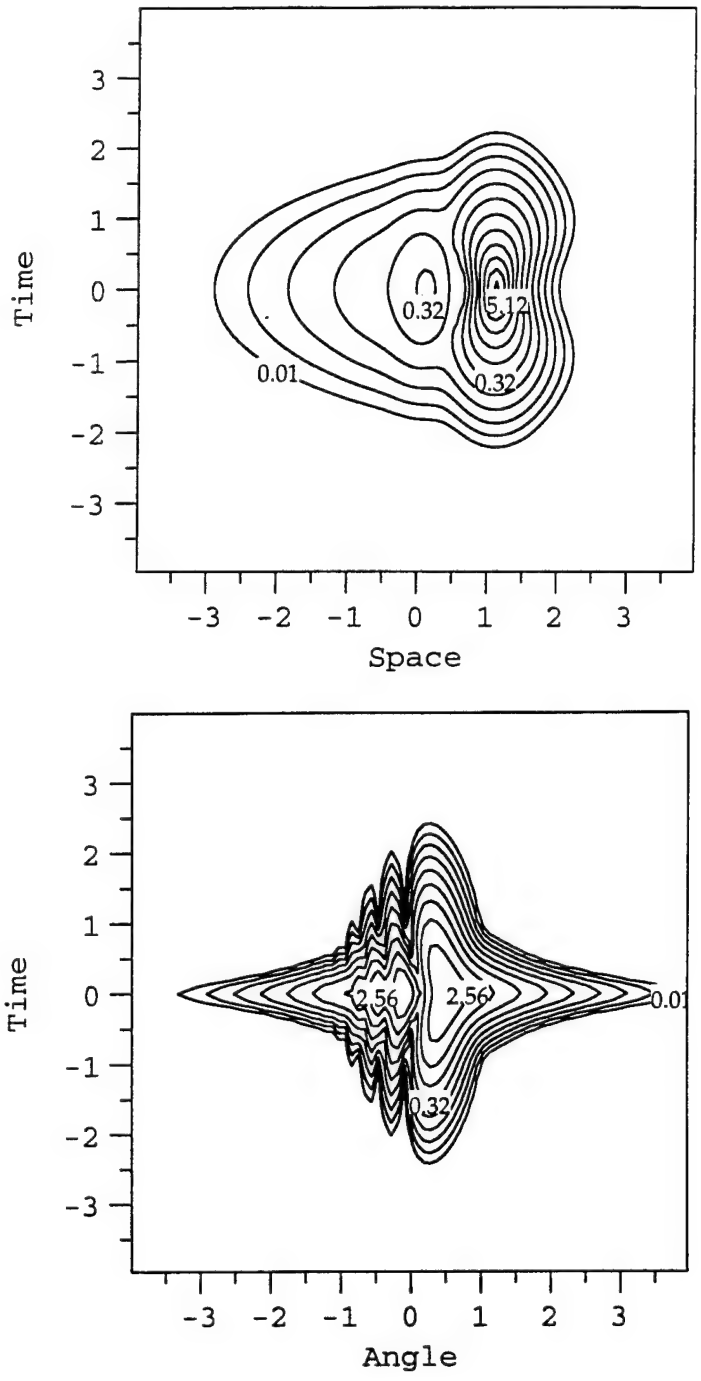

Figure (4.27) The results of a simulation of propagation in bulk media with the input intensity N = 3. (a)The intensity distribution of the field in the plane $\eta = 0$ after propagation to $\zeta = 0.2$. . The logarithmic contour lines are necessary in this case in order to be able to see even the secondary peak as the primary peak is very large due to the self-focusing in the η direction. (b) The far-field intensity distribution indicates the problems that arise due to spatial self-focusing.

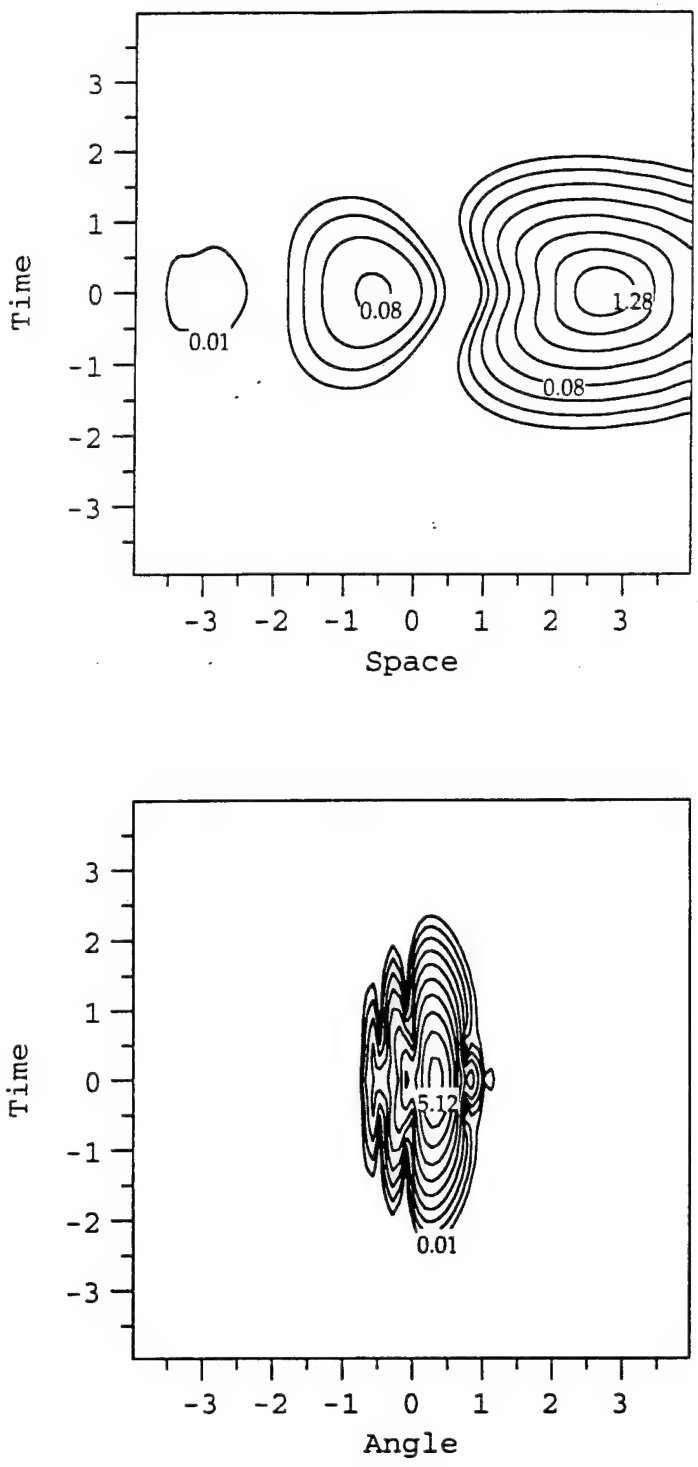

Figure (4.28) Propagation in bulk media with an N = 2 input field. (a) The weaker nonlinearity results in a weaker pulse shaping, but (b) the far-field is better behaved.

field intensity distribution shown in fig. (4.27b). In order to have a manageable spatial phase distribution at the output of the medium, we must choose an input field weak enough that the two-dimensional spatial self-focusing does not dominate the field behavior, yet strong enough that the nonlinear sub-beam coupling can still play an important role. In figs. (4.28) we see the effects of steering a field with an input intensity such that N = 2. As we observed in the (spatially) one-dimensional simulations, the sub-beam coupling (and consequently the pulse shaping) is weaker here as indicated by the less-pronounced temporal curvature of the peaks in fig. (4.28a). Yet the spatial-self-focusing is no longer dominant at this power level as indicated by the well-defined peaks of the far-field intensity distribution shown in fig. (4.28b).

The next issue to address is the light source. As an example let us compare the pulses from an actively modelocked Nd:YAG laser and those from a self-modelocked Ti:Sapphire as possible sources. A modelocked Nd:YAG laser may produce pulse of 60 ps duration with 60 μJ per pulse. For a collimated beam with a 100 μm diameter, the peak intensity would be on the order of $5\text{x}10^{10}$ W/cm^2. Thus, for this field a nonlinear index of $n_2 = 2\text{x}10^{-16}$ cm^2/W would be required to produce an N = 1 input field. The effect of dispersion in this case would be negligible since this type of pulse propagating in glass would have a dispersion length of 180 km compared to 2.2 cm for the diffraction length. With a Ti:Sapphire pulse the numbers are somewhat different. Such a pulse typically has an energy of 5 nJ and a duration of 30 fs for a peak power of 167 kW. Collimated into a 100 μm beam it would require a nonlinear index $n_2 = 7\text{x}10^{-16}$cm^2/W to produce an N = 1 pulse. Further, in this case the pulse would have a dispersion length of 3 cm in glass, which means d ≈ 0.95 for this field.

Although both lasers can produce sufficient intensity for the observation of these pulse shaping effects, the negligible dispersion associated with the Nd:YAG pulses make this laser the better choice.

4.5 Conclusions

In this chapter we have discussed the effects of sinusoidal spatial phase modulation on optical wave propagation in nonlinear dispersive media. We showed how this type of modulation breaks the input beam into a series of overlapping sub-beams. In the case of linear media we showed the effects of the various modulation parameters on the sub-beam behavior and we noted that there is a range of modulation frequencies for which the sub-beams always overlap. For this range of modulation frequencies the beam shape is a result of interference among the overlapping sub-beams rather than the sub-beams themselves. We then discussed beam steering in this modulation regime in nonlinear media. We showed that because of the nonlinearity the position of the peaks created by the sub-beam overlap is peak-intensity dependent. Thus when pulses are modulated, their deflection becomes time dependent. Employing a slit for filtering then allows us to shape the pulse. Thus the combination of spatial phase modulation, filtering and nonlinearity gives us some control over the time-domain behavior. Hence, we have spatiotemporal coupling even in the absence of dispersion. When we included dispersion in the simulations, we found that this coupling still exists but is much weaker than that provided by the dispersion interacting with the nonlinearity. We showed that for dispersion parameters $|d| > 0.1$ the dispersive effects overwhelmed the pulse shaping influence of the

spatial phase modulation and filtering. Although the initial simulations were performed for a waveguide geometry, we found that simulations in bulk media produce new challenges. In particular, in order for this mechanism to be effective the intensity of the input field must be chosen carefully so as to avoid the problems due to spatial self-focusing. We also showed that because of the possible dominance of dispersive effects it would be more advisable to use pulses from a Nd:YAG laser rather than those from a Ti:Sapphire laser in this experiment. The large dispersive effects obtained with the ultrafast pulses (20-40 fs) coming from a Ti:Sapphire laser are the subject of the next chapter.

4.6 References

1. Y. Li, D. Y. Chen, L. Yang, R. R. Alfano, "Ultrafast all-optical deflection based on an induced area modulation in nonlinear materials," Opt. Lett. **16**, 438 (1991)

2. A. C. Boccara, D. Fournier, W. Jackson, and N. M. Amer, "Sensitive photothermal detection technique for measuring absorption in optically thin media," Opt. Lett. **5**, 377 (1980)

3. W. B. Jackson, N. M. Amer, A. C. Boccara, and D. Fournier, "Photothermal deflection spectroscopy and detection," Appl. Opt. **20**, 1333 (1981)

4. A. L. Smirl, T. F. Bogess, J. Dubard, and A. G. Cui, "Single and multiple beam nonlinear absorption and refraction measurements in semiconductors," Proc. Soc. Photo-Opt. Instrum. Eng. **1307**, 251 (1990)

5. A. W. Snyder, A. P. Sheppard, "Collisions, steering, and guidance with spatial solitons," Opt. Lett. **18**, 482 (1993)

6. P. V. Mamyshev, A. Villeneuve, G. I. Stegeman, J. S. Aitchison, "Steerable optical waveguides formed by bright spatial solitons in AlGaAs," Electron. Lett. **30**, 726 (1994)

7. B. Luther-Davies, X. Yang, "Steerable optical waveguides formed in self-defocusing media by using dark spatial solitons," Opt. Lett. **17**, 1755 (1992)

8. W. Goltsos, M. Holz, "Binary micro optics: an application to beam steering," SPIE **1052**, 131 (1989)

9. F. Vasey, F. K. Reinhart, R. Houdre, J. M. Stauffer, "Elecrto-optic AlGaAs spatial light deflector/modulator based on a grating phased array," Appl. Phys. Lett. **58**, 2874 (1991)

10. S. Zhou, P. Yeh, and H.-K. Liu, "Dynamic two-dimensional beam-pattern steering technique," Opt. Lett. **18**, 843 (1993)

11. A. J. Stentz, M. Kauranen, J. J. Maki, G. P. Agrawal, and R. W. Boyd, "Induced focusing and spatial wave breaking from cross-phase modulation in a self-defocusing medium," Opt. Lett. **17**, 19 (1992)

12. A. Barthelemy, C. Froehly, S. Maneuf, F. Reynaud, "Experimental observation of beams' self-deflection appearing with two-dimensional spatial soliton propagation in bulk Kerr material," Opt. Lett. **17**, 844 (1992)

13. A. Dreischuh, E. Eugenieva, S. Dinev, "Pulse shaping and shortening by spatial filtering of an induced-phase-modulated probe wave," IEEE J. of Quant. Electron. **30**, 1656 (1994)

14. A. T. Ryan, G. P. Agrawal, "Steering of optical beams in nonlinear Kerr media by spatial phase modulation," Opt. Lett. **18**, 1795 (1993)

15. X. D. Cao, D. D. Meyerhofer, G. P. Agrawal, "Optimization of Optical beam steering in nonlinear Kerr media via spatial phase modulation," J. Opt. Soc. Am. B **11**, 2224 (1994)

16. R. W. Boyd, *Nonlinear Optics*, (Academic Press, San Diego, 1992)

Chapter 5

Spatiotemporal Coupling in Z-scan Measurements of Optical Nonlinearities

5.1 Background

Throughout this thesis we have been attempting to describe the unique behavior of ultrashort optical pulses in the presence of the Kerr nonlinearity, or intensity-dependent index of refraction. Quantitative experimental verification of any of the effects described in previous chapters necessarily includes an accurate measurement of the nonlinear index, n_2, of the material in which the experiment is to be performed. Recently, the Z-scan measurement, a relatively simple technique for determining the nonlinear index of a material was introduced by Sheik-Bahae et al.[1] The basic idea is to measure the change in the axial transmittance of an aperture in the far-field of a focusing Gaussian beam as the sample being measured is translated through the focus of the beam. For a sample thin enough that the beam does not reshape itself while in the sample, the difference in peak and minimum transmittance is linearly proportional to the nonlinear refractive index.

Since its introduction, several modifications and improvements to the basic technique have been proposed and implemented by both the original authors[1-5] and new workers[6-11] in the field. The consequences of using non-Gaussian beams[6,7] or thicker samples[6,8] have been investigated and demonstrated by several workers. The response time of the optical

nonlinearity has been investigated using pump-probe Z-scans.[4,9] Different beam polarizations have also been employed in the investigation of the anisotropy of the optical nonlinearity.[3,12] The Z-scan technique has been employed in a number of papers as the primary method for characterizing both the nonlinear index and nonlinear absorption of a variety of materials ranging from semiconductor-doped[13] and high-index glasses[12] to polymers,[6] semiconductors[12-15] and composite materials.[6] Proper characterization of these materials requires that the dispersion of the nonlinear index be determined by measurements made at several wavelengths. Frequently the only available light source at a given wavelength consists of ultrashort pulses, in which case the linear index dispersion and the resultant nonlinear pulse reshaping must be considered.

5.2 Theory

The Z-scan apparatus is depicted in fig. (5.1). It consists essentially of a spatially Gaussian beam incident on a lens of focal length F. The beam is focused to a waist, w_0, at which we define the zero of sample position. The typical practice is to measure the sample position in diffraction lengths of the focused beam, defining $Z = z/z_0$ where $z_0 = 2\pi w_0^2/\lambda$ is the diffraction length of the beam with wavelength λ. The "Z-scan" takes placed as the sample is scanned along the axis of the lens through the region about Z = 0. A detector measures the power transmitted through an aperture in the far-field. When the sample is between the lens and the focus, the nonlinear refraction complements the focusing effects of the lens which results in a broader far-field and reduced transmission through the

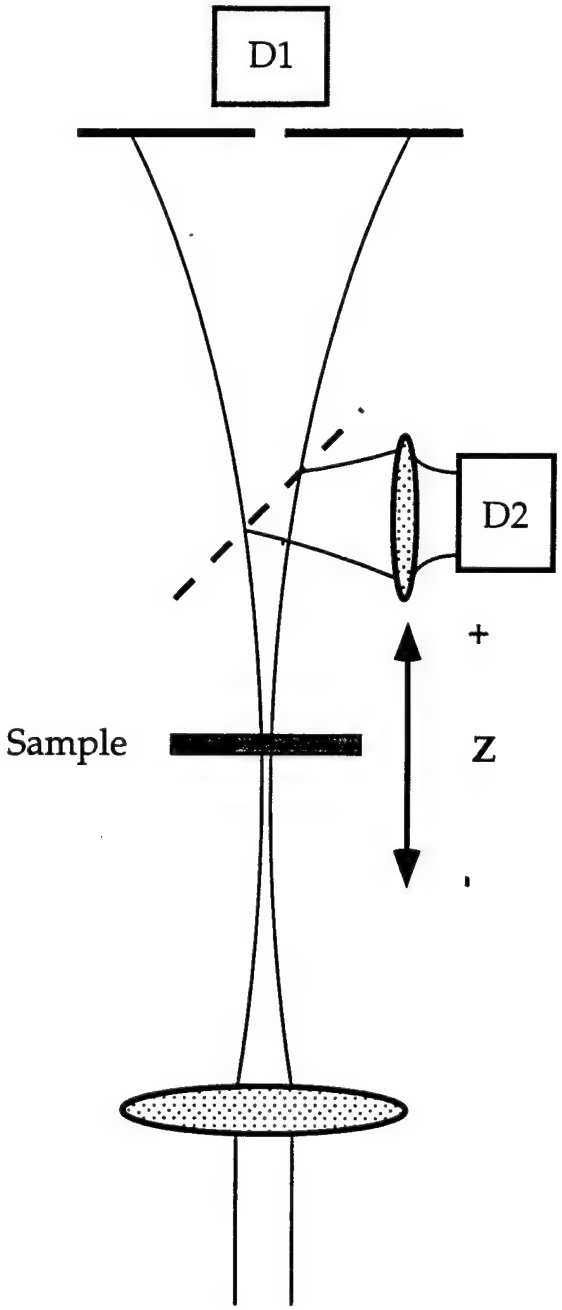

Figure (5.1) The Z-scan experiment is performed when a sample is translated through the focal region (in the 'Z' direction) of an intense beam of light. The effect of the nonlinear refraction in the sample is quantified by detecting the light transmitted through an aperture in the far-field with detector D1. The effect of nonlinear absorption is quantified by measuring the total transmittance of the sample with detector D2.

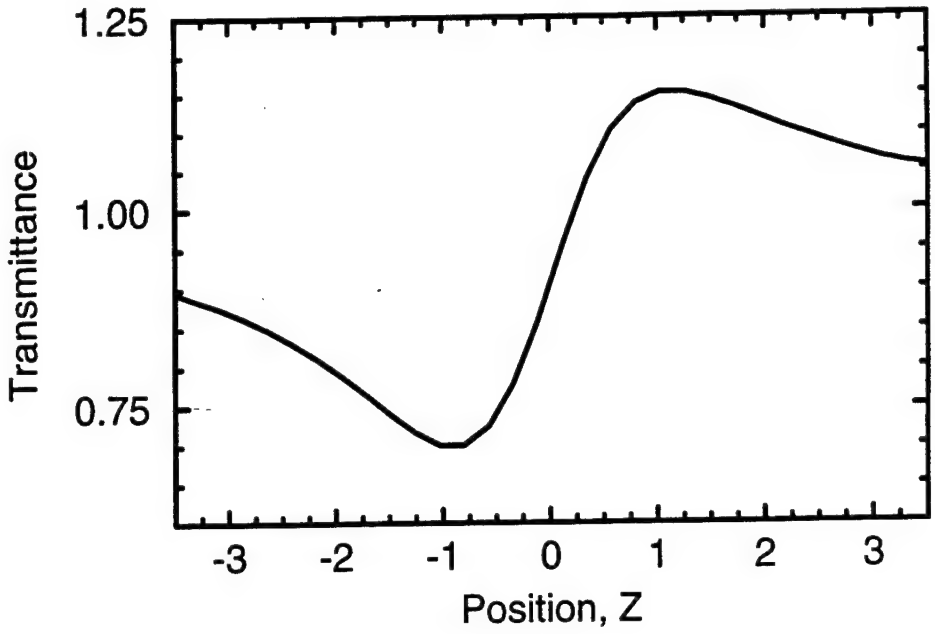

Figure (5.2) A typical closed-aperture Z-scan signal as measured by detector D1 in fig. (5.1). With the sample on the lens-side (Z < 0) of the focus, the nonlinear refraction adds to the phase curvature of the beam, increasing the size of the beam in the far-field. When the sample is on the far side of the focus, the nonlinear refraction reduces the phase curvature of the beam, narrowing the far-field.

aperture. On the far side of the focus the nonlinear refraction narrows the beam, increasing the transmission through the aperture producing the characteristic Z-scan signal depicted in fig. (5.2). For a self-defocusing nonlinearity the sample has the opposite effect and the behavior is reversed. For a sample with nonlinear absorption, we employ an open-aperture Z-scan to determine the nonlinear absorption coefficient, α_2. The effect of opening the aperture allows us to measure the total transmission of the sample as a function of its position. As the sample is translated along Z, the peak intensity of the beam goes through a maximum as does

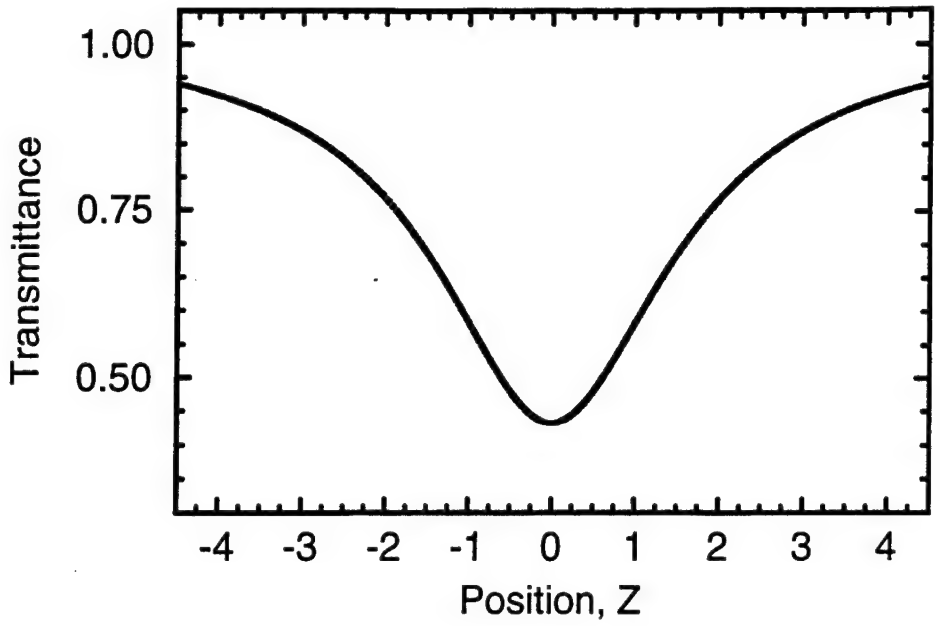

Figure (5.3) A typical open-aperture Z-scan signal as measured by detector D2 in fig. (5.1). As the sample moves through the focus the intensity of the beam increases; thus the light lost due to nonlinear absorption increases as well, as a result the total power transmitted by the sample goes through a minimum at the focus.

the amount of light lost due to nonlinear absorption. Consequently, the measured total transmittance of the sample goes through a minimum with the characteristic shape shown in fig. (5.3). Alternatively, both measurements may be made simultaneously with the aid of a beam splitter as depicted in fig. (5.1) where detector D1 reads the closed-aperture scan and detector D2 measures the open-aperture data.

5.2.1 Analytical Description

One of the chief advantages of the Z-scan technique, as pointed out by Sheik-Bahae et al. in their original paper on the subject,[1] is that the apparatus of fig. (5.1) is simple enough that an analytical description of the signal is possible provided a few simplifying assumptions are made. They found that in order to obtain consistent measurements, generally it was sufficient to constrain the sample length L such that $L < z_0$. They postulated that if the sample is thin enough that the changes in the beam shape within the sample due to both diffraction and nonlinear refraction can be neglected, then the effect of the sample on the field can be treated as an instantaneous, spatially dependent phase shift. The magnitude of the phase shift is dependent on sample position through the relation

$$\Delta\phi_0(Z,t) = \frac{\Delta\Phi_0(t)}{1 + Z^2} \ . \tag{5.1}$$

Here the peak phase shift $\Delta\Phi_0(t)$, as derived with the slowly varying envelope approximation (SVEA), is related to the nonlinear index, n_2, peak intensity at the focus, $I_0(t)$, and wave number, k, via the relation

$$\Delta\Phi_0(t) = k\, n_2\, I_0(t)\, L_{eff} \tag{5.2}$$

where $L_{eff} = [1 - \exp(-\alpha_0 L)]/\alpha_0$ is the effective length of the sample and α_0 is the linear loss. The spatial dependence of the phase of the light exiting the sample is determined by the spatial dependence of the intensity. For a spatially Gaussian beam, the beam decomposition method of Weaire et al.[16] is used to derive the intensity distribution at an aperture in the far-field. The Z-scan signal for a given sample position is then calculated by

integrating the far-field intensity distribution so derived, over the area of the aperture. A typical result is shown in fig. (5.2). The most important features of the Z-scan signal are the peak and valley. From their positions relative to the focus we can immediately obtain the sign of n_2. The authors of ref. 1 also noted that for a cubic nonlinearity the peak-valley separation is nearly constant and is given by

$$\Delta z_{p\text{-}v} \approx 1.7\, z_0 . \tag{5.3}$$

The magnitude of the nonlinearity is then obtained from the change in transmittance between the peak and the valley. For small phase distortions and small apertures, the change in transmittance is nearly linearly related to the peak axial phase shift

$$\Delta T_{p\text{-}v} \approx 0.406\, |\Delta\Phi_0|, \tag{5.4}$$

where the transmittance is normalized so that when the sample is far from the focus the transmittance is one. Thus, once we have measured the peak to valley change in transmittance we can immediately obtain the magnitude of the nonlinearity as well, provided we know the thickness, absorption and linear index of the sample as well as the wavelength and intensity of the beam. In the case of pulsed beams, the intensity is not constant and it becomes necessary to determine the time-averaged index change based on assumptions about the response and decay times of the nonlinearity.

In the presence of nonlinear absorption, the total transmitted energy is not constant with respect to sample position. The nonlinear absorption coefficient, α_2 is defined by the relation,

$$\alpha(I) = \alpha_0 + \alpha_2 I, \tag{5.5}$$

where α is the total absorption coefficient. With the aperture removed, the SVEA can be used to compute the total transmitted power as a function of sample position,

$$P(Z,t) = P_i(t)\exp(-\alpha_0 L)\frac{\ln[1 + q_0(Z,t)]}{q_0(Z,t)} \tag{5.7}$$

where

$$q_0(Z,t) = \frac{\alpha_2 I_0(t) L_{eff}}{1 + Z^2} \tag{5.8}$$

and $P_i(t) = \pi w_0^2 I_0(t)/2$ is the input power. At large Z, the right-hand-side of eqn. (5.7) reduces to $P_i(t)\exp(-\alpha_0 L)$, thus we define our normalized open-aperture transmittance, $T_{oa}(Z) = P(Z,t)/P_i(t)\exp(-\alpha_0 L)$. In an open-aperture Z-scan $T_{oa}(Z)$ is plotted, displaying the characteristic single-valley behavior shown in fig. (5.3). The depth of the valley can be quickly computed from eqn. (5.7) by setting Z = 0. It is useful to construct the conversion chart of fig. (5.4) based on eqn. (5.7) where we plot $T_{oa}(0)$ as a function of $q_0(0,0)$. For the pulsed case we assume a Gaussian pulse and integrate eqn. (5.7) in time. Once the effective length is computed and the beam intensity is measured fig. (5.4) can be used to quickly obtain α_2 for a given $T_{oa}(0)$.

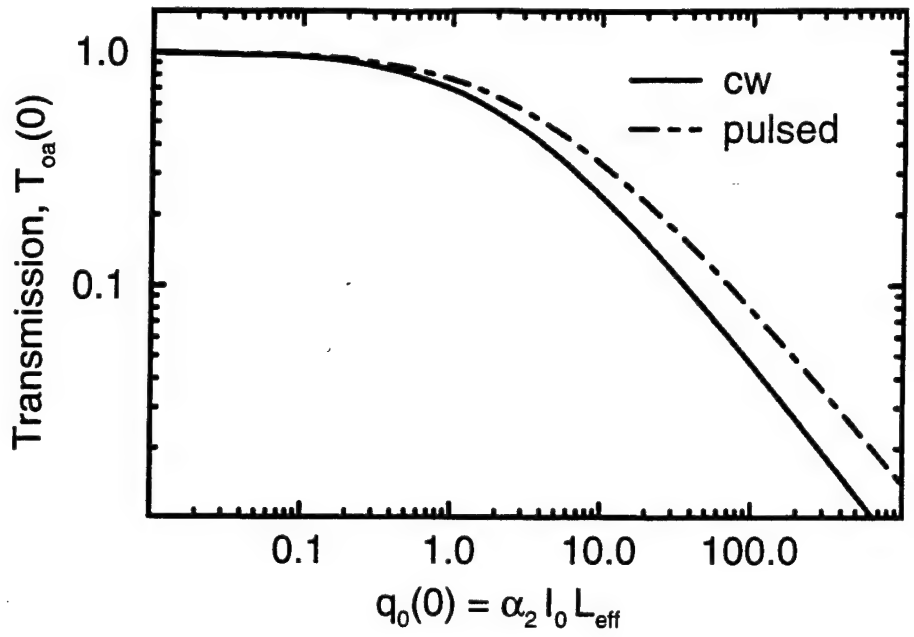

Figure (5.4) The minimum normalized transmittance of an open-aperture Z-scan is dependent on the product of nonlinear loss, α_2, peak intensity, I_0, and effective length, L_{eff} in a logarithmic fashion. The reduced absorption in the pulsed case occurs because the pulse is less intense on average than a cw beam of the same peak intensity.

Determining the nonlinear refraction in the presence of nonlinear absorption is more complicated. In the presence of nonlinear absorption, the SVEA gives the phase shift at the exit of the sample[1] as

$$\Delta\phi(Z,r,t) = \frac{kn_2}{\alpha_2} \ln\left[1 + q(Z,r,t)\right] \tag{5.9}$$

where $q(Z,r,t) = \alpha_2 I(Z,r,t)L_{eff}$. A zeroth-order Hankel transform is used to derive a new more complicated expression for the power transmitted by the far-field aperture.[1] Once the nonlinear absorption is determined from fig. (5.4), it can be used with eqn. (5.9) and the resulting far-field expression

to determine n_2. A simpler technique,[1] although less accurate, is to divide the closed aperture Z-scan (with the background subtracted) by the open aperture Z-scan and treat the resulting data as a purely refractive Z-scan. This is accurate to within 10% provided $q_0(0,0) < 1$ and $\alpha_2/2kn_2 < 1$.

Using the expressions found in Ref. 1 for the field at the aperture, it is a relatively simple procedure to write a computer program to compute the Z-scan for a given beam shape, pulse shape and nonlinear index. Just as it is assumed the beam shape is unchanging due to nonlinear refraction or diffraction, it is also assumed that the pulse shape does not change due to nonlinear self-phase-modulation or dispersion. Although several authors[6,7] have described methods to adapt the analysis for media thick enough to reshape the beam, none have discussed the effects of pulse reshaping in the sample. The criterion $L < z_0$ works well provided the sample dispersion length can be neglected relative to the diffraction length. However, as we have seen in chapter 3 and chapter 4 a modest amount of dispersion can significantly affect the beam shape over distances much less than the diffraction length. Unfortunately, in this case analytical solutions are difficult to obtain and we must return to numerical simulations.

5.2.2 Numerical Simulations of Ultrashort Pulse Z-scans

In order to simulate the Z-scan experiment as performed with beams of ultrashort pulses we adapt the code used to obtain the results of the previous chapters to fit the system described by fig. (5.1). In our normalized coordinates, an input Gaussian field is first spatially phase modulated,

$$u(\xi,\eta,\tau,0) = \exp\left(-\frac{\xi^2+\eta^2+\tau^2}{2}\right)\exp\left[i\phi(\xi,\eta)\right], \tag{5.10}$$

where the phase modulation is now quadratic or lens like such that $\phi(\xi,\eta) = -(\xi^2 + \eta^2)/2f$ with $f = F/L_d$ is the focal length of the lens normalized via the diffraction length L_d of the incident beam. Propagation from the lens to the sample is through air which we can take to be linear and non-dispersive. The field at the sample is then obtained by solving the Helmholtz equation,

$$i\frac{\partial u}{\partial \zeta} = -\frac{1}{2}\left(\frac{\partial^2}{\partial \xi^2}+\frac{\partial^2}{\partial \eta^2}\right)u \tag{5.11}$$

with the Fourier transform method. The solution is simply,

$$u(\xi,\eta,\tau,\zeta) = \frac{\exp(-\tau^2/2)}{\left[1+i\zeta\left(1+\frac{i}{f}\right)\right]}\exp\left\{-\frac{\xi^2+\eta^2}{2}\left[\frac{1+\frac{i}{f}}{1+i\zeta\left(1+\frac{i}{f}\right)}\right]\right\}. \tag{5.12}$$

where ζ is the distance of the sample beyond the lens. Rather than continue with this cumbersome formula, we note that the beam width reaches a minimum at $\zeta_0 = f/(1 + f^2)$ which is related to the incident beam width, σ, by

$$\frac{w_0}{\sigma} = \frac{f}{\sqrt{1+f^2}} \tag{5.13a}$$

and this results in a new diffraction length, z_0 related to the diffraction length before the lens by

$$\frac{z_0}{L_d} = \frac{f^2}{1 + f^2}, \tag{5.13b}$$

respectively. Eqns. (5.13) are then used to obtain a new set of coordinates, normalized to the new beam width and diffraction length. In these coordinates, eqn. (5.12) can be rewritten,

$$u(\xi',\eta',\tau,Z) = \exp(-\tau^2/2)\,\frac{1}{(1 + iZ)}\exp\left\{-\frac{\xi'^2 + \eta'^2}{2}\left(\frac{1}{1 + iZ}\right)\right\}, \tag{5.14}$$

where $\xi' = \xi\sigma/w_0$, $\eta' = \eta\sigma/w_0$ and $Z = (\zeta - \zeta_0)L_d/z_0$ is the same Z used to describe the sample position in the Z-scan measurements.

The field is propagated through the sample using the split-step Fourier method algorithm described in chapter 2. The field at the exit face of the sample, $u_e(\xi',\eta',\tau,Z)$ is then propagated a distance z_a to the aperture using the Fresnel diffraction formula,

$$u(\xi_a,\eta_a,\tau,Z) = \frac{\exp(ikz_a)}{i\lambda z_a}\exp\left[i\,\frac{k}{2z_a}(\xi_a^2 + \eta_a^2)\right]$$

$$\int_{-\infty}^{\infty}\int_{-\infty}^{\infty}\left\{u_e(\xi',\eta',\tau,Z)\exp\left[i\,\frac{k}{2z_a}(\xi'^2 + \eta'^2)\right]\right\}\exp\left[-i\,\frac{k}{z_a}(\xi'\xi_a + \eta'\eta_a)\right]d\xi\,d\eta \tag{5.15}$$

which can be written as a Fourier transform of the field at the exit face. Thus this last step is performed with a FFT algorithm. The value of the detected pulse energy for a given sample position is then obtained by

integrating over all time and spatially over the aperture area. This process is repeated for many sample positions. Parameters such as sample thickness, aperture size, pulse duration, beam size, wavelength, linear and nonlinear index of refraction, and medium losses are read as input and translated into the normalized parameters and coordinates of the previous chapters.

As the preceding discussion indicates, this code is more complicated than the generic propagation code we have been employing to this point. As a check on the accuracy of the results, the simulation was performed in the dispersionless approximation and compared to results obtained using the formulae of the previous section. When dispersion was included in the model, we used the invariance of the results with respect to grid and step size as the criterion for accuracy. As indicated by our discussion of the numerical model in chapter 2 and the difficulties associated with calculations involving three-dimensional fields due to the memory requirements, the simulation of a single pulsed Z-scan was extremely computationally intensive. Consequently, we would perform simulations designed to calculate the point in the Z-scan corresponding to the sample positioned exactly at the focus as an error check rather than an entire (much lengthier) Z-scan. This was done because the field is most intense with the sample positioned there and thus the resultant computation errors are largest there as well. Also, most of the work was performed simulating Z-scans with only one spatial dimension in order to get a qualitative understanding of the influence of spatiotemporal pulse reshaping on the n_2 measurements. Moreover, the spatially one-dimensional Z-scans are verifiable in the laboratory by performing the measurements with an elliptical beam.

5.3 Numerical Experiments

The goal of the numerical experiments was to establish a qualitative understanding of the effects which the spatiotemporal coupling induced pulse and beam shaping could have on the nonlinear refraction and absorption measurements obtained from a Z-scan experiment. With an eye to the eventual laboratory verification of the results, the code was rewritten to translate information from the laboratory into the normalized parameters for which the code was originally designed.

5.3.1 Nonlinear Refraction

For the case of a purely refractive nonlinearity (no nonlinear absorption) the split-step Fourier algorithm did not need to be modified. But, because of the computationally intensive nature of the simulations, much of the work was done simulating spatially one-dimensional Z-scans. As in chapter 3, the spatially one-dimensional simulations still allow us to observe the spatiotemporal coupling and obtain a qualitative understanding of its influence on the measurement. With the eventual goal of experimental verification, we sought to explore the four regimes of propagation (defined by the signs of the dispersion and nonlinear index) to establish in which the effect was most noticeable.

The affects of dispersion on the Z-scan signal in the four regimes in the weak nonlinearity limit is exhibited in fig. (5.5). Here we have performed a simulation of a Z-scan with one spatial dimension as we might obtain with light from the Ti:Sapphire system described below. The value of $\chi^{(3)} = 2 \times 10^{-13}$ and our incident pulse energy of 2 nJ combine to give a peak nonlinear phase shift of 0.57 radians, with an effective

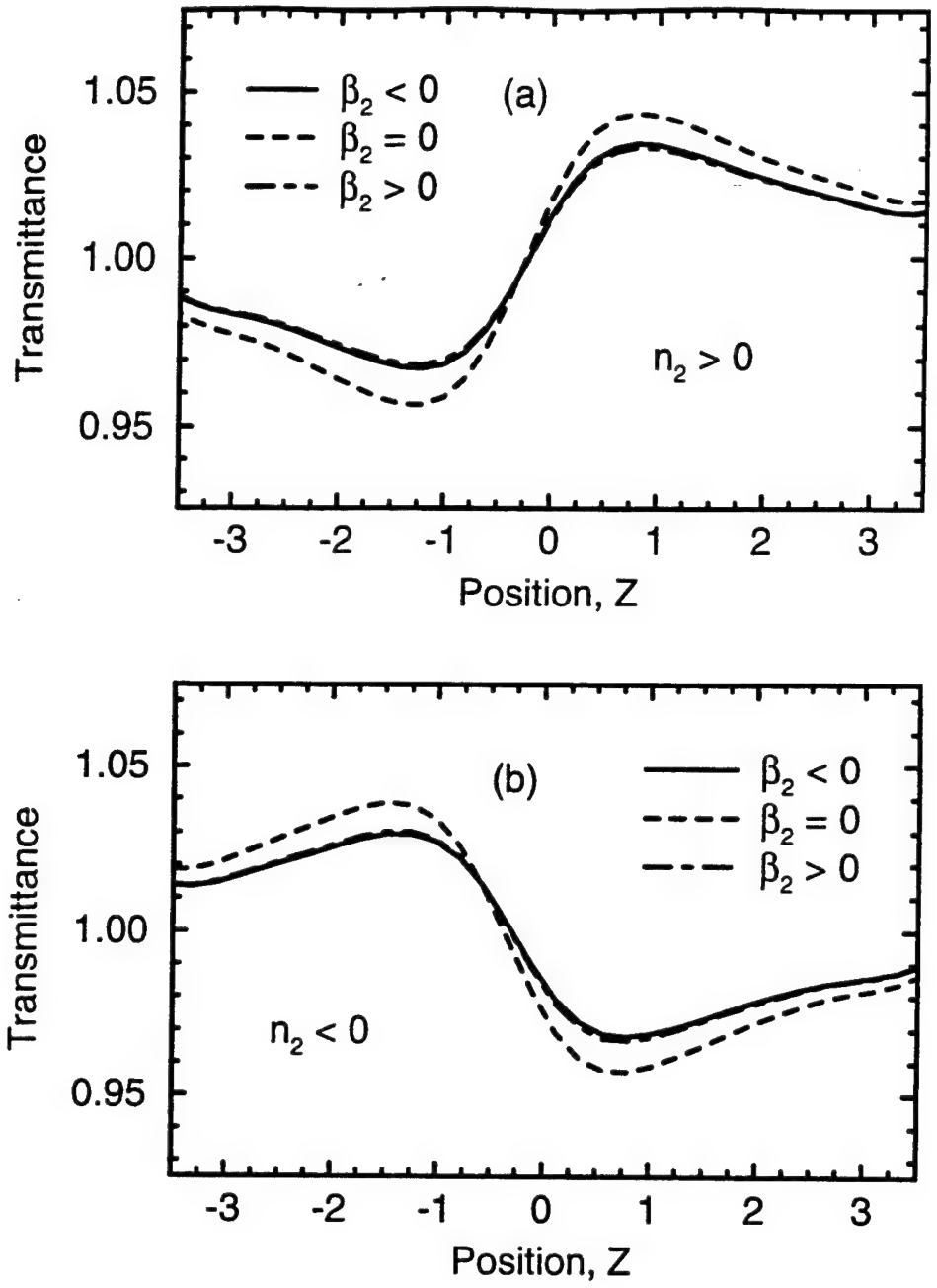

Figure (5.5) In the weak nonlinearity limit dispersive broadening has the effect of reducing the Z-scan measurement in both the normal and anomalous dispersion regimes for both types of nonlinearity.

$N^2 = 0.77$ at the focus. The dispersion of the material and the pulse length are such that there is no nonlinear pulse compression, hence in both the anomalous and normal dispersion regimes the peak field strength is reduced by the dispersion. Thus in both regimes, the effect of the dispersion on the measurement is to reduce the change in transmittance and resultant measured value of $\chi^{(3)}$. Note that in the self-focusing case the normally dispersive medium gives a marginally smaller change in transmission than the anomalously dispersive case because what little temporal nonlinear phase is accumulated aids the pulse broadening in the normally dispersive medium and reduces it in the anomalously dispersive medium. The opposite effect with regard to dispersion type occurs in the self-defocusing medium.

Given that linear dispersion can affect the Z-scan measurement, a natural question to ask is what role may be played by frequency chirp. We try to answer that question with fig. (5.6) where plot simulations under the same conditions as figs. (5.5) yet with a chirped input pulse. We define our chirp parameter C such that our normalized input field has the form

$$u(\xi,\eta,\tau,0) = \exp\left(- \frac{\xi^2 + \tau^2}{2} \right) \exp(- iC\tau^2) \qquad (5.16)$$

As we can see in figs. (5.6) the effect of chirp can be quite dramatic. In the self-focusing case [fig. (5.6a)] a chirp pulsed such that C = 2 almost perfectly compensates for the dispersive broadening in the anomalous dispersion case. Moreover the chirp in this case results in an overestimate of $\chi^{(3)}$, the opposite of the error observed for an unchirped pulse. Conversely, the chirped pulse in the Z-scan of a normally dispersive self-focusing medium

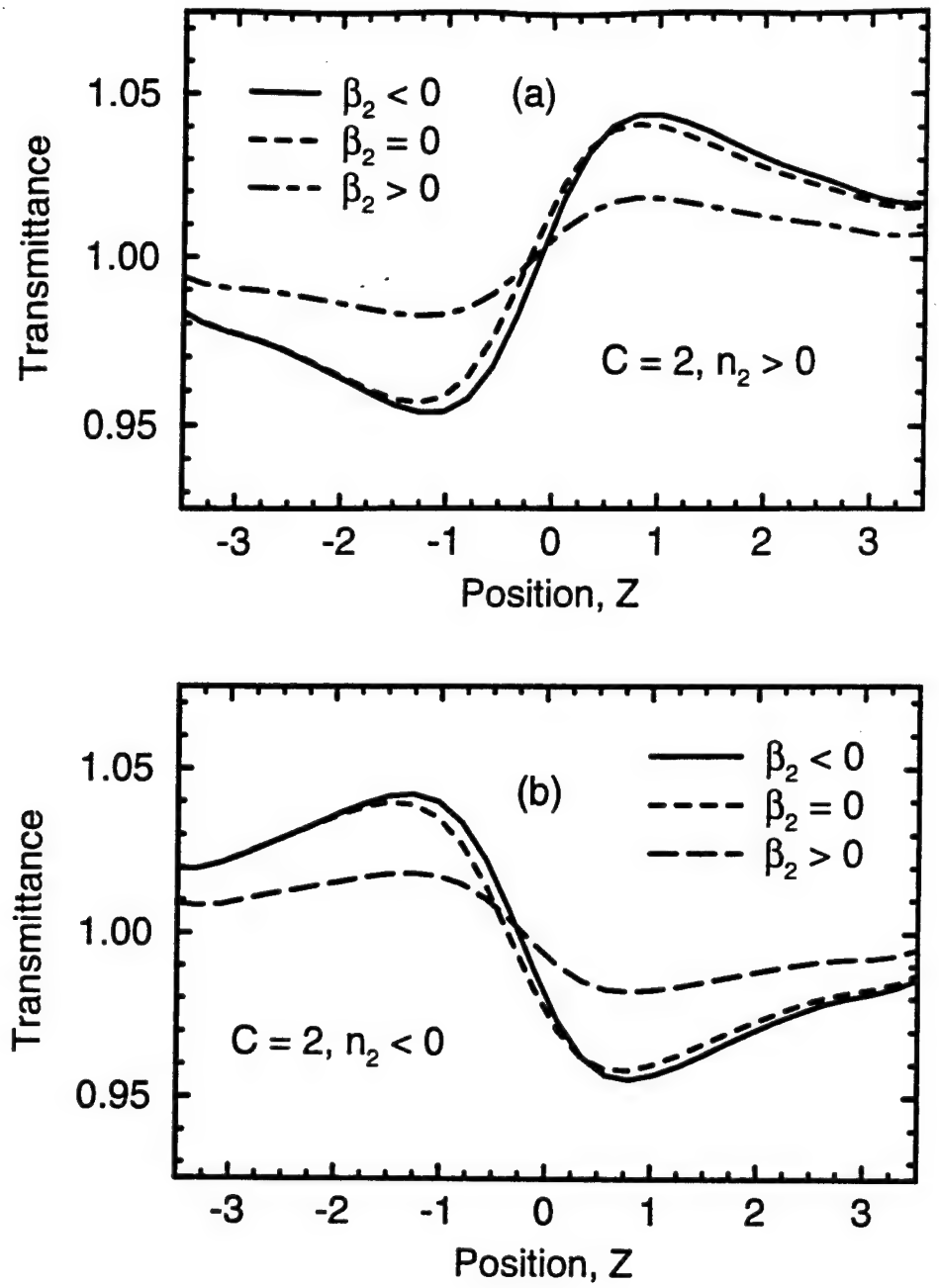

Figure (5.6) In the presence of frequency chirp, pulse reshaping due to linear effects can dominate the Z-scan measurement for either type of nonlinearity. The error is dependent on the product of C and β_2.

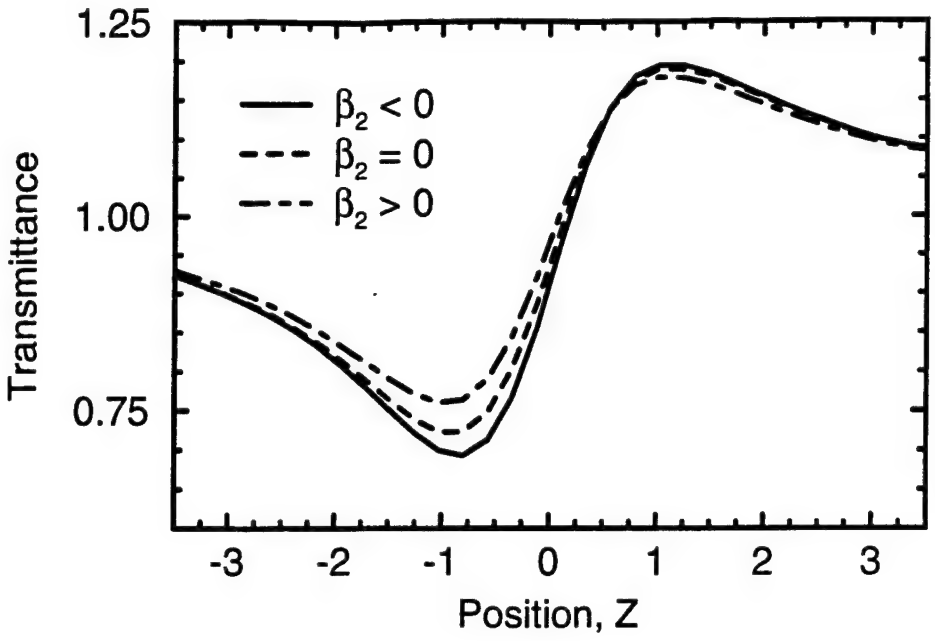

Figure (5.7) When the nonlinearity is strong enough that there is nonlinear pulse reshaping the sign of the error in the Z-scan depends on the type of dispersion in the material.

results in an underestimation of $\chi^{(3)}$. In fig. (5.6b) we see that chirped pulses in the Z-scan of a self-defocusing medium also lead to misleading results such that the effects due to the chirp can either add to the errors due to dispersive broadening or negate them.

The next issue to address is the effect of nonlinear spatiotemporal pulse reshaping which occurs when the nonlinear phase accumulated by the pulse is of the same order or greater as that described by the frequency chirp in fig. (5.6). For a simulation such that $\chi^{(3)} = 10^{-11}$ esu the nonlinear pulse reshaping dominates the effect of the spatiotemporal coupling on the Z-scan measurement as shown in the simulations of fig. (5.7). Here the nonlinear pulse compression due to the anomalously dispersive

medium occurs so rapidly that Z-scan reads erroneously large, whereas the normal dispersion leads to a rapid pulse broadening which reduces the measured value of $\chi^{(3)}$. Depending on the size of $\chi^{(3)}$ the error due to nonlinear spatiotemporal coupling may be even larger than that due to the dispersive reshaping of a chirped pulse.

5.3.2 Nonlinear Absorption

In order to determine the effects of spatiotemporal coupling on open-aperture Z-scans which are designed to measure the nonlinear absorption of a sample, it was first necessary to include nonlinear absorption in the model. The nonlinear absorption can be traced to the imaginary part of the nonlinear susceptibility, $\chi^{(3)}$ but eqn. (5.10) gives a more intuitive representation for the nonlinear absorption coefficient, α_2. With nonlinear absorption included in the model the NSE becomes,

$$i\frac{\partial u}{\partial \zeta} = -\frac{1}{2}\left(\frac{\partial^2}{\partial \xi^2} + \frac{\partial^2}{\partial \eta^2}\right)u + \frac{d}{2}\frac{\partial^2}{\partial \tau^2}u - (\mathrm{sgn}(n_2)\,N^2 + i\,N_a^2)\,|u|^2 u. \quad (5.17)$$

where N_a is related to the nonlinear absorption coefficient, α_2 of eqn. (5.10) via

$$N_a = \frac{2\pi n_0 \sigma^2}{\lambda}\frac{\alpha_2 I_0}{2} \quad (5.18)$$

This added nonlinear term is included simply as a multiplicative factor in the nonlinear part of the split-step algorithm. The results of simulated spatially one-dimensional Z-scans with an open aperture are shown in fig. (5.8) for a self-focusing nonlinearity and the cases of normal and

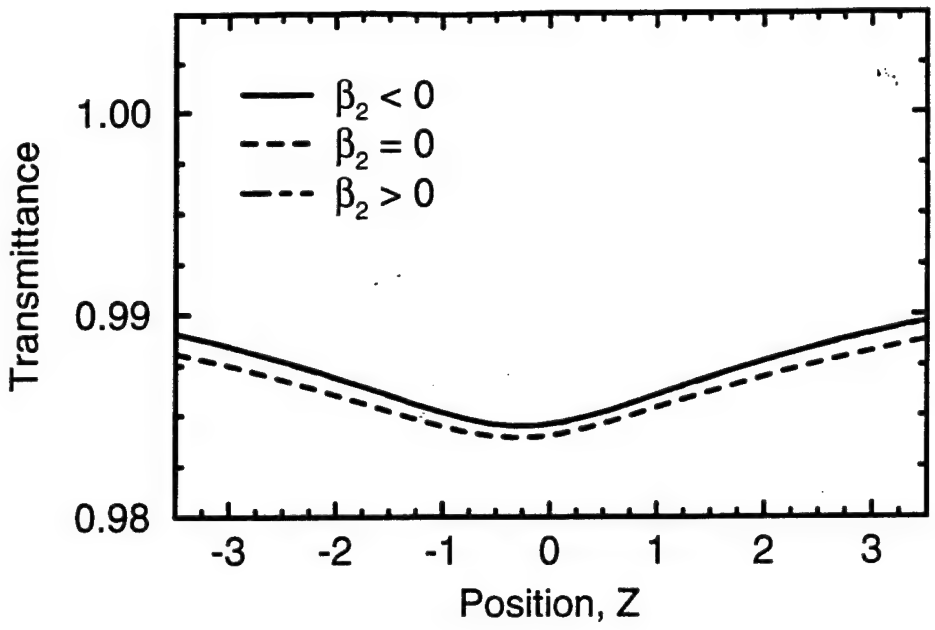

Figure (5.8) In the weak nonlinearity limit both types of dispersion affect the open-aperture Z-scan measurement in a similar manner. The Z-scan for the normally dispersive medium (dot-dashed line) is invisible because it is laying on top of the anomalous medium Z-scan (solid line).

anomalous dispersion. Here the parameters are identical to those of figs. (5.5) but with a nonlinear absorption coefficient chosen such that α_2 = 7 cm/GW. Results similar to that obtained for the closed-aperture case are observed here. In the absence of chirp and a weak nonlinearity both types of dispersion lead to pulse broadening and a diminished signal. When chirp is included in the model, the effect of the chirp is to enhance or reduce the measurement depending on whether or not the chirp broadens or compresses the pulse. The effect on the nonlinear absorption measurements of dispersive pulse broadening and increasing nonlinear pulse reshaping with peak power is demonstrated in fig. (5.9). Here we

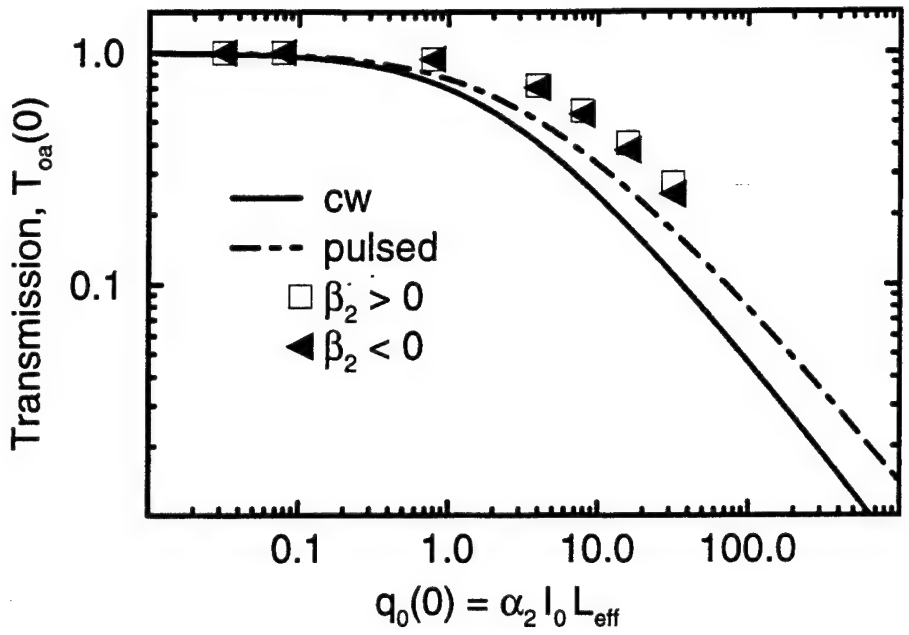

Figure (5.9) For higher nonlinearities, the nonlinear pulse reshaping affects the open-aperture measurement in a manner dependent on the type of dispersion present in the material.

reproduce the conversion chart of fig. (5.4) with points added corresponding to the results of three-dimensional simulations in anomalously (dark triangles) and normally (light squares) dispersive media. As in the closed-aperture case, the effect of the dispersion in both types of media at low powers is to reduce the open-aperture signal by reducing the peak power. As the pulse energy is increased the nonlinear pulse shaping begins to effect the results and the error due to pulse broadening is reduced in the anomalously dispersive medium and increased in the normally dispersive medium. For a less dispersive medium the effective temporal nonlinearity ($N_\tau = N/\sqrt{d}$) would be greater and the nonlinear pulse shaping effects would dominate at lower

powers causing the triangles to separate faster. The result would be different measured nonlinear absorption coefficients for different pulse energies. As in the closed aperture case, the pulse compression in the anomalous dispersion regime would lead to an enhanced signal while the pulse broadening in the normal dispersion regime would diminish the signal (assuming a self-focusing nonlinearity).

5.4 Laboratory Experiments

The Z-scan simulations discussed above have assumed a Gaussian beam of ultrashort pulses with a well-determined phase distribution incident on a highly dispersive nonlinear medium. In order to perform these experiments in the laboratory it is first necessary to acquire both a pulse source and highly dispersive nonlinear medium. The former was the greatest obstacle to experimental verification.

5.4.1 The Pulse Source

In fig. (5.10) is a schematic layout of the system used to generate the pulses employed in this experiment. The system is an Argon-ion laser pumped self-modelocked Ti:Sapphire laser with a prism-pair pulse compressor. The Argon pump beam is first focused by the lens L1, then enters the Ti:Sapphire cavity through the dichroic mirror M1. The pump beam is absorbed by the crystal X. The mirrors M1 and M2 focus the intracavity beam into the crystal. The long arm of the cavity is composed primarily of the pair of prisms P1 and P2 which were introduced to compensate for the gain and index dispersion in the crystal. Both P1 and

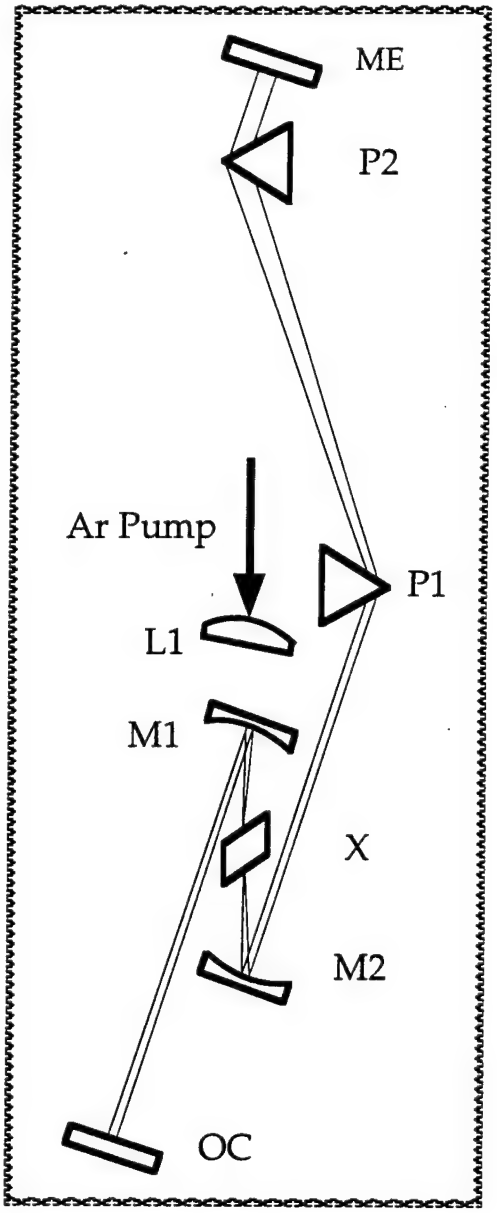

Figure (5.10) A schematic layout of the Argon-laser pumped Ti:Sapphire cavity used to generate the pulses in this experiment. The pump beam is focused by the lens, L1, into the crystal X. The folding mirrors, M1 and M2, focus the intracavity beam into the crystal and redirect the beam towards the output coupler, OC, and dispersive delay arm of the cavity respectively. The prisms in the dispersive delay arm, P1 and P2, give the lower frequencies a longer optical path thus compensating for gain and material dispersion in the crystal.

P2 could be translated into the intracavity beam path to increase or decrease the overall dispersion in the cavity which had the effect of narrowing or broadening the pulse spectrum. The pulse spectrum as measured by a Digikrom 240/480 monochromator is shown in fig. (5.11). The spectrum shown here has a FWHM of 50 nm or 22.5 THz with a peak at 820 nm. The laser was capable of producing pulses with spectra as broad as 60 nm (~30 THZ), but it was difficult to achieve such spectra and long-term (~2 hours) stability simultaneously. The problems with stability stemmed primarily from environmental conditions, in particular the temperature of the pump laser cooling water and the crystal cooling water. The starting or ending of an experiment in another laboratory which had a

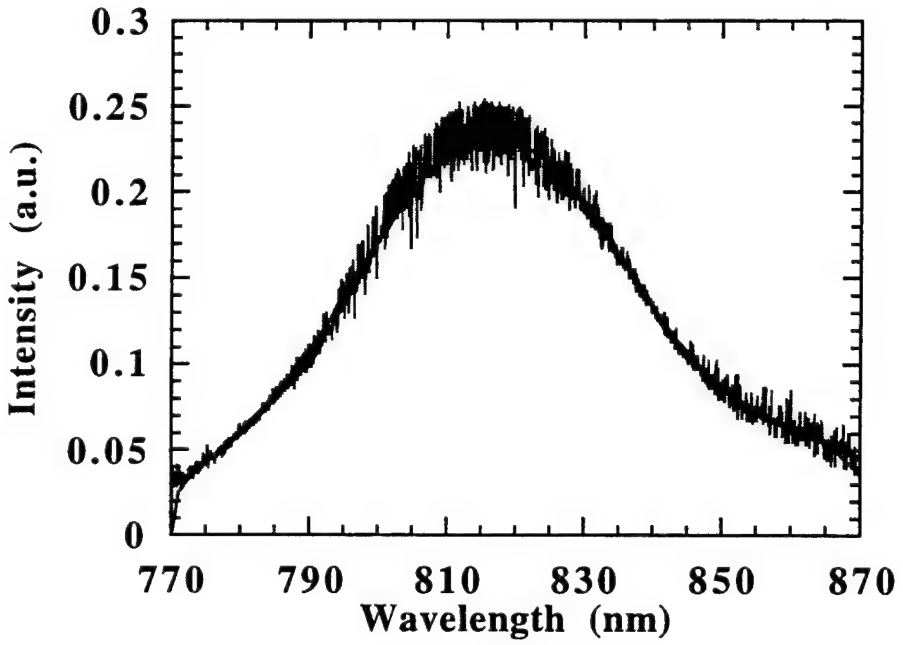

Figure (5.11) The typical spectrum of the pulses produced by the laser in fig. (5.10) had a bandwidth of 50 nm (22.5 THz) centered at 820-830 nm.

laser on the same water line could change the state of the laser (We became accustomed to working around the "4:30 effect" so named because 4:30 pm was typically the time several of the other lasers in the building were shut off every day and it was almost expected that our laser modelocking would be lost at this hour). In general, the narrower the spectrum the more stable the pulses but in order to witness strong dispersive effects the broadest spectrum possible was desired. Moreover, a broader spectrum made shorter pulses possible which lead to a higher possible peak power. The spectrum of fig. (5.11) represents the most reproducible compromise between stability and dispersion. We were able to produce this spectrum to within the measurement error (± 5 nm due to the noise from the photodetector) on a daily basis.

The next criterion for determining the acceptability of the laser mode was the autocorrelation trace of the compressed pulses. The autocorrelator[19] was the modified Michelson interferometer shown in fig. (5.12). The incoming pulse is split into the two arms of the interferometer by the beam splitter. The optical path of one arm is varied by moving the corner cube with a servo motor controlled by the signal from a function generator. The optical path difference of the two arms produces a time-delay, τ_d, between the arrival of the two pulses at the microscope objective. The KD*P crystal and filter combination at the focus of the microscope objective result in a second-harmonic signal at the photodetector. The signal at the photodetector, $s(\tau_d)$, was related[19] to the intensity of the pulses via

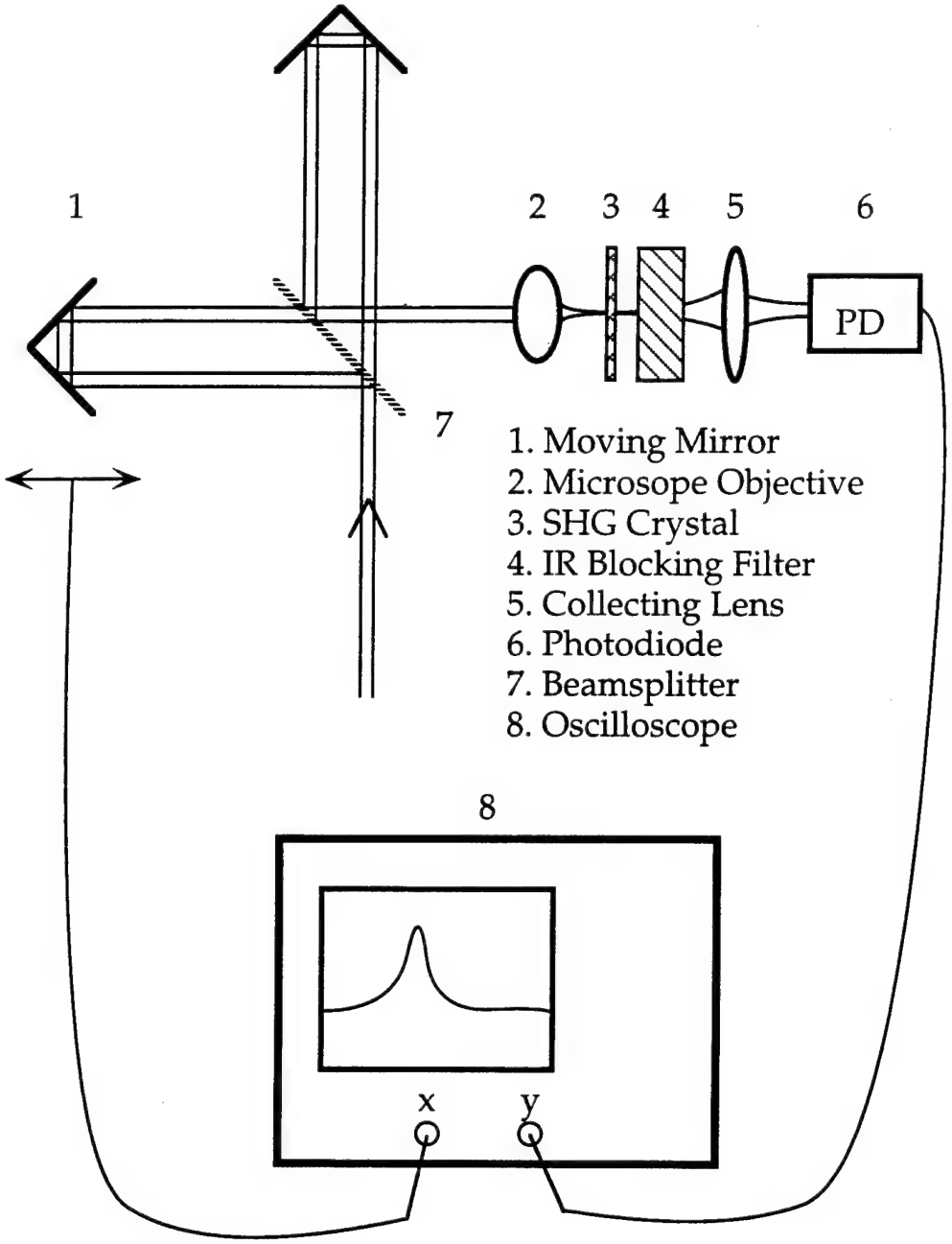

Figure (5.12) A modified Michelson interferometer is used as an intensity autocorrelator to characterize the pulses.

$$s(\tau_d) = C_1 \left[1 + \frac{2 \int_{-\infty}^{\infty} I(t)I(t-\tau_d)\,dt}{\int_{-\infty}^{\infty} I(t)^2\,dt} \right] \qquad (5.19)$$

where C_1 is a normalization constant generally chosen such that $s(\tau_d) = 1$ for large τ_d. The slow response of the photodiode relative to the pulse duration performs the indicated integration. The signal from the photodiode and the function generator are then sent to a storage oscilloscope which allows us to retrieve the function of eqn. (5.19) for analysis. The shape of the peak above the background is simply the autocorrelation of the pulse intensity. There is a constant relationship between the width of the autocorrelation trace and the width of the pulse which is dependent on the pulse shape. For hyperbolic secant pulses as may come from a Kerr-lens modelocked Ti:Sapphire laser, the pulsewidth is 0.636 times the autocorrelation width.

With the autocorrelator we could directly observe the effect of the pulse compressor.[20] In fig. (5.13) we show the different autocorrelations produced by different prism positions. Note that since this compressor is outside the laser cavity (and the peak intensity of the pulse is such that spectral broadening due to self-phase-modulation can be neglected), the spectrum is constant for the different autocorrelations shown here, however there is a significant increase in pulse width from adding just 4 mm of prism glass (note that this distance is a translation of the base of the prism and that the pulse traverses the prism twice thus the actual amount of glass the pulse sees is increased approximately 9.2 mm). This is

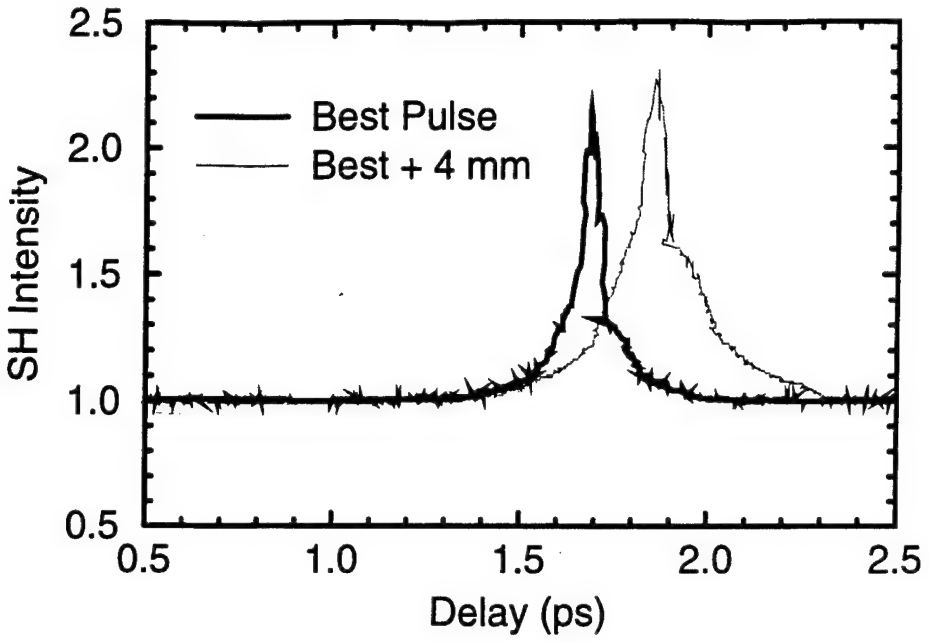

Figure (5.13) An external cavity prism-pair pulse compressor was used to control the pulse width in the experiment. Adding 4 mm of glass into the path of the beam could drastically affect the pulse width.

due to simple dispersive broadening of the pulse as it travels through those few mm. Given that our autocorrelator itself has a rather thick microscope objective contained within it, we must assume that it too broadens the pulse. In order to compensate for the broadening caused by the autocorrelator, it was necessary to obtain an estimate of its effect. This was achieved by passing the pulses through two simultaneous microscope objectives positioned so that there was no net effect on the spatial behavior of the field, then measuring the change in prism position necessary to reacquire a minimum autocorrelation width. A similar procedure was performed with the focusing lens to be used in the Z-scan measurements [see fig. (5.1)]. The distances necessary to move the prism

in order to reacquire the minimum pulse width in both cases were halved and the prism moved to that position relative to the position of the measured minimum. This was done in an effort to both minimize the chirp on the pulse and to obtain the most accurate estimate of the width of the pulse as it interacted with the sample in the Z-scan measurement. Although we could attempt to minimize the chirp with the pulse compressor, higher-order dispersion was beyond our control. Due to third- and higher-order dispersion the minimum pulse width achievable always increased as more optical elements were placed in the beam path. Moreover, we were not equipped to accurately measure the phase distribution of the field. Thus, unlike the simulations described above, the phase of the field was an unknown quantity. By compensating for the dispersion of the lens and using the minimum pulse width we attempted to keep the unknown phase distribution constant and minimum, thus making it more likely that the nonlinear phase accumulation would produce a measurable effect.

The dispersion from the microscope objective and the focusing lens in the Z-scan were not the only sources of error in the pulse measurements. Inasmuch as the pulses we were measuring were on the order of a few tens of femtoseconds in time, their spatial length was approximately 10 μm (for a 33 fs pulse). Thus the optical path of the two arms of the interferometer were equal to within a pulse length for only a very small range (± 5 μm) of mirror positions. Determining the ratio of servo signal voltage to mirror position thus became the limiting factor in the pulse width measurement. For a given voltage the mirror position could be measured to ± 1μm. Combined with errors due to the assumed linearity between driving voltage amplitude and mirror position as well

as the phase uncertainties discussed above, the error in the pulsewidth was generally taken to be ± 15 fs.

The simulations above also assume a circularly symmetric Gaussian beam. In the event of nonuniformities in the spatial intensity distribution, spatial filtering is typically employed to produce Gaussian output. Unfortunately, beam power is frequently sacrificed to beam shape in this case. In the experiments described here no spatial filtering of the Ti:Sapphire beam was performed for several reasons. First, the microscope objective needed for the spatial filtering would have added yet more unwanted chirp to the pulse. Second, when the Ti:Sapphire is most stably modelocked, its output is very nearly Gaussian. Moreover, when it is passed through the external cavity compressor an effective alignment check is to see that the beam remains Gaussian after exiting the compressor. The beam shape was measured using a 25-μm pinhole as it was translated across the beam path in both the x- and y-directions at the point where the focusing lens for the Z-scan was to be placed and again at a distance 50 cm further. Typical results are shown in figs. (5.14) as well as Gaussian fits to the data. In this case the beam is slightly astigmatic in that the modest ellipticity observed at the first position has increased by the second. Minor deviations from circular symmetry such as this are due to misalignment of the pulse compressor and resulted in an uncertainty in the minimum beam width of approximately 15%. Although the pulse energy could be measured relatively accurately (± 2 %), the uncertainty in beam width and pulse width combined to give an estimate of the peak intensity of the focused beam to be 11 ± 7 GW/cm^2 for a 4 nJ pulse focused by an 8.8 cm lens.

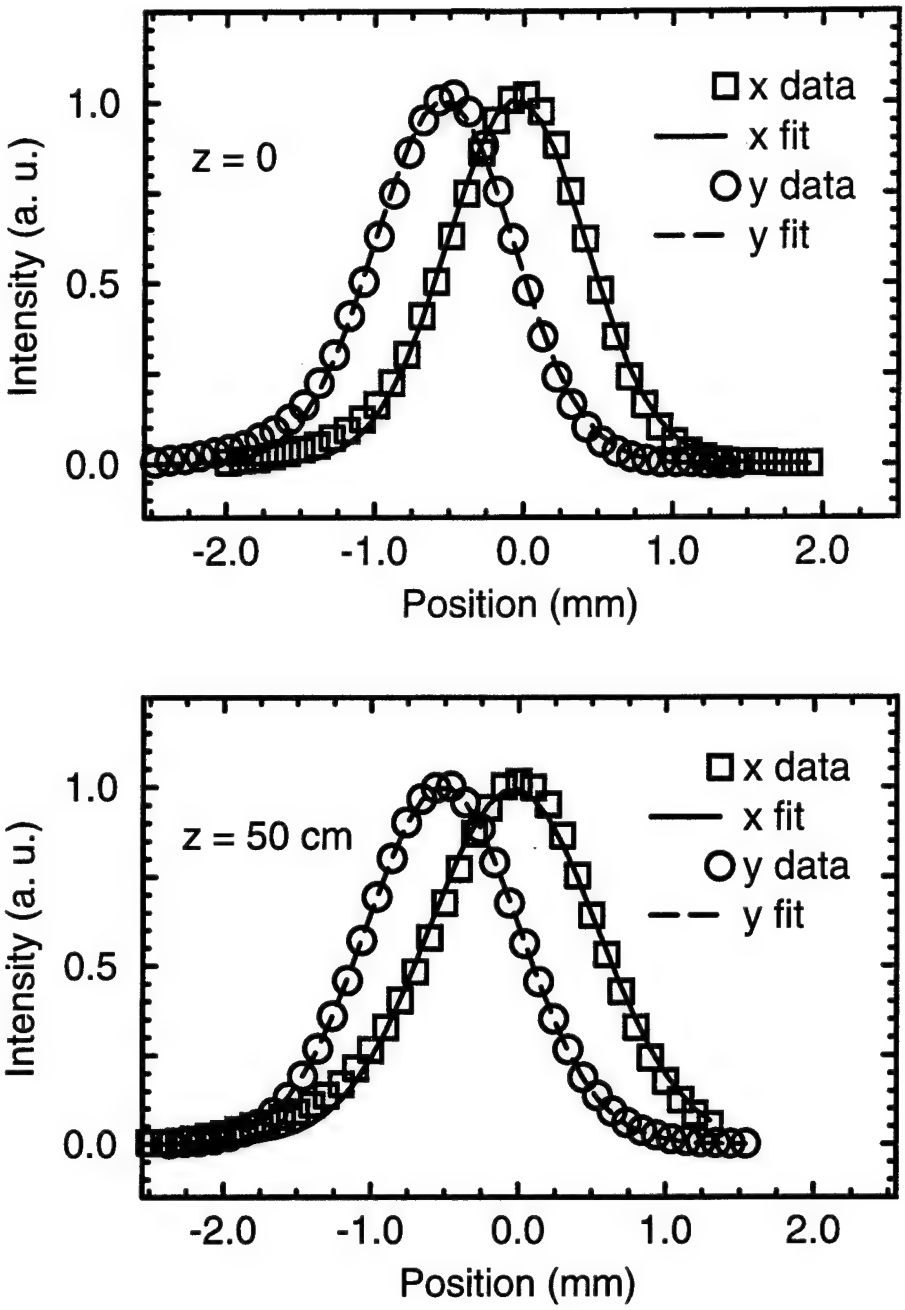

Figure (5.14) In order to measure the beam width and shape a 25 μm pinhole was scanned across the beam path. The data obtained in the x- and y-directions indicate a slightly elliptical beam.

5.4.2 The Samples

Two types of nonlinear media were employed in the Z-scan experiments: high-index glasses and conjugated polymer solutions. The criterion for selecting these samples was their reported large electronic nonlinearities.[13,17,18] Limited to pulse energies of less than 5 nJ and pulse peak powers of 150kW, samples with large third-order susceptibilities were desired. The polymer nonlinearity was reported[18] to be $\chi^{(3)} = 10^{-10}$ esu, which reduces to 10^{-13} in a 0.1% solution. The high-index glasses had reported[13] $\chi^{(3)}$ values of as high as 7.6×10^{-12} esu at 770 nm and were also know to be quite dispersive.

There were two high-index glass samples, obtained from workers at Corning Inc., denoted DY and DZ. The glasses were composites made of $Tl_2O(40);Bi_2O_5(40):Ga_2O_3(20)$ and $Tl_2O(30);Bi_2O_5(50):Ga_2O_3(20)$ respectively, with indices of refraction estimated at approximately 2.5. The index of refraction of the glasses was measured by a simple technique which is the basis of ellipsometry. The sample was mounted on a rotating stage and the angle at which the reflected, linearly polarized light was minimized was taken as Brewster's angle from which the index of refraction could be determined via the relation, $n_0 = n_a \arctan(\theta_{min})$. Taking the index of air, n_a, as unity the indices of the samples were measured with the modelocked Ti:Sapphire light and found to be 2.44 and 2.42 respectively. The linear absorption of the samples was measured with a simple transmission experiment. After accounting for losses due to Fresnel reflection, the linear absorption coefficients for the two glasses were determined to be 1.53 ± 0.05 cm^{-1} and 1.18 ± 0.05 cm^{-1} for DY and DZ respectively. The 5-mm samples thus had effective lengths of 3.49 mm and 3.77 mm respectively.

The polymer samples were 0.1 wt % solutions of the fused aromatic ladder polymer poly(benzimidazobenzophenanthroline), BBL-20 and BBL-32, with estimated nonlinear susceptibilies[18] of 10^{-10} esu before solution. The solutions were placed in quartz cuvettes for the experiments. The linear index of the polymer solutions were obtained with the aid of the autocorrelator. The difference in position, Δx, of the autocorrelation peak with and without the cuvette in the reference arm of the interferometer was related to the index difference via $n = 1 + \Delta x/h$ where h is the thickness of the solution and Δx has been corrected for the contribution due to the quartz walls of the cuvette. Using this technique we obtained indices of 1.40 and 1.44 for the BBL-20 and BBL-32 solutions respectively. The absorption measurements were carried out in the same manner as for the glasses and we obtained absorption coefficients of $\alpha_0 = 0.59 \pm .05$ cm^{-1} for the BBL-32 and $\alpha_0 = 0.35 \pm 0.05$ cm^{-1} for the BBL-20. Using the 5-mm cuvette, these absorptions gave effective lengths of 4.3 mm and 4.6 mm respectively.

In as much as we were attempting to observe the effects of dispersive and nonlinear pulse broadening on Z-scan measurements, we tried to quantify the broadening influence of the samples on the pulse. This was done by inserting the sample into the beam path prior to the autocorrelator and measuring the increase in pulse width due to its presence. It was at this stage that the first problems arose. A number of factors made obtaining a dispersion measurement for the glass samples difficult. First, imperfections in the surfaces of the samples badly degraded the beam quality upon transmission. Second, absorption, transmission and scattering losses significantly reduced the optical power of the beam that was transmitted. Finally, the faces of the samples were not ground

plane parallel thus deflecting and distorting the beam. This last problem proved insurmountable. The cuvettes in which the polymer samples were contained had no surface imperfections of any kind. The problem with the polymer solutions was the large defocusing thermal nonlinearity. The effect was so strong that the unfocused circular beam was converted into an annulus upon propagation through the 5-mm cuvette. A weak beam passing through the 1-mm cuvette filled with BBL-20 solution broadened the pulse autocorrelation trace by an amount less than the uncertainty of the autocorrelation measurement, as a result the strength of the dispersion of the samples remained unknown. However, the lack of measurable broadening in the 1-mm cuvette gave an upper bound to the dispersion of the BBL-20 solution of 100 ps^2/km.

5.4.3 The Z-scan Measurements

The experimental set-up was as shown in fig. (5.15). The arrangement of the Z-scan apparatus is as shown in fig. (5.1) except that the open- and closed-aperture measurements were not performed simultaneously. A lens was also added after the aperture to aid the collection of light by the detector. The focal length of the lens was typically between 7.5 cm and 10.0 cm giving a diffraction length of between 5 mm and 7 mm for our 830 nm input pulses. The aperture was a variable iris diaphragm and the detector was a Newport model 818-IR photovoltaic detector. Because there was no equipment available to select individual pulses from the 85 MHz pulse train, the detector measured average power. In order to obtain consistent results, we required constant pulse shape and energy over the course of the measurement. Previous work characterizing

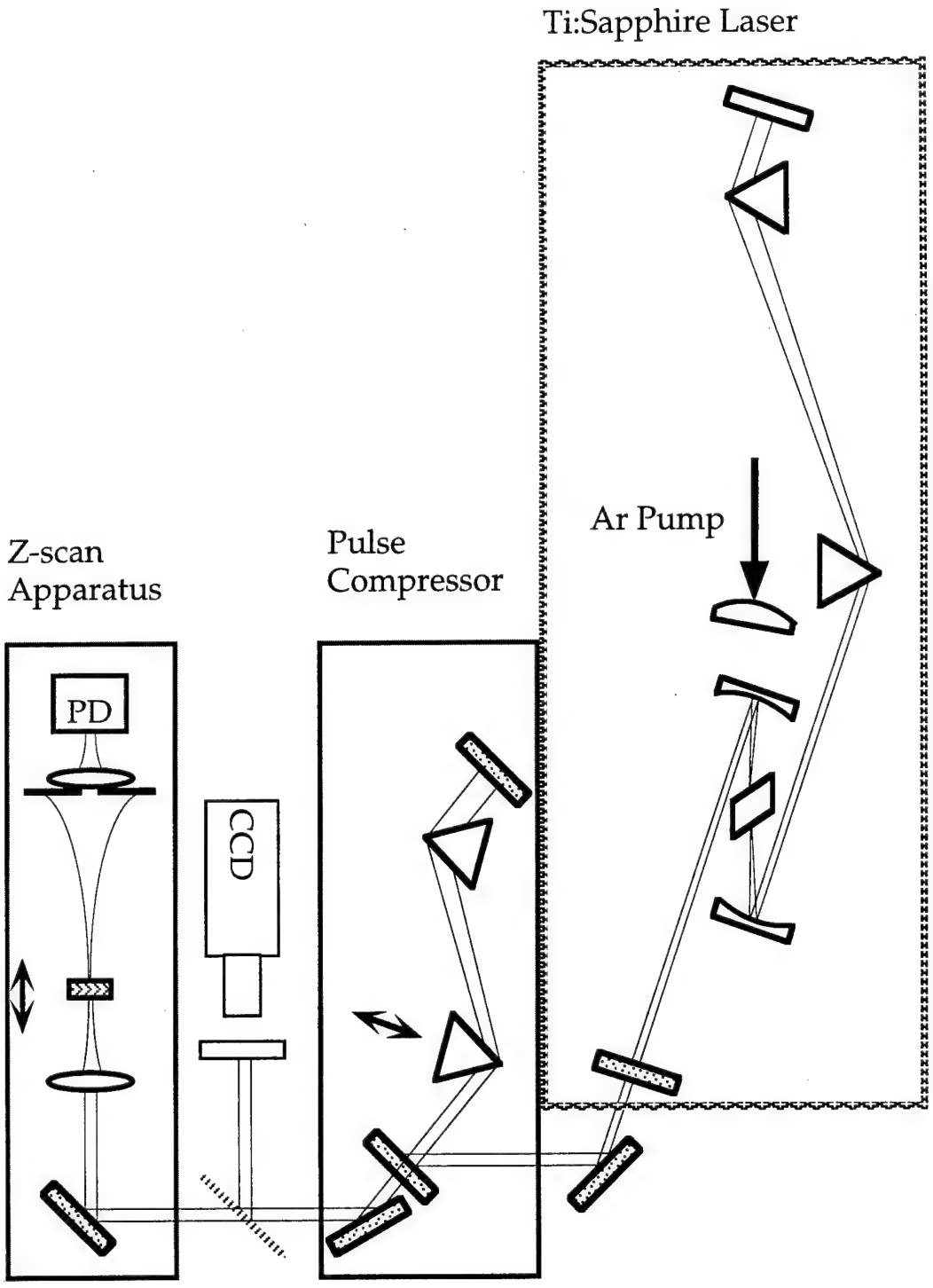

Figure (5.15) The experimental set-up consisted of the Z-scan apparatus of fig. (5.1) and a video camera to monitor the spatial mode of the laser which was related to the pulse shape. Prior to the Z-scan, the pulses were characterized with a monochromator and autocorrelator (not shown).

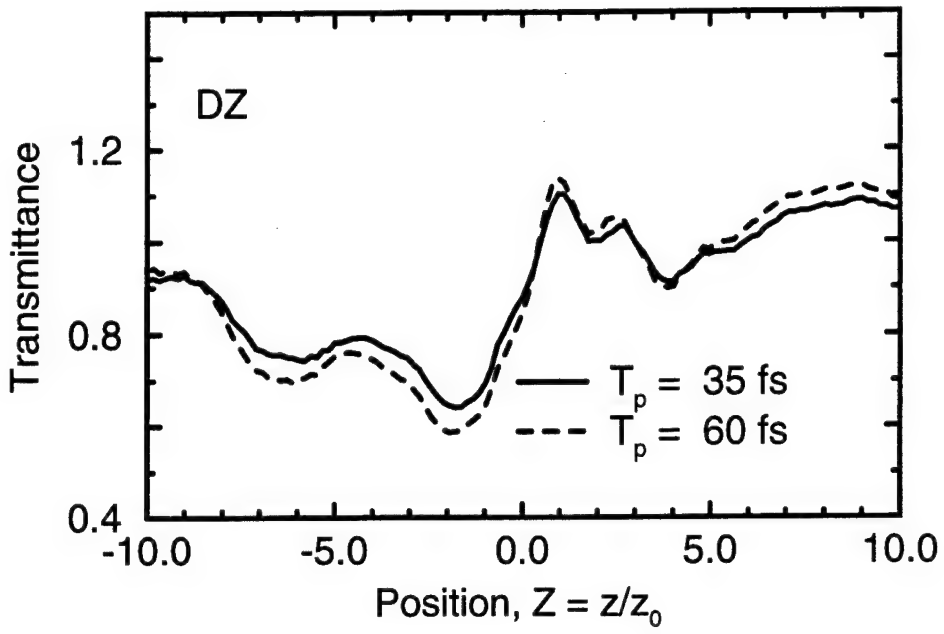

Figure (5.16) The closed-aperture Z-scans of the high-index glasses were affected by the non-plane-parallel nature of the samples.

the pulses with the autocorrelator and a photodiode had indicated that consistent pulse shape and energy could be maintained provided the laser stayed in the same spatial mode. The laser mode was monitored by splitting a small percentage of the beam from the pulse compressor to a video camera. Changes in the spatial mode could be as subtle as a switch from a circular to an elliptical beam shape or as obvious as a loss of modelocking characterized by the appearance of speckle in the video image. Occasionally, the mode change would be too subtle for even a trained eye to detect, but such changes were usually discernible when observing the data from a Z-scan.

The typical procedure was to first measure and store the autocorrelation traces of the pulse for several prism positions, then insert

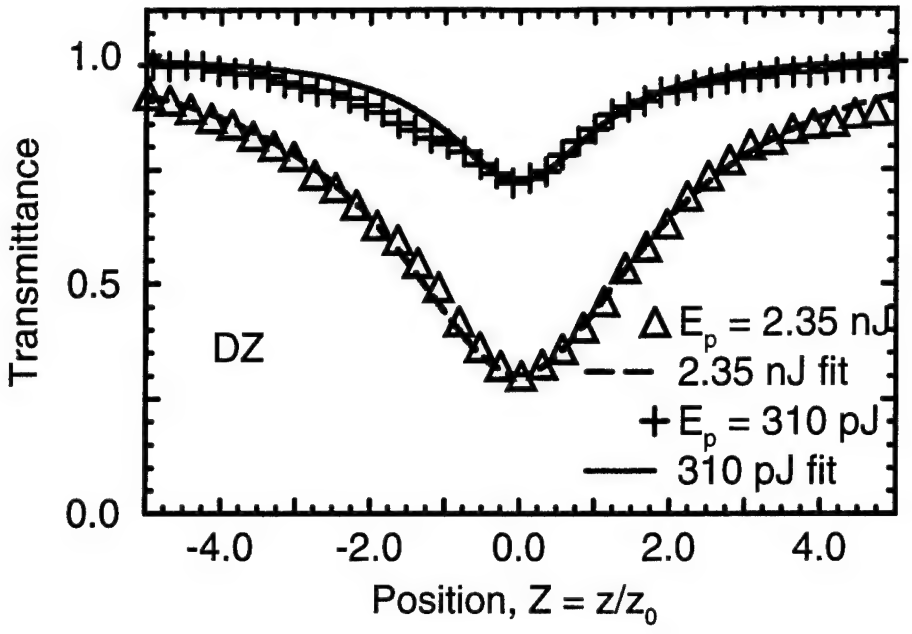

Figure (5.17) The open-aperture Z-scans of the DZ glass produced consistently low results for the nonlinear absorption measurements as expected for the case of dispersive pulse broadening in the sample. The result $\alpha_2 = 2.1 \pm 1.4$ cm/GW was lower than the value of $\alpha_2 = 9.4$ cm/GW measured at 770 nm by other workers.

the Z-scan apparatus, and commence taking data. First a low power (< 1 pJ/pulse) Z-scan was taken which was stored so that it could later be subtracted from the higher power data to account for losses due to surface roughness. Next Z-scans with a range of powers and prism positions were taken. The different pulse energies were obtained with the aid of neutral density filters. The first measurements undertaken were those of the high-index glasses. In fig. (5.16) we plot the results of closed-aperture Z-scans of the DZ glass. After correcting for the nonlinear absorption [see fig. (5.17) above], there are still obvious differences between the results depicted here and those predicted by the analytical or even numerical

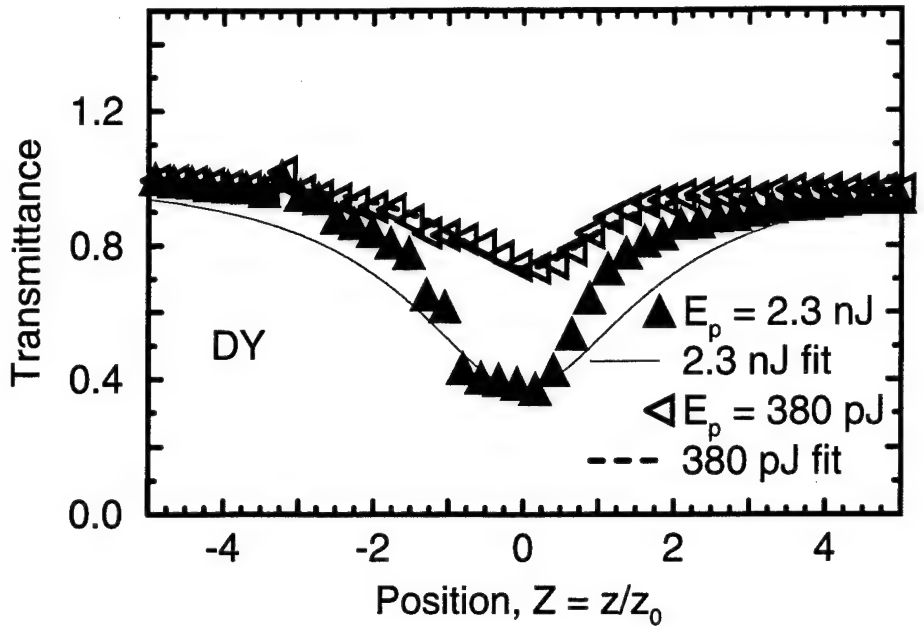

Figure (5.18) The open aperture Z-scans of the DY glass gave $\alpha_2 = 1.7 \pm 1.3$ cm/GW at both power levels.

theory of the earlier sections of this chapter. The surface irregularities have already been accounted for by subtracting the low-power Z-scan for the data shown here. However, the effects of the non-plane-parallel nature of the samples could not be accounted for by simple low-power subtraction, nor by any other means of which we are aware. The effect of the wedge in the sample was to make it impossible to keep the aperture positioned at the center of the beam for every sample position because the center of the far field moved laterally as the sample moved through the focus. In fig. (5.16) the observed change in transmission is greater for the broader (and hence lower peak power) pulse. This indicates that the effects of the wedge in the sample are strong enough to dominate any effects due to spatiotemporal coupling. As a result, we concentrated

our efforts on observing the effects of spatiotemporal coupling in the nonlinear absorption measurements from open-aperture Z-scans.

In general the open-aperture data was much more consistent. A lens placed shortly after the sample could collect all of the light exiting the sample regardless of small changes in position due to the wedge. The open-aperture results shown in fig. (5.17) were obtained with 35 fs pulses and the fits to the data come from the analytical result of eqn. (5.7). The high-power (2.35 nJ pulse) Z-scan resulted in a measurement of 2.3 ± 1.5 cm/GW and the lower-powered (310 pJ pulse) result was 2.1 ± 1.4 cm/GW both of which are well below the reported[13] values for this glass of 9.4 cm/GW measured at 770 nm with much broader pulses. These lower values are consistent with a dispersively broadened pulse reducing the expected peak power of the pulse in the medium. Moreover, if the glass was anomalously dispersive the higher α_2 measurement for the 2.35 nJ pulse would be consistent with our understanding of the affect of spatiotemporal coupling on the measurement. The results obtained for the open aperture scans of the DY glass are shown in fig. (5.18). The 2.3 nJ pulses returned values $\alpha_2 = 1.6 \pm 1.3$ cm/GW, while the 380 pJ pulses produced scans which measured $\alpha_2 = 1.7 \pm 1.3$ cm/GW. While there have been no measurements of the nonlinear absorption coefficient reported for this glass, its similar composition to the DZ glass indicates that it should have similar characteristics. In this case, normal dispersion in the glass would be needed to account for the small discrepancy between the α_2 measurements at the different powers. In both cases, the size of the experimental errors in the measurement from other sources prohibits decisively ascribing the discrepancies to dispersion or nonlinear pulse reshaping.

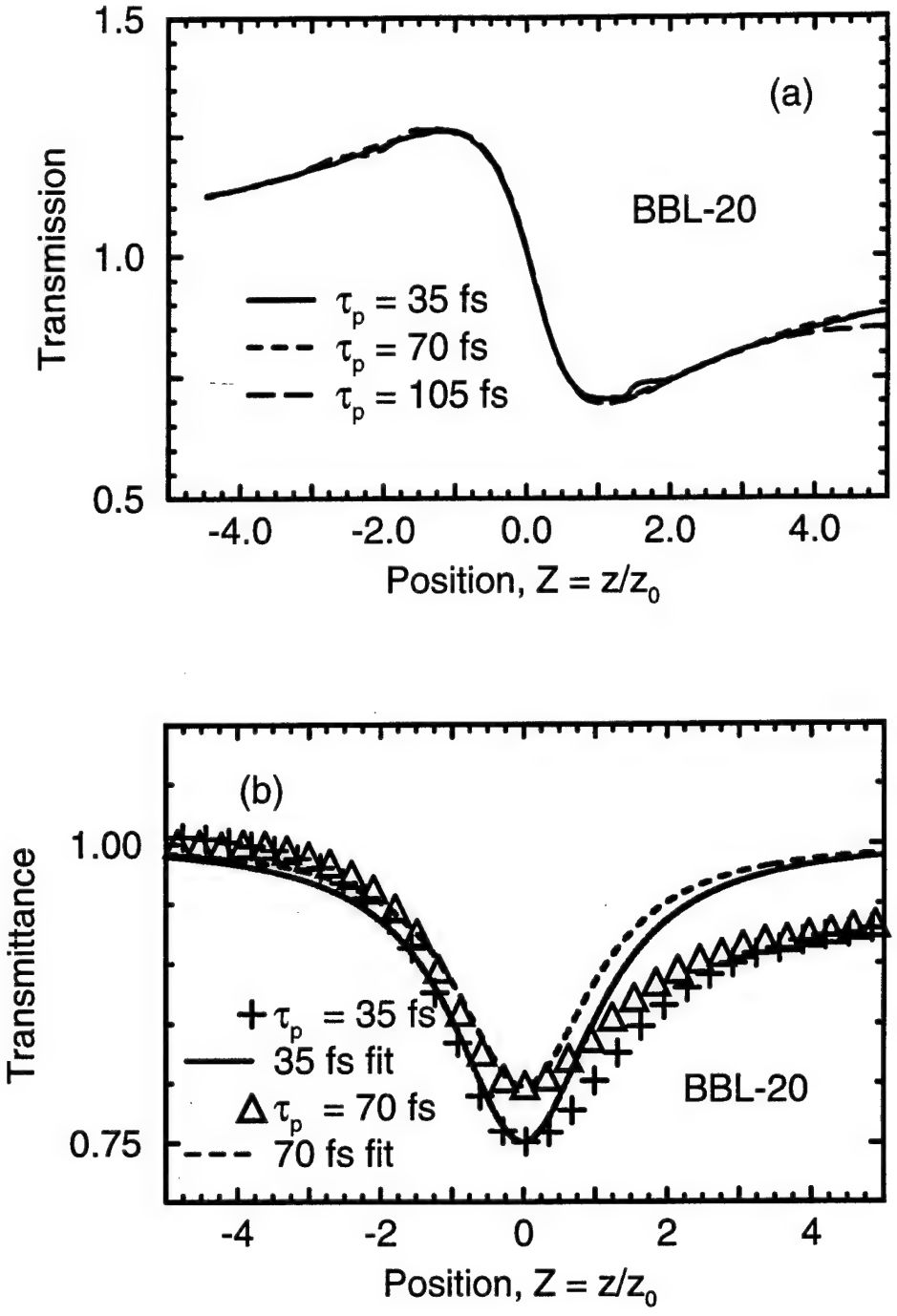

Figure (5.19) The Z-scan measurements of the conjugated polymer solutions were not affected by poor surface quality. Unfortunately, (a) the closed aperture Z-scans were dominated by a slow thermal nonlinearity which even affected (b) the open aperture data. The measured value of α_2 was 0.8 ± 0.5 cm/GW.

The large thermal nonlinearities of the BBL-20 polymer solution are evidenced by the closed-aperture Z-scan of fig. (5.19a). The peak on the lens-side of the focus corresponds to a defocusing nonlinearity such as one would expect when the index change is due to the heating of the solution. Moreover, the change in transmittance of the sample as well as the position of the transmittance peak and valley are independent of the pulse duration, hence the conclusion that the nonlinear refraction effects are due to the average power of the pulse train (~200 mW) rather than the peak power of the individual pulses (~100 kW). Thus, studying ultrafast spatiotemporal coupling in the nonlinear refraction measurements of the polymer was not possible since the slowly-responding thermal nonlinearity dominated the measurement. The thermal nonlinearity was so large in fact that it even affected the open-aperture results, shown in fig. (5.19b). The defocusing beam, traversing the sample when it was positioned on the far-side of the focus, was broadened so rapidly that the lens, positioned 5 cm from the sample, could not collect all the exiting light. Fortunately, when the sample was on the lens-side of the focus the nonlinearity was competing with rather than adding to the phase curvature from the lens. As a result we believe the data for $Z \leq 0$ is unaffected by the thermal defocusing of the beam. Moreover, because the nonlinear absorption measurement is really only dependent on two data points, [$T_{oa}(0)$ and $T_{oa}(\infty)$] we were able to obtain a measurement of α_2 for each of the Z-scans in fig. (5.19b). The Z-scan with the 35 fs pulse gave a value of $\alpha_2 = 0.8 \pm 0.5$ cm/GW while the 70 fs pulse Z-scan gave a value of $\alpha_2 = 1.2 \pm 0.4$ cm/GW. These results are consistent with our understanding of the affect of dispersive pulse broadening on the measurements as discussed in section 5.3 and depicted in fig. (5.9). The

shorter pulse will broaden more in the medium thus leading to less absorption than would be expected based on the input peak power. As a result, the measured value of α_2 is lower for the shorter pulse. Unfortunately, without proper phase characterization of the field, this is merely speculation.

5.5 Conclusions

In this chapter we have discussed the effects of spatiotemporal coupling on Z-scan measurements performed with ultrashort pulses. The simulations of Z-scans with one spatial and one temporal dimension showed that dispersion can indeed affect the measurement when ultrashort pulses are employed. For weak nonlinearities, linear dispersion can influence the Z-scan measurement by broadening the pulse as it propagates in the sample. The effect is the same in all four of the propagation regimes defined by the sign of the nonlinearity and the dispersion: the dispersive broadening leads to a reduced $\chi^{(3)}$ measurement. When the input pulse has a frequency chirp then the effects become even more dramatic. Because the pulse can be either compressed or broaden depending on whether or not $\beta_2 C > 0$, the chirp can produce a result that is either erroneously large or small. When the nonlinearity being measured is large enough that nonlinear pulse compression is possible then the dispersion regimes exhibit quite different behavior.

Although the experimental results were consistent with the numerical predictions on several points, experimental verification of these phenomena was hampered by several factors. The primary problem

that needs to be dealt with is our inability to accurately characterize the shape and phase of the pulses used in the experiment. Given that the phase of a sub-100 fs pulse is difficult to measure and even more so to control, a transform limited pulse is more closely related to theoretical fantasy than it is to experimental reality. Moreover, due to the large influence of frequency chirp on the measurement, as indicated by figs. (5.5), and the limited expected nonlinear phase accumulation, uncertainties in the initial phase of the field dictate a large uncertainty in our ability to ascribe discrepancies in the measurements to the nonlinear spatiotemporal coupling described by the previous chapters of this thesis. There may also have been a related problem from the pulse compressor contributions to the spatial phase distribution of the field. There were other problems with the samples themselves. The wedge in the glass samples as well as poor surface quality eliminated the possibility of accurately performing the phase-sensitive closed-aperture Z-scans that were the initial motivation for the experiment. Although the glass samples were hygroscopic we did attempt to polish them using ethylene glycol; this approach was unsuccessful, resulting in the destruction of one of the samples. The surfaces of the cuvettes and hence the optical quality of the polymer samples were excellent, however the large thermal nonlinearity could not be avoided with the large average power of our 85 MHz pulse train. Without a Pockel's cell or some other means of selecting single pulses, the slow thermal contribution to $\chi^{(3)}$ will dominate any measurements of nonlinear index change made with the polymers and can even corrupt the open-aperture Z-scans.

Inasmuch as this entire chapter has been spent searching for problems with the Z-scan measurement technique, it is only fair to point

out that in order to find measurable errors due to nonlinear spatiotemporal coupling it was necessary to postulate some fairly extreme conditions in the simulations. In particular, the samples were nearly as large as the diffraction length of the focused beam and the assumed dispersion of the material was on the order of ten times that of bulk silica. Although we did find that frequency chirp may play an important role, this should merely serve as a motivation for the development of more effective ultrashort pulse characterization techniques. Given well-characterized pulses, the Z-scan technique appears to be a very robust measurement tool.

5.6 References

1. M. Sheik-Bahae, A. A. Said, T.-H. Wei, D. J. Hagan, E. W. Van Stryland, "Sensitive measurements of optical nonlinearities using a single beam," IEEE J. Quant. Electron. **26**, 760 (1990)

2. E. W. Van Stryland, M. Sheik-Bahae, A. A. Said, D. J. Hagan, "Characterization of nonlinear absorption and refraction in advanced materials," SPIE Vol. 1852 , 135 (1993)

3.R. DeSalvo, M. Sheik-Bahae, A. A. Said, D. J. Hagan, E. W. Van Stryland, "Z-scan measurements of the anisotropy of nonlinear refraction and absorption in crystals," Opt. Lett. **18**, 194 (1993)

4. J. Wang, M. Sheik-Bahae, A. A. Said, D. J. Hagan, E. W. Van Stryland, "Time-resolved Z-scan measurements of optical nonlinearities," J. Opt. Soc. Am. B **11**, 1009 (1994)

5. T. Xia, D. J. Hagan, M. Sheik-Bahae, and E. W. Van Stryland, "Eclipsing Z-scan measurement of $\lambda/10^4$ wave-front distortion," Opt. Lett. **19**, 317 (1994)

6. R. E. Bridges, G. L. Fischer, R. W. Boyd, "Z-scan measurement technique for non-Gaussian beams and arbitrary sample thicknesses," Opt. Lett. **20**, 1821 (1995)

7. J. A. Herrmann, R. G. McDuff, "Analysis of spatial scanning with thick optically nonlinear media," J. Opt. Soc. Am. B **10**, 2056 (1993)

8. W. Zhao, P. Palffy-Muhoray, "Z-scan technique using top-hat beams," Appl. Phys. Lett. **63**, 1613 (1993)

9. K. Y. Tseng, K. S. Wong, "Femtosecond time-resolved Z-scan measurements of optical nonlinearities in solids and liquids," Quantum Electronics and Laser Science Conference (QELS'95), Baltimore, Maryland, (1995) paper QWD13

10. A. Hochbaum, "Simultaneous determination of two or more nonlinear refractive constants by Z-scan measurement," Opt. Lett. **20**, 2261 (1995)

11. A. Marcano, H. Maillotte, D. Gindre, and D. Metin, "Picosecond nonlinear refraction measurement in single-beam open Z-scan by charge-coupled device image processing," Opt. Lett. **21**, 101 (1996)

12. T. D. Krauss, F. W. Wise, "Femtosecond measurement of nonlinear absorption and refraction in CdS, ZnSe, and ZnS," Appl. Phys. Lett. **65**, 1739 (1994)

13. I. Kang, T. D. Krauss, F. W. Wise, B. G. Aitken, N. F. Borrelli, "Femtosecond measurement of enhanced optical nonlinearities of sulfide glasses and heavy-metal-doped oxide glasses," J. Opt. Soc. Am. B **12**, 2053 (1995)

14. M. Sheik-Bahae, D. C. Hutchings, D. J. Hagan, E. W. Van Stryland, "Dispersion of bound electronic nonlinear refraction in solids," IEEE J. Quant. Electron. **27**, 1296 (1991)

15. A. A. Said, M. Sheik-Bahae, D. J. Hagan, T. H. Wei, J. Wang, J. Young, E. W. Van Stryland, "Determination of bound-electronic and free-carrier nonlinearities in ZnSe, GaAs, CdTe, and ZnTe," J. Opt. Soc. Am. B **9**, 405 (1992)

16. D.Weaire, B. S. Wherrett, D. A. B. Miller, and S. D. Smith, "Effect of low-power nonlinear refraction on laser beam propagation in InSb," Opt. Lett. **4**, 331 (1979)

17. N. F. Borrelli, B. G. Aitken, and M. A. Newhouse, "Resonant and non-resonant effects in photonic glasses," J. of Non-Crystalline Solids **185**, 109 (1995)

18. J. S. Meth, H. Vanherzeele, S. A. Janekhe, M. F. Roberts, A. K. Agrawal, C. Yang, "Dispersion of $\chi^{(3)}$ in fused aromatic ladder polymers and their precursors probed by third harmonic generation," Proc. SPIE **1560**, 13 (1991)

19. J.-C. M. Diehls, J. J. Fontaine, I. C. McMichael, F. Simoni, "Control and measurement or ultrashort pulse shapes (in amplitude and phase) with femtosecond accuracy," Appl. Opt. **24**, 1270 (1985)

20. R. L. Fork, O. E. Martinez, J. P. Gordon, "Negative dispersion using pairs of prisms," Opt. Lett. **9**, 150 (1984)